Spring 5-5-2018

Inhibition of RAD52-based DNA repair for cancer therapy

Mona Al-Mugotir
University of Nebraska Medical Center

Inhibition of RAD52-based DNA repair for cancer therapy

By

Mona Hadi Al-Mugotir

A DISSERTATION

Presented to the Faculty of the University of Nebraska Graduate College in Partial Fulfillment of the Requirements for the Degree of Doctor of Philosophy

Biochemistry & Molecular Biology

Graduate Program

Under the Supervision of Professor Gloria E. O. Borgstahl

University of Nebraska Medical Center

Omaha, Nebraska

April, 2018

Supervisory Committee:

Amarnath Natarajan, Ph.D.

Justin L. Mott, M.D.- Ph.D.

Youri I. Pavlov, Ph.D.

Acknowledgment

Any line I could think of to start my acknowledgment contains the phrase “my mother.” My mother has a generous, giving nature that drove her since early times in her life to assume motherhood responsibilities towards her younger siblings which continued in full capacity as she became a parent herself for the eight surviving of us. Not a single time in my life growing up do I recall her going to a bakery to buy bread. She kneaded her dough and fired up her oven (tanoor) practically daily. We would show up from school and consume all that she made with little thought as to how much of her health was consumed standing during those extremely hot summers of Iraq in front of that oven. As war circumstances did not make life any easier for her, she persisted by quietly absorbing all the pain of mounting losses we endured and continued her art of providing the absolute best from the least. The debt I owe to my mother goes far in time and magnitude beyond the years of working on my Ph.D., during which she made sure to call every night, when she could, just to hear my voice and ensure that I was surviving. I miss living within the warmth of her love. The closest I get to replicating those times is to wait for her visits and do something like feigning sleep on a couch just to get her to do the predictable: walk quietly with a blanket to cover and tuck me around. She would do that and often walk back to ensure that I did not kick that blanket off. I tried to keep those pretending games to a reasonable limit but it’s hard to get enough when you are on the receiving end of that. Today, as I am watching her back arching and joints painfully swelling, I feel the inadequacy of saying thank you. She had humbly raised every bar for me in parenthood, integrity, and generosity. I dedicate all the work here to my mother as she was the power behind every good in my life.

I also dedicate my work to my father who provided me with his love and support throughout. I draw much of my strength from the example he is in my life as a strong and patient man. There were days where life difficulties brought him down on his knees but that never lasted longer than the time needed to think and get back up on his feet. As every graduate student can attest to, that type of persistence is the best example one can ask for and I have it in the form of a father.

Many thanks to my siblings who have been a wonderful source of support, love, and care. A person who is literally the reason I am still alive to write this acknowledgment is my older brother Baqir. During difficult and petrifying times of war, he showed up with a cylindrical-rear tanker, loaded all of us along with other frightened families in our home town of Shinafiya, and drove us all to safety. Another particularly special bond that fills my heart with warmth is that provided by my younger siblings. Starting with my brother Hassan who, despite receiving a permanent little mark on his forehead from one of our childhood rivalries that I started, has been giving me nothing short of absolute love and support. My brother Abdulbari is another magical character that can turn any situation or a place into a world of fun when he shows up, earning him the "favorite uncle" title. Many thanks to my sister Heba for being a source of support and encouragement. All my other siblings who live far away: Natheema, Essam, Nahtha, Hisham, and Sindus were supporting and encouraging me in every way they can. I am also grateful for the amazing sisters-in-law who helped tremendously to make it possible for me to study for exams or travel for conferences knowing that my family were cared for.

My nieces and nephews have been a source of joy and happiness and I am very lucky to be their aunt. I would like to particularly acknowledge my nephew Mohammad Baqir,

who can send all my stress away with a single hug. He always inspires me with his strength and determination.

I am thankful for my husband Ihsan, who showed me the way to true happiness through his love, care, and support. It fills me with pride to call a reliable, compassionate, and an intelligent man like him as a partner and a friend. His love and support made every challenge in life worthwhile. Our boys, Ayman and Ibraheem, have been the best two human beings a parent can ask for. With their cheerful attitude, they managed to turn my time in graduate school into a magical journey. They kept me in check in hope of successfully finishing the invention of a superhero-antidote to inject them with. The truth is, the two of them along with their father have been my superheroes all along and no effect of an antidote can measure up to that. I am also very grateful for the wonderful parents-in-law who supported me immensely during early years of my studies. Their presence was always a source of happiness and fulfillment for the four of us.

Much of the great opportunities that paved the path for me in science are attributed to the generous support and guidance I received from Dr. Mary McNamee. She was the first person I was lucky to meet as I was seeking an opportunity at UNMC. Ever since, she and Keith made me and my family part of their own and were there in every milestone.

Few can say that they had the ideal role model in science and I was beyond lucky to have three of the finest examples of women in science: Dr. Mary McNamee, Dr. Gloria Borgstahl, and Carol Kolar. Those three women made a lasting impact in my knowledge and training in ways that cannot be simply found in a textbook. I would like to particularly express my deep gratitude to Dr. Borgstahl for giving me an opportunity and

trusting me to join her team at an unconventional turning time of my doctoral years. I am honored to have been mentored by a brilliant and humble scientist like her.

My gratitude is also extended to my colleagues who contributed to a positive, jovial, and supportive work environment. Screening 8,000 -10,000 molecules on an average week for the high throughput screening was only possible because Carol joined with me on that project. Her contribution experimentally and intellectually was tremendous and I have been very lucky to have worked with her. I am also very grateful for all the valuable insights she had giving me out of her many years of experience and I hope to always meet her meticulous standards as a scientist and an person. Dr. Lucas Struble and I had a common path through course work, comprehensive exam, thesis project, and down to the final steps of defense and graduation. His genuine, kind, and helpful attitude made that path both tolerable and enjoyable. Many thanks to Willian Lutz, Jahaun Azadmanesh, and Jeffrey Lovelace for their considerable support and kindness. My great appreciation is also extended to past lab members: Krysten Vance, Jacob Remsza, and Phillion Hoff, who contributed much help to the completion of my project.

The work on my project demanded new techniques and instruments that my lab did not have at certain points in time, and I have many people to thank for giving me the space and training to make my work possible. I thank Dr. Luis Marky, Dr. Alexander Lushnikov, and Dr. Calliste Reiling for the ITC work; Dr. David Kelly and Amy Wells for the HTS work; Dr. Amarnath Natarajan and his team and Tadayoshi Bessho for the cell culture work; and Dr. Chanty Morris for early SPR work.

The completion of my dissertation would have not been easy without the generous support I and my family received from friends. Special thanks to the community

members of Alhadi Center for being a constant source of spiritual support and genuine help. Our friends Mayraj Fathima and Syed Javed Ali are among the most amazing friends, and have been my anchors in times of challenge. During the onerous processes of writing my dissertation, I received from them countless messages of encouragement as well as delicious food that was sometimes courteously left by my door. I would also like to acknowledge my friend Dr. Jennifer Kopanic for her sensible advises and tremendous support. Many thanks to my friend Raghda Mukbil who was a wonderful help with Ayman and Ibraheem during the early years of my studies. I am also grateful for my friend Maha Farid who has been both an inspiration and support. My great appreciation is extended to Mohammed Alkhadhim and his family who have been a source of constant encouragements.

Finally, this was a remarkable journey of my life that nuanced my perception and perspective on many levels. Ironically, while working on this dissertation that holds implications in breast and ovarian cancer, I learned that my childhood friend and cousin Huda is battling triple negative subtype of breast cancer due to BRCAness. While I had access to observe the somber side of this disease at work, the way she maintains her courageous and positive attitude after two rounds of chemotherapy is spectacular. It is my hope that one day a more targeted treatment for this disease would be possible and we continue to see her amazing smile and lively spirit.

Abstract

Germline BRCA mutations underlay a significant risk for breast and ovarian cancer that increases in age. BRCA mutations are usually associated with the most aggressive subtypes of these cancers such as triple negative breast cancer and high-grade serous ovarian cancer. Conventional chemotherapeutic or hormonal therapies do not address the molecular deficiencies responsible for their resistance and there is a high rate of recurrence. Targeted therapy that can address the unique molecular features in these subtypes of cancer is the only way to cure the disease or, at the very least, improve patients' quality of life.

Homologous recombination repair is an accurate repair pathway that utilizes a copy of a homologous sequence to relay information to the break site. Cancer cells copy their DNA extensively meeting the principle demand for this high-fidelity repair pathway. Homologous recombination repair is utilized by cancer cells to cope with the most challenging forms of DNA damage such as DNA double strand breaks, stalled replication forks, adducts, and interstrand crosslinks. Among the key proteins in homologous recombination repair, RAD52 activity promotes cancer cells' tolerance and survival. Therefore, there is a therapeutic opportunity in inhibiting RAD52 activity to push DNA damage levels in homologous recombination repair-deficient tumors beyond the limits of viability.

One of the early events in this repair is resection of the broken strand and generation of single strand DNA. Replication protein A cover and protect those strands and interact with key DNA repair proteins. RAD52 activity in DNA repair is dependent on its

interaction with replication protein A. The hypothesis of this thesis is that it is possible to inhibit RAD52 activity by inhibiting its interaction with RPA and this inhibition will have therapeutic benefits for cancer patients. We explored the binding activity and affinity of the RAD52 interaction with RPA. Kinetic, and thermodynamic parameters dictating this protein:protein interaction were measured. The characterization of RAD52:RPA interaction data guided remapping of the RPA interaction domains on RAD52. To target RAD52 activity by inhibiting its interaction with RPA, we designed an *in vitro* fluorescent-based protein-protein interaction assay. This assay was further optimized for high throughput settings with a robust signal, minimal steps, statistical accuracy, and low cost. We screened over 100,000 compounds to look for small molecule inhibitors. Eleven hits were found and five were selected for their high EC_{50} values. Three of the five hits are FDA approved drugs and were selected for cytotoxicity tests in BRCA-deficient cell lines.

The outcome of our characterization for these three candidate small molecule inhibitors may shed light on the variation of their efficacy and sensitivity among breast or ovarian cancer patients with BRCA-defective pathway versus those with none. Additionally, we present fluorescent-based protein-protein interaction assay as an affordable method to detect many protein:protein interactions in low-scale or high throughput settings applicable to finding small molecule inhibitors or aptamer modulators for protein:protein interactions.

Table of Contents

List of Figures

List of tables

Abbreviations

ATM, ataxia telangiectasia mutated

BER, base excision repair

DDR, DNA damage response

DLS, dynamic light scattering

DSB, double stranded break

EC_{50}, half-maximal effective concentration

EGFP, enhanced green fluorescent protein

ELISA, enzyme-linked immunosorbent assay

FluorIA, Fluorescence-based protein-protein Interaction Assay

HTS, high throughput screening

HRR, homologous recombination repair

NER, Nucleotide excision repair

MMR, mismatch repair

PARP, poly(ADP-ribose) polymerase

PPI, protein-protein interactions

RFU, relative fluorescent unit

RPA, replication protein A

SAXS, small-angle X-ray scattering

SMI, small molecule inhibitor

ssDNA, single stranded DNA

SSB, ssDNA-binding proteins

wHLH, Winged Helix-Loop-Helix

Chapter 1

1.1. Introduction

1.1.1. Normal cell division and DNA damage repair machinery. Regulation of cell division is essential for tissue homeostasis. This regulation involves utilization of molecular signals and critical decision-making regulated at discrete stages of a cell's lifecycle [1]. A major driver of this decision-making process is DNA damage due to metabolic or environmental insults. Cells response in the face of these challenges involves initiating DNA repair processes while activating cell cycle checkpoints to allow the time needed for repair. Ataxia telangiectasia mutated (ATM), AT and Rad3-related (ATR), and DNA-dependent protein kinase, for example, are kinases that regulate the DNA damage response by establishing phosphorylation cascades in cell cycle checkpoint kinases and support the initiation progression of the appropriate repair mechanisms [2-4]. Cells resort to apoptosis when the damage is beyond their repair capacity [5]. DNA repair pathways have a common capacity of repairing DNA lesions but vary in their efficiency as a function of the site, nature of the lesion, cell's genotype, stage in the cell cycle, and the risk of mutagenesis in the process. Figure 1.1 summarizes the different DNA lesions and corresponding specialized repair pathways [6].

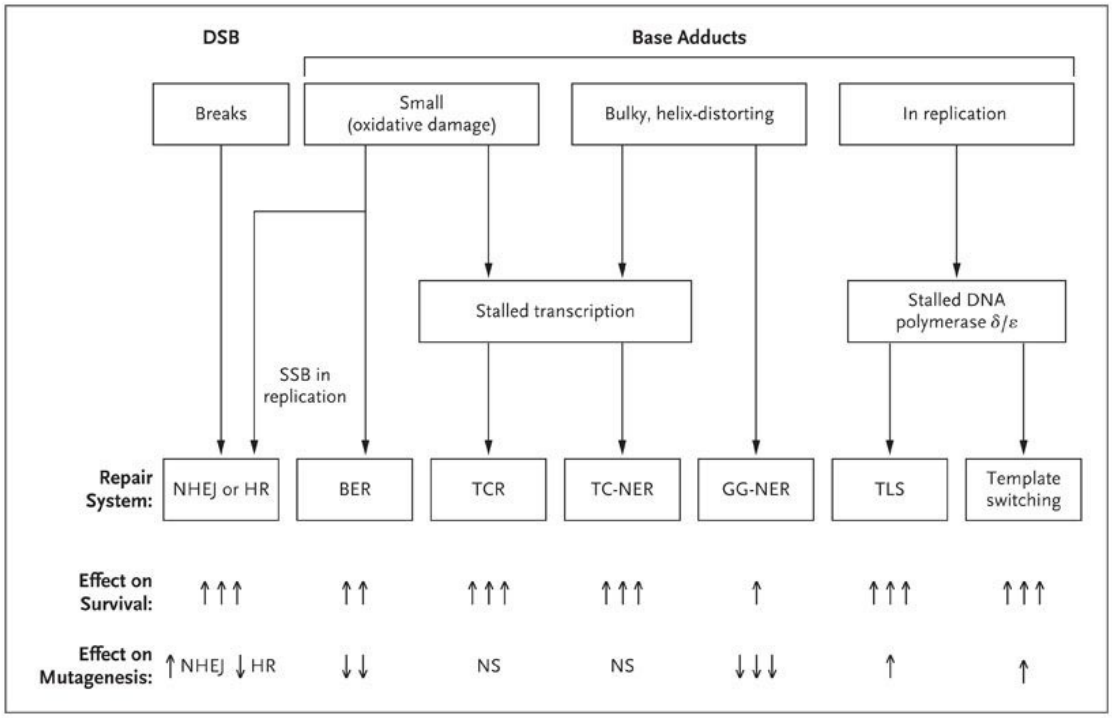
DSB
Base Adducts
Breaks
Small (oxidative damage)
Bulky, helix-distorting
In replication
Stalled transcription
Stalled DNA polymerase δ/ε
SSB in replication
Repair System:
NHEJ or HR
BER
TCR
TC-NER
GG-NER
TLS
Template switching
Effect on Survival:
↑↑↑
↑↑
↑↑↑
↑↑↑
↑
↑↑↑
↑↑↑
Effect on Mutagenesis:
↑NHEJ ↓HR
↓↓
NS
NS
↓↓↓
↑
↑

Figure 1.1 Types of DNA damages and repair mechanism. DNA is damaged in various ways during normal metabolism or by exogenous factors. The top panel of boxes show the types of DNA damage and arrows point down to specialized repair systems. DSBs are repaired through NHEJ or HR. The beneficial outcome of different repair pathways is measured by promoting cell survival and variation in that is indicated by the number of upward arrows. Accurate repair pathways such as HR are least mutagenic and that is indicated by an upward arrow. Less accurate repairs are mutagenic and indicated by a downward arrow. BER is involved with small DNA adducts. Transcription-coupled repair (TCR) deals with lesions that block elongating RNA polymerase. Transcription-coupled nucleotide-excision repair (TC-NER) repairs transcription-blocking bulky adducts. The path of DNA polymerases can be stalled due to encountered adducts or cross-links. Such damage can be repaired, bypassed (template switching or translational synthesis). Figure is adapted from Jan Hoeijmakers, 2009: The New England Journal of Medicine.

The level of challenge for the cell to repair DNA damage varies. For example, DNA single strand breaks are frequent but relatively undemanding. These breaks are ligated either directly within the phosphodiester backbone or after removal of abnormal structures with as the intact strand holding the ends together [7]. Single strand breaks are inevitable intermediates in base excision repair BER, nucleotide excision repair NER, and mismatch repair MMR are among the main DNA repair pathways.

The most taxing form of DNA damage in a cell is the DNA DSB [6]. DSBs are an unavoidable consequence for a number of physiological processes such as the process of relaxing DNA supercoils, or during normal cell death by apoptosis [8]. Generally, the availability of a template on a sister chromatid makes it possible to search for homologous or near-homologous sequence to copy information accurately in HRR pathway. This is possible when damage occurs during the S or G_2 phase of the cell cycle, otherwise nonhomologous end joining (NHEJ) is an error-prone alternative repair choice for non-proliferative cells in G_0 and G_1 [9, 10]. NHEJ simply involves alignment and ligation of broken strands. Lahav's and coworkers avoided the approach of fixing cells after damage to measure the type of repair activity in relation to cell cycle phase. Instead, they employed long-term, time-lapse microscopy and fluorescent reporters to obtain quantitative data that suggested a direct link between HRR and increased active replication events (Figure 1.2) [11]. Therefore, they argued that it is not the availability of replicated DNA that dictates the transition to HRR, but rather the extent of active replication. Single strand annealing (SSA) is another repair process for DSBs occurring at site of already existing homology, in particular repetitive DNA sequences [12].

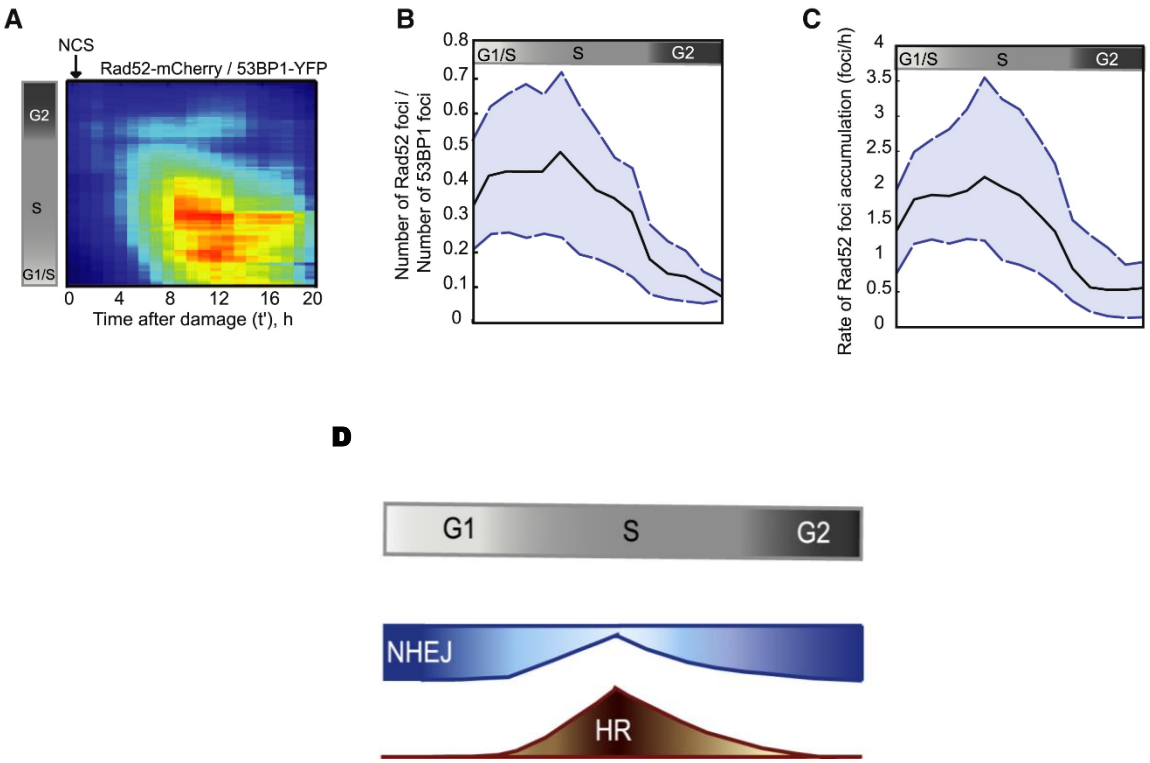
A
NCS
Rad52-mCherry / 53BP1-YFP
G2
S
G1/S
0 4 8 12 16 20
Time after damage (t'), h
B
G1/S
S
G2
Number of Rad52 foci / Number of 53BP1 foci
0 0.1 0.2 0.3 0.4 0.5 0.6 0.7 0.8
C
G1/S
S
G2
Rate of Rad52 foci accumulation (foci/h)
0 0.5 1 1.5 2 2.5 3 3.5 4
D
G1
S
G2
NHEJ
HR

Figure 1.2 Repair choice by HRR or NHEJ and cell cycle. 53BP1 is a DNA damage response protein which forms subnuclear compartments called foci that provide experimental assessment of DSBs in cells. RAD52 is a protein that forms foci at DSB sites that are committed to HRR. (A) Heat map showing the proportion of DSBs repaired by HR (RAD52-mCherry foci) post damage (53BP1-YFP foci) shown as a function of the time (hours) from the induction of DSBs and cell-cycle progression (gray bar on the left). Higher proportion of HRR activity is observed (red color) with longer extent in replication phases of cell cycle.

(B) The proportion of DSBs repaired by HRR in individual cells post damage is plotted against their cell-cycle progression at the time of damage indicated by the reference bar on top. The three lines shown are the median (black line), 25^{th}, and 75^{th} percentile (dashed blue lines above and below the black line).

(C) Relative accumulation of RAD52 foci in individual cells after damage is plotted against cell-cycle progression. The three lines shown are the median (black line), 25^{th}, and 75^{th} percentile (dashed blue lines above and below the black line).

(G) A model summarizing collective data from time-lapse microscopy and fluorescent reporters and represents the transition between NHEJ and HR with cell-cycle progression. In G1, DSBs are exclusively repaired by NHEJ. HRR activity gradually increase as cells progress into early S phase and a peak is reached by mid S phase. HRR then decreases gradually as cells progress toward late S and G2. Cells in late G2 repair their DSBs almost entirely by NHEJ.

Figure is adapted and modified from Karanam et al., 2012: Molecular Cell.

1.1.2. The tolerance for DNA damage by cancer cells. Cancer cells usually exhibit an abnormal extent of active replication with a large capacity to divide and replicate their DNA [13]. Accompanying these events is a heavy load of genotoxic stress that when combined with cytotoxic treatments, results in an intensified amount of DNA damage mostly in the form of DSBs. Stalled replication forks, interstrand crosslinks, and adducts are prevalent in the stressful tumor environment and tend to induce more DSBs. At this level, normal cells would have exhausted their repair capacity mechanisms and resorted to cell death to prevent the propagation of damage and preserve genomic stability. Cancer cells on the other hand are not only able to survive, but also are propelled into further expansion. Resistance to cell death becomes a hallmark for them and they acquire the ability to maintain the *status quo* by tolerance for genomic instability [14].

1.1.3. The rise of malignancies and the vision for targeted therapy. The vitality of a tissue is judged by the ability of its cells to divide with orchestrated control throughout its life cycle. Cells differentiate into their fateful identity through a tightly regulated process. This is no surprise, given that a vast portion of our genome encodes regulatory elements and a much smaller part encodes functional proteins. Although this may seem to be a rigid process, we now know that a degree of plasticity is offered by our chromatin structure and associated transcriptional regulators. For example, studies have shown that in the face of some challenges, the responsibility of DNA replication can be handed over to other classes of DNA polymerases with more malleable base-pairing capacity [15]. This plasticity allows for an appropriate and adaptive response to environmental or metabolic stimuli. Flavahan and colleagues postulated that when a cell is faced with a

challenge, this plasticity allows it to assume alternative functional and regulatory pathways [14]. For example, cells can shift DNA damage response or repair to alternative mechanisms or pathways [16]. While these alternative pathways may contribute to a cell's fitness in the face of potentially pro-oncogenic stimuli, some can drive the cell into malignancy. This unfortunate consequence itself gives cancer cells distinctive molecular features when compared to normal ones, a concept of great importance to researchers interested in shifting cancer therapeutics to specific and targeted approaches.

Current promising therapies involve targeting pathways that are vital to cancer cells' survival, proliferation, and the maintenance of their tumor microenvironment [17]. Components of the DNA damage response are at the center of these processes and are, not surprisingly, among the most frequently mutated in cancer [18]. Evidence includes the acceleration of hepatocarcinogenesis by constitutive upregulation of different DNA repair pathways [19], the upregulation of the HRR component *RAD51* [20-22], or the downregulation of tumor suppressors *BRCA1/2* [23] in driving breast and ovarian cancers.

1.1.4. Homologous recombination repair machinery. HRR is initiated by a resection process at the DSB site in a 5′-3′ direction by the Mre11-RAD50-NBS1 (MRN) complex producing exposed ssDNA on opposite ends of the break site (Figure 1.3, step 1, 2, and 3) [24]. This outcome is immediately addressed by replication protein A (RPA) binding ssDNA at the break site. Aside from physical shielding and protection, RPA contributes to an accurate repair choice by preventing insufficient homologies to lead the repair process or haphazard end joining [25]. In addition, RPA prevents the formation of DNA secondary structures during replication and repair, thereby contributing to the

maintenance of genomic stability [26, 27]. This role for RPA continues until RAD51 takes over the repair process by forming presynaptic filaments to catalyze homologous strand invasion and annealing [28]. An active ongoing HRR is usually experimentally observed in the form of discrete subnuclear structures called RAD51 foci [29]. The replacement of RPA with RAD51 requires a mediator protein.

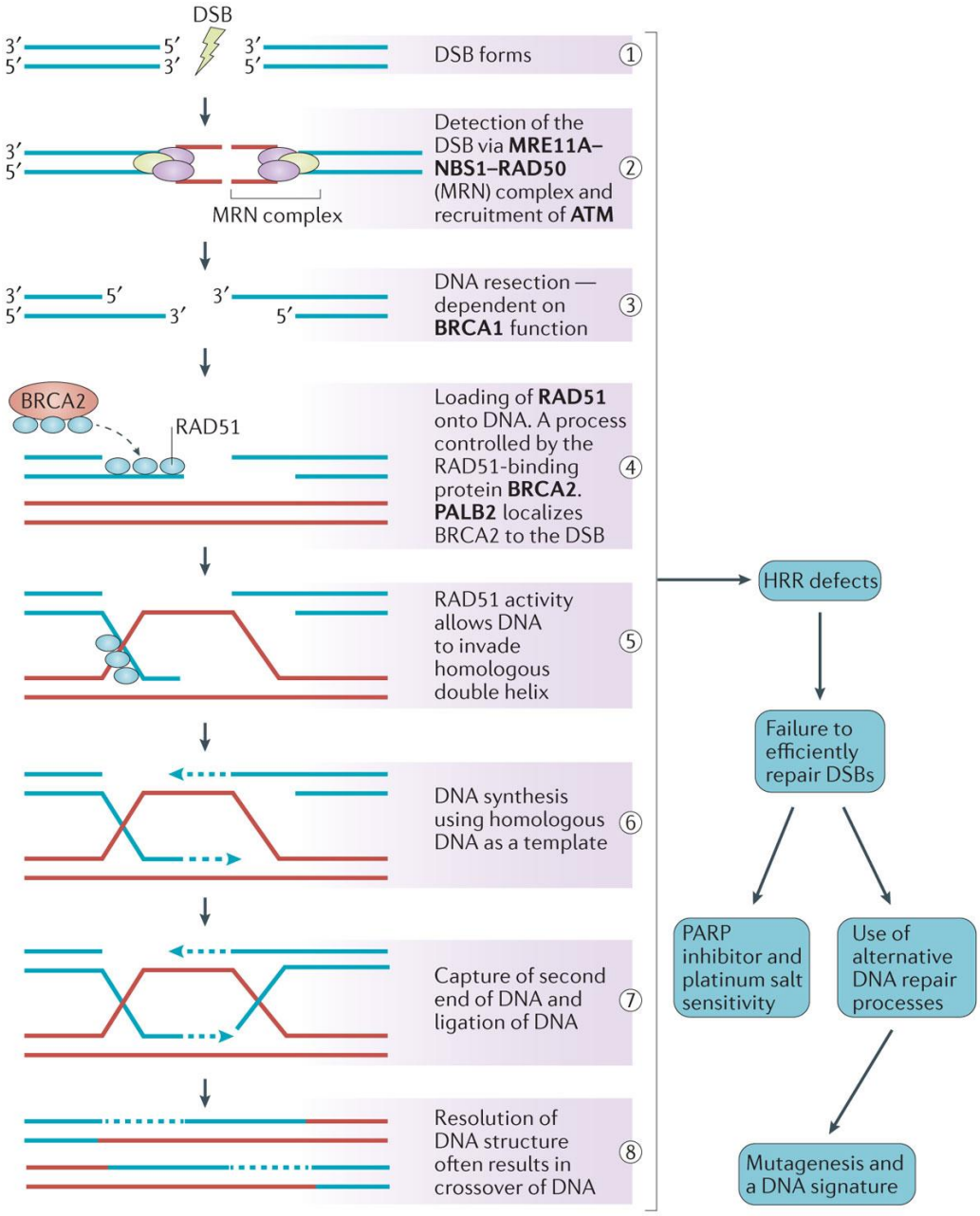
DSB
3′
5′
5′
3′
3′
5′
DSB forms
①
3′
5′
MRN complex
Detection of the DSB via **MRE11A–NBS1–RAD50** (MRN) complex and recruitment of **ATM**
②
3′
5′
5′
3′
3′
5′
DNA resection — dependent on **BRCA1** function
③
BRCA2
RAD51
Loading of **RAD51** onto DNA. A process controlled by the RAD51-binding protein **BRCA2**. **PALB2** localizes BRCA2 to the DSB
④
RAD51 activity allows DNA to invade homologous double helix
⑤
DNA synthesis using homologous DNA as a template
⑥
Capture of second end of DNA and ligation of DNA
⑦
Resolution of DNA structure often results in crossover of DNA
⑧
HRR defects
Failure to efficiently repair DSBs
PARP inhibitor and platinum salt sensitivity
Use of alternative DNA repair processes
Mutagenesis and a DNA signature

Figure 1.3 HRR and BRCAness. A schematic representation of the repair steps of DSBs by HR. Tumor suppressor proteins involved in the process are shown in bold. BRCA1 is an example of those proteins and is essential for the early step in repair where MRE11A-NBS1–RAD50 (MRN) complex detects and bind broken strands. This complex, along with recruited ATM, leads the resection process and generation of ssDNA on either side of the break. The next tumor suppressor proteins in the process is BRCA2, which localizes RAD51 to the exposed ssDNA regions to perform homology search. PALB2 is an additional tumor suppressor that is crucial for the localization of BRCA2. Next, nucleoprotein filament formed by RAD52 recombinase invade an intact DNA double helix containing a homologous, sequence (indicated in red). This sequence is used by DNA polymerases as a template to synthesize new DNA that repair the break. Finally, resulting cross-over structures are resolved by DNA ligases and endonucleases. Blue branching boxes on the right represent the vulnerabilities of cells with defected HRR and ways to exploit that vulnerabilities in targeted therapy. For example, pharmacological inhibition of PARP leads to accumulation of DSBs that cannot be efficiently repair by HR when *BRCA1, PALB2, or BRCA2* are mutated. Also, loss of HRR probably cause shunting of DSBs repair to alternative mutagenic DNA repair pathways such as NHEJ resulting in gross chromosomal instability and cell death. Figure is adapted from Lord and Ashworth, 2016: Nature Reviews Cancer.

1.1.5. The status of BRCA1/2 in RAD51-mediated HRR. BRCA1 and BRCA2 play a crucial role in both detection and repair of DSBs. BRCA2 joins BRCA1 in a complex that co-localizes with RAD51 and activates DSB repair [30, 31]. BRCA1 is implicated in regulating the activities of the DNA repair by HRR such as the formation and function of the MRN complex (Figure 1.3, step 3) [32-34].

While BRCA1 function in HRR is focused on recruitment, activation, and assembly of repair components, BRCA2 plays a more direct role. For RAD51 subunits to load and nucleate a protein filament on the ssDNA strands, RPA must be displaced. In eukaryotes, the BRCA2 proteins are the main mediators of this process [35]. Heyer and colleagues have shown that BRCA2 plays an integral role in HRR not only as a mediator, but as a driver of the process as it stimulates RAD51 binding to ssDNA [36]. In fact, direct interaction and regulation of RAD51 repair activities defines the role of BRCA2 in HRR(Figure 1.3, step 4) [37].

1.1.6. The significance of 'BRCAness' in cancer. Germline mutations in the tumor suppressor *BRCA1, BRCA2, or PALP2* are associated with the majority of hereditary breast and ovarian cancers [38, 39] and contribute, less frequently, to the risk for prostate, pancreas, fallopian tube, bile duct, stomach, and male breast cancer [40-43]. Moreover, *BRCA1* was identified as *FANCS* while *BRCA2* as *FANCD* comprising the Fanconi anemia-BRCA pathway. Mutations are also associated with predisposition to acute myelogenous leukemia and epithelial cancers [44-46]. In a broad sense, BRCAness is defined as defect in DSBs repair by HR. Figure 1.3 depicts DSBs repair by HR and the significance BRCA1, BRCA2, and PALP2 in the process [34]. Tumors with BRCAness

share molecular features across their different subtypes [47]. Hallmarks of BRCAness' include basal-like phenotype, ER-negativity, EGFR expression, sensitivity to DNA-crosslinking agents, and loss of RAD51 foci formation [48]. BRCAness predisposes women to the most aggressive subtypes such as triple-negative breast cancer (TNBC) [49]. The majority of high-grade serous carcinoma (HGSC), which account for over half of all ovarian epithelial tumors with the lowest survival rate, demonstrate BRCAness [50]. TNBC and HGSC remain challenging in the face of available conventional hormone or cytotoxic chemical therapies due to lack of hormone receptors, poor prognosis, and high rate of recurrence [51, 52]. Due to the significance of the BRCAs in DSB repair, exploiting their malfunctions can offer selective killing of cancer cells.

1.1.7. The status of RAD52 in RAD51-mediated homologous recombination repair. Knowing the indispensable role of Rad52 and its epistasis group of genes in HRR in *Saccharomyces cerevisiae*, West and colleagues were motivated to investigate its status in human HRR. Accordingly, they developed an *in vitro* system using purified human RPA, RAD51, and RAD52 proteins to reconstitute the HRR processing of DSBs. In addition to their detailed finding of the overall repair process, RAD52 was found to function in stimulating RAD51 interaction with ssDNA [53]. However, the significance of RAD52 remained perplexing as two *in vivo* model studies at that time showed the unhampered ability of mammalian cells to mount an HRR response in the absence of a functional RAD52. The first of these studies measured the number of RAD51 foci after gamma-irradiation of normal verses. $RAD52^{-/-}$ in the DT40 chicken B cell lines [54]. No difference was found in the formation or cycling of RAD51 foci indicating an unhindered HRR process. Another independent study found that RAD52 knock-out mice were

aphenotypic and relatively similar in their ability to mount HRR compared to mice with wild-type RAD52 [55]. Interest in RAD52 function in DSB repair eventually sparked with the series of siRNA targeting studies by Simon Powell and collaborators that demonstrated dependence of cells deficient in BRCA2 function on RAD52 to carry RAD51-mediated HRR of DSBs [56]. RAD52 indeed is capable of taking over this BRCA2 function in HRR given its reported direct interaction with RAD51 [57]. In fact, a synthetic lethal relationship was concluded to exist between RAD52 and BRCA2 as well as BRCA1 and PALB2 as explained in the next section [58].

1.1.8. BRCA proteins & RAD52: Synthetic lethality relationship. In the face of mounting DNA damage challenges cancer cells become "addicted" to DNA repair pathways. These alternative pathways are usually not the same ones that led to their malignant phenotype. Having lost the function of their main DNA repair pathway(s) by oncogenic alterations, selective cell death can be achieved by toxic accumulation of DNA damage when the alternate pathway(s) is targeted by an inhibiting or a modulating agent. Cancer cells deficient in BRCA1/2 function show reliance on RAD52 to mediate RAD51-facilitated HRR and SSA of DSBs [59-61]. These findings motivated a number of studies aimed at targeted cancer therapy exploiting the synthetic relationship between the BRCAs and RAD52. Indeed Cramer-Morales and colleagues demonstrated potential targeted therapeutic effects in leukemia cells harboring impaired BRCA1 function by targeting RAD52 activity [60]. A number of similar efforts followed to find ways to inhibit RAD52 to induce selective cell death in BRCA-deficient tumors and recently reviewed by Spies et al.[62-65].

1.1.9. RAD52 and tumorigenesis, beyond filling-in for BRCA2. Targeted therapy efforts rely on identifying specific molecular factors that enable tumor cell survival and growth. Recent expanded understanding of RAD52 activity suggests that it can assume "emergency" roles and is specifically recruited to DNA replication stress sites [66]. Therefore, RAD52 appears to promote tumorigenesis extending beyond the narrow scope of providing a backup pathway in BRCA-deficient cells. For example, *RAD52* upregulation was reported in liver cancer [19] and RAD52 is required for the recovery of a collapsed replication fork [67, 68]. RAD52 is also the main player in SSA, a repair process that was reported to increase in some cancers [69]. Moreover, some cancer-associated genes are reported to be enriched for repetitive sequences suggesting potentially increased SSA activity [70]. SSA repair activity of DSBs was also observed to increase in response to general decrease in RAD51-mediated HRR [71].

Recently a new inverse strand exchange activity for RAD52 was identified to drive RNA-templated DSBs repair [72]. It is no surprise, therefore, that targeting RAD52 activity was not only selectively lethal to BRCA-deficient cell [56], but also suppressed cancer stem and progenitor cell expansion [60], and even augmented the activity of the tumor immune response [73].

1.1.10. Approach to target RAD52 repair activity. RAD52 function has been correlated with several stress-induced responses that foster survival during uncontrolled cell growth. Targeting RAD52 is detrimental to BRCA-deficient tumors and may very well deprive other types of tumor microenvironments of an essential survival and maintenance factor. Different SMIs and aptamers have been identified and developed however, the common goals have been targeting RAD52 interaction with substrate DNA

and RAD52 annealing activity. Among the early approaches was the targeting of a residue on the RAD52-DNA binding domain (F79) by an aptamer to achieve synthetic lethality in chronic myelogenous leukemia cells deficient in BRCA1 activity [60]. More work followed to find a SMI to disrupt the ring structure of RAD52 and prevent the formation of the presumed ssDNA-binding grooves [74], RAD52 SSA repair activity of DNA [63], and inhibition of RAD52-ssDNA inhibitors [62, 64]. The outcomes of these studies are promising and motivating, however, our expertise in DNA repair proteins suggests for a different approach.

Aside from the innate ssDNA annealing capability demonstrated *in vitro* by Sugiyama and colleagues [75], all RAD52 repair activities described earlier require interaction with RPA. Given its abundance [76] and high intrinsic affinity for ssDNA [77], any single stranded region formed is immediately bound by RPA. This strong hold of DNA enables RPA to coordinate repair components arriving at the break site. Indeed, RAD52 function in HRR seems to be dictated by RPA. Early studies demonstrated that a mutated RPA-binding domain on Rad52 impairs its recruitment to the damage site [78]. We have shown that in the absence of RPA, RAD52 exists in rings and aggregates of rings and that monomeric RAD52 purifies in a stable complex with RPA-ssDNA. RPA was capable of promoting the breaking of the RAD52ring structure supporting RPA role in RAD52 activity [79]. In the recently described role for RAD52 in RNA-templated DNA DSB repair, the addition of RPA noticeably stimulated the repair activity [72]. Inhibiting RAD52's interaction with RPA is probably detrimental to all its functions in repair. The feasibility of this approach, however, has been met with reluctance as it involves targeting of a PPI with small molecule inhibitors. Among candidate cancer

targets, PPIs were historically discounted due their large and discontinuous epitopes. However, protein mutations are among the drivers for tumorigenesis as well as the development of resistance [80]. Remarkable strides were achieved recently in pharmaceutical targeting PPI of the Bcl-family of proteins to impede cancer cell survival [81]. These recent advances have improved the outlook on targeting PPIs for the development of new therapies.

The hypothesis of this thesis is that RAD52 can be as a targeted through its interaction with RPA. This PPI constitutes a repair pathway to mediate RAD51 activity in HR offering a backup survival path in BRCA-deficient tumors. The therapeutic value of targeting RAD52 activity can apply to several types of tumors. We investigated both kinetic and thermodynamic parameters of the RAD52:RPA complex deciphering important domains of interactions. Our work here acknowledges that there are still many potential targets to explore for targeted therapeutics which raises the need for a reliable high throughput experimental technique to search for compounds capable of modulating the function of a target. To address this need and contribute to the efforts, we developed a PPI assay and utilized it to confirm interacting domains. The assay was optimized for use in high throughput settings and used to screen over 100,000 small molecules looking for inhibitors. Finally, we detail our cell-free and cell-based methods characterizing candidate SMIs to determine their therapeutic value. Characterization results of some hits show reduced survival of cancer cells when RAD52 interaction with RPA is inhibited and thus validate the hypothesis.

Chapter 2

A simple fluorescent assay for the discovery of protein-protein interaction inhibitors

2.1. Abstract

Due to the therapeutic potential of targeting PPIs there is a need for easily executed assays to perform HTS of inhibitors. We have developed and optimized an innovative and robust fluorescence-based assay for detecting PPI inhibitors, called FluorIA (Fluorescence-based protein-protein Interaction Assay). We use targeting the PPI of RAD52 with RPA as an example and describe the FluorIA protocol design and optimization for future HTS of large chemical libraries. Here EGFP-tagged RAD52 detects the PPI using RPA coated, black microtiter plates and loss in fluorescence intensity identifies SMIs that displace the EGFP-tagged RAD52. The FluorIA design and protocol can be adapted and applied to detect PPIs for other protein systems. This should push forward efforts to develop targeted therapeutics against protein complexes in pathological processes.

2.2. Introduction

High throughput screening (HTS) has evolved into a specialized key drug discovery tool [82, 83]. With this advancement, the ambitions of scientific research shifted from the delivery of indiscriminate agents to drugs with more selectivity for the target. Current targets in cancer, for example, include abnormally expressed proteins, tumor microenvironment components, and alternative survival pathways adapted by tumor cells [17]. In each of these categories of therapeutic approaches, targeting pathologic PPIs are as promising as targeting mutated genes. PPIs orchestrate the signaling of normal cellular proliferation, the very trait that defines malignancies when deregulated. To sustain chronic proliferation, cancer cells acquire alternative signaling pathways defined by unique and specific PPIs [13].

Modulation of PPI with small molecules was, justifiably, described as “undruggable” or the “high-hanging fruit” [84]. Over the past two decades, however, interest in targeting PPIs increased with advanced knowledge of proteomics. Large PPI interfaces, for example, once regarded as a major challenge to target with small drug-like molecules are now desirable to bolster selectivity [85, 86]. Also, the community no longer thinks SMIs must mimic the interacting partner of the targeted protein and this realization led to a more comprehensive screening of available libraries [87-89]. Mutational studies demonstrated that only some residues in the PPI, or “hot spots”, contribute the majority of binding energy for the SMIs to bind and block the targeted protein partner from binding[85, 90]. With this finding, the quest for targeting PPIs with SMIs became plausible and the development of robust and cost-effective assays for HTS of SMI libraries for PPIs are in demand. Successful HTS screens that target PPIs include nuclear magnetic resonance [91], differential scanning fluorimetry[92], Fluorescence polarization/anisotropy[93], virtual screening with docking[94] and cell-free, enzyme-linked immunosorbent assay (ELISA) [95, 96].

Here, we describe our design and optimization of a fluorescent-based protein-protein interaction assay (FluorIA) applicable for HTS. As an example, we applied our assay to target the PPI of two important DNA repair proteins: RAD52 and replication protein A (RPA). RAD52 is a multi-domain protein that mediates homologous recombination repair of DNA double-strand breaks, a role mainly played by BRCA2 in mammalian cells [36, 97-99]. Tumor cells that have lost BRCA2 function rely on RAD52 to survive the breaks encountered from replication stress or cytotoxic treatments [61, 100, 101] and this presents a therapeutic opportunity to target RAD52 activity in BRCA-deficient tumors [56, 58, 60,

63, 102]. For homologous recombination, breaks are initially processed to produce single-stranded DNA tails that are then bound by RPA. The PPI of RAD52 with RPA is extensive and essential for RAD52 activity in the subsequent steps of repair [75, 79, 103]. Plate and co-workers demonstrated by mutational analysis that the ability of RAD52 to form repair foci required the RPA-binding domain [78]. Since the structure of the RAD52:RPA PPI is unknown, the FluorIA was developed using full length proteins and designed to screen for SMIs of the RAD52:RPA PPI in an unbiased manner. The application of this protocol to other PPI will support quests to find therapeutic SMIs or modulators targeting cancer or other pathological conditions.

2.3. Materials and methods

2.3.1. Protein expression and purification. The plasmid for full-length RPA (Figure 2.1A) in pET29a vector, a gift from Dr. Marc Wold, was transformed into Rosetta2(DE3) *Escherichia coli* with chloramphenicol and kanamycin selection. A single colony was inoculated into 5 mL starter culture and grown with selection for 6-8 hours at 37 ºC. Large cultures were made by inoculating 1 mL starter culture into 2 L sterilized LB with antibiotics in 4 L flasks and incubating at room temperature or 37 ºC overnight without shaking. The following day, the cultures were incubated at 37 ºC with shaking and induced with 0.5 mM isopropyl-β-D-l-thiogalactopyranoside (IPTG) at an A_{600} of 0.6-0.8. After 3 hours, cells were collected by centrifugation at 8,500 xg for 20 min. Pellets were divided into 5 gram portions and stored frozen at -20 ºC.

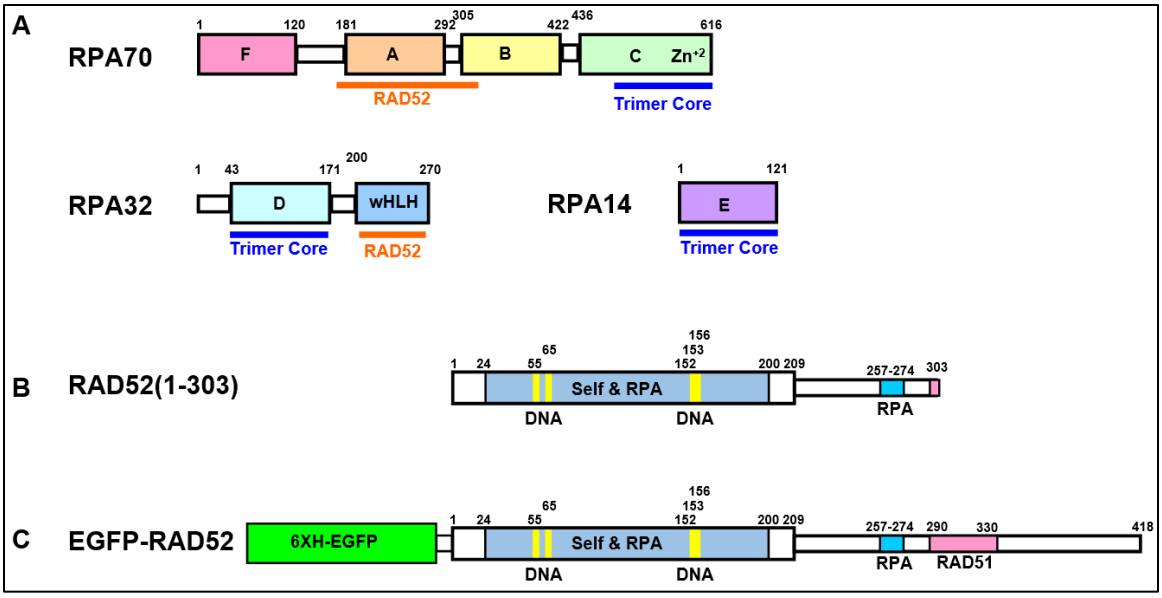
A
RPA70
1
120
181
292
305
422
436
616
F
A
B
C
Zn+2
RAD52
Trimer Core
RPA32
1
43
171
200
270
D
wHLH
Trimer Core
RAD52
RPA14
1
121
E
Trimer Core
B
RAD52(1-303)
1
24
55
65
152
153
156
200
209
257-274
303
Self & RPA
DNA
DNA
RPA
C
EGFP-RAD52
6XH-EGFP
1
24
55
65
152
153
156
200
209
257-274
290
330
418
Self & RPA
DNA
DNA
RPA
RAD51

Figure 2.1 Domain maps of proteins used in this study. (A) RPA, (B), RAD52(1-303), (C) Full length RAD52 tagged with 6x His EGFP. Structured domains and flexible linkers indicated as thick and thin boxes respectively.

Each RPA cell pellet was thawed and resuspended in 25 mL of HI-0 buffer [30 mM HEPES pH 7.8, 0.25% inositol, 0.25 mM EDTA, and 1mM dithiothreitol] with 500 mM sodium thiocyanate (NaSCN) plus 250 µL of protease inhibitor cocktail (PIC, Sigma, Cat. #P8849) before lysis using an Emulsflex-C3. Lysate was clarified by centrifugation at 45,000 xg for 30-45 min. The NaSCN content was reduced by either dilution or dialysis against HI-0 buffer and then filtered through a 0.45 µm filter. All chromatography steps employed HI-0 with varying salts. First the lysate was applied to a HiTrap Blue HP column (5 mL, GE Life Sciences # 17-0412-01) and washed For 5 CVs with 800 mM KCl followed by 5 CVs with 0.5 M NaSCN and then eluted with 1.5 M NaSCN into 1 mL fractions. The NaSCN content was reduced by either dilution or dialysis against HI-0 buffer and then applied to a hydroxyapatite column (3 mL, BioRAD # 157-0040) and eluted in a 25 CV gradient of 0-75% 160 mM $NaPO_4$. The column was cleaned by washing with 2 M KPO_4 in HI-0 after each use. RPA fractions were pooled and diluted with 4 volumes HI-0 before polishing with a monoQ anion exchange column (1 mL, GE Life Sciences # 17-5166-01). RPA was eluted in a 25 CV gradient of 0-100% 1 M KCl. Throughout the purification procedures described above, fractions were examined by 10% polyacrylamide gel electrophoresis (SDS-PAGE) with Coomassie stain (Figure 2.2). A NanoDrop1000 was used to measure concentrations using a molecular weight of 110 kDa and ε_{280}=87.2 $M^{-1}cm^{-1}$. Finally, purified RPA was stored at -20 °C in 500 mM KCl in HI-0 with 30% glycerol

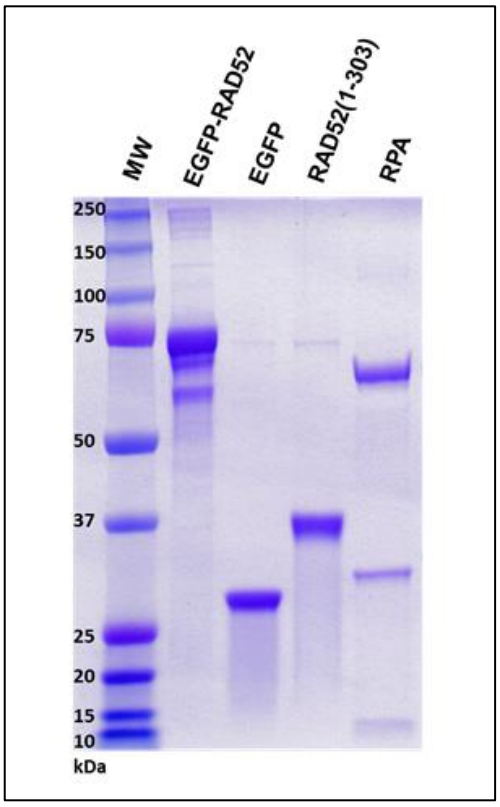
MW
EGFP-RAD52
EGFP
RAD52(1-303)
RPA
250
150
100
75
50
37
25
20
15
10
kDa

Figure 2.2 Proteins used in FluorIA. SDS-PAGE gel of the purified proteins.

The RAD52(1-303) (Figure 2.1B) in pET28b plasmid was a gift from Dr. Min Park. It has a 6xHis tag on the C-terminus that is not cleavable. Transformation was done into Rosetta2(DE3). Expression and growth were the same as described for RPA with the exception of allowing large cultures to cool in an ice bath for 30 min before inducing with IPTG. Cultures were then transferred to a pre-chilled shaker at 18 ºC for 15-18 hours. Pellets were processed in the same manner described above.

A thawed RAD52(1-303) cell pellet was resuspended in 25 mL of buffer A [50 mM Tris-HCl pH 7.8, 300 mM KCl, 2 mM β-mercaptoethanol (β-ME), 10 mM imidazole, and 10% glycerol] with 250 µL of PIC and lysed. Clarified and filtered lysate was then loaded onto a HisTrap FF column (5 mL, GE Life Sciences). The protein eluted with a 25 CV gradient to 1 M imidazole in buffer A. Eluted fractions were pooled and dialyzed against heparin buffer (50 mM Tris-HCl pH 7.5, 200 mM KCl, 2 mM β-ME, 0.5 mM EDTA, and 10% glycerol). The dialyzed protein was loaded onto a HiTrap Heparin HP column (5 mL, GE Life Sciences) and eluted with a 25 CV gradient to 1 M KCl in heparin buffer. The recovered protein was dialyzed overnight into a storage buffer (20 mM HEPES pH 6, 400 mM NaCl, 100 mM KCl, 1 mM EDTA, 2 mM β-ME, and 10% glycerol). The protein was stored frozen with 30% glycerol. A NanoDrop1000 was used to measure concentrations using a molecular weight of 34.6 kDa and ε_{280}=20.4 $M^{-1}cm^{-1}$. Purity of fractions was assessed by SDS-PAGE (Figure 2.2).

Full-length RAD52 tagged with 6X-His enhanced green fluorescent protein (EGFP-RAD52) (Figure 2.1C and Figure 2.3), in pET28a vector was ordered from GenScript with codons optimized for *E. coli* expression and the overall design is described in the

supplement. BL21(DE3) were transformed and selected with kanamycin. Expression, growth, and pellet storage was as described for RAD52(1-303). It is noteworthy that overnight growth at 18 ºC was mandatory for protein expression.

EGFP (MW = 29.1 kDa)

```
MGSSHHHHHH SSGLVPRGSH MVSKGEELFT GVVPILVELD GDVNGHKFSV 50
SGEGEGDATY GKLTLKFICT TGKLPVPWPT LVTTLTYGVQ CFSRYPDHMK 100
QHDFFKSAMP EGYVQERTIF FKDDGNYKTR AEVKFEGDTL VNRIELKGID 150
FKEDGNILGH KLEYNYNSHN VYIMADKQKN GIKVNFKIRH NIEDGSVQLA 200
DHYQQNTPIG DGPVLLPDNH YLSTQSALSK DPNEKRDHMV LLEFVTAAGI 250
TLGMDELYK  259
```

Note, the F64L\S65T EGFP mutations are highlighted in green and the thrombin cleavage site is underlined.

EGFP-RAD52 (MW = 76.2 kDa)

```
MGSSHHHHHH SSGLVPRGSH MVSKGEELFT GVVPILVELD GDVNGHKFSV 50
SGEGEGDATY GKLTLKFICT TGKLPVPWPT LVTTLTYGVQ CFSRYPDHMK 100
QHDFFKSAMP EGYVQERTIF FKDDGNYKTR AEVKFEGDTL VNRIELKGID 150
FKEDGNILGH KLEYNYNSHN VYIMADKQKN GIKVNFKIRH NIEDGSVQLA 200
DHYQQNTPIG DGPVLLPDNH YLSTQSALSK DPNEKRDHMV LLEFVTAAGI 250
TLGMDELYKG GSGGSGGSGG SGGMSGTEEA ILGGRDSHPA AGGGSVLCFG 300
QCQYTAEEYQ AIQKALRQRL GPEYISSRMA GGGQKVCYIE GHRVINLANE 350
MFGYNGWAHS ITQQNVDFVD LNNGKFYVGV CAFVRVQLKD GSYHEDVGYG 400
VSEGLKSKAL SLEKARKEAV TDGLKRALRS FGNALGNCIL DKDYLRSLNK 450
LPRQLPLEVD LTKAKRQDLE PSVEEARYNS CRPNMALGHP QLQQVTSPSR 500
PSHAVIPADQ DCSSRSLSSS AVESEATHQR KLRQKQLQQQ FRERMEKQQV 550
RVSTPSAEKS EAAPPAPPVT HSTPVTVSEP LLEKDFLAGV TQELIKTLED 600
NSEKWAVTPD AGDGVVKPSS RADPAQTSDT LALNNQMVTQ NRTPHSVCHQ 650
KPQAKSGSWD LQTYSADQRT TGNWESHRKS QDMKKRKYDP S  691
```

Figure 2.3 Details of EGFP and EGFP-RAD52 expression plasmids and proteins. All expression plasmids were made by Genscript®. Codons were optimized for expression in *Escherichia coli*. Enhanced green fluorescent protein (EGFP) was cloned into the pET28a plasmid using the NdeI site so that a thrombin cleavable, 6X His tag was placed at the N-terminus. The NT-EGFP-RAD52 was cloned into pET28a in a similar manner. For the later construct a disordered soluble linker was inserted between EGFP and RAD52. Note, the amino acid sequences with a dotted underline are disordered in the EGFP crystal structure (PDB ID 2Y0G). The soluble disordered linker has a double underline and the human RAD52 sequence is highlighted in yellow.

Thawed EGFP-RAD52 cell pellets were resuspended in 25 mL buffer B (50 mM BICINE pH 9, 300 mM KCl, 200 mM NaCl, 10 mM imidazole, 10% glycerol, and 2 mM β-ME) with 250 µL of PIC and lysed. The clarified lysate was loaded onto a HisTrap column and eluted in a 25 CV gradient to 1 M imidazole in buffer B. Keeping the lysate and buffers ice-cold throughout was necessary to prevent the loss of the EGFP tag from the protein. A NanoDrop1000 was used to measure concentrations using a molecular weight of 76 kDa and ε_{280}=63.0 $M^{-1}cm^{-1}$. The protein product was verified by SDS-PAGE gel (Figure 2.2). The protein solution was then mixed with 30% glycerol and stored at -20 ºC. EGFP-RAD52 must be made fresh the week of HTS.

A plasmid of 6xHis-tagged EGFP in pET28a vector was ordered from GenScript with *E. coli* optimized codons and transformed into BL21(DE3) with kanamycin selection. Expression, growth, and pellet storage was as described for RAD52(1-303). EGFP cells were resuspended in 25 mL buffer C (50 mM BICINE; pH 9, 20 mM imidazole, 200 mM NaCl, and 2 mM β-ME) with 50 µL of PIC and lysed. The lysate was loaded onto HisTrap column and eluted with 25 CV gradient up to 500 mM imidazole in buffer C. The tag was removed by thrombin digestion to give pure EGFP (Figure 2.2).

2.3.2. FluorIA procedure. The first step of the FluorIA procedure is to prepare RPA plates (Figure 2.4 top left). Purified RPA, diluted to 0.2 µM with milli-Q water, is dispensed by Multidrop Combi (ThermoScientific) to uniformly fill each well of a 384-well, high-binding, “MaxiSorp”, black Plastic, flat bottom, opaque microtiter plate (Thermo Fisher Scientific, #460518) to 75 µL volume. Centrifugation at 500 xg for a few seconds prevents air bubble formation and evenly coats the well. Plates are then

incubated on an orbital shaker for 1 hour at room temperature, then excess protein solution is decanted by flicking plates upside down several times and striking repeatedly against a pad of paper toweling to remove residual liquid. Unbound RPA is removed by two washes, 85 µL per well, using wash buffer (1X PBS with 0.2% Tween-20) with elimination of residual liquid after each washing step as described above. Freezing-blocking buffer (5% milk in 1X PBS with 30% glycerol) is then dispensed at 85 µL per well and plates briefly centrifuged. Following a 10 min room temperature incubation on an orbital shaker, each plate is sealed with an aluminum adhesive sheet (Thermo Scientific, Cat. # AB-0626) and stored in the -20 ºC freezer until use. Typically, we can make 60 to 80 RPA plates per day.

On a screening day, the desired number of RPA plates are thawed for 1 hour at room temperature. Then the aluminum seal is removed, and the freezing-blocking buffer decanted. The plates are washed once and decanted. Two protein mixtures are prepared on the day of the screen: mixture-A is 1.33 µM RAD52(1-303) with 2.67 µM EGFP-RAD52 in 1xPBS-5% milk, and mixture-B is 2.67 µM EGFP-RAD52 alone in 1xPBS-5% milk. In the optimized protocol 75 µL of each protein mixture is used per well. Mixture-A is dispensed into one column per plate to serve as a positive control (known inhibitor, Figure 2.4, column 21) while mixture-B is dispensed into all wells that receive a test compound from the chemical library or buffer only control. A column is reserved for 1xPBS-5%-milk as a buffer blank (Figure 2.4, column 22). At this point, the RPA plates are ready to receive compounds from a chemical library. A Biomek F/X liquid handler (Beckman Coulter LifeSciences) automated the transfer of test compounds from a chemical library source plate into the wells of a RPA plate. After test compound

addition, RPA plates are centrifuged at 500 xg for a few seconds. The plates are covered with aluminum foil and placed on an orbital shaker for 1 hour at room temperature. Then three washes are performed to remove unbound chemicals and excess protein before the relative fluorescence (RFU) is measured using a POLARstar OPTIMA plate reader (BMG LABTECH) on emptied plates at an excitation/emission (for EGFP) of 485/520 nm at 2500 gain setting. Plates must be read decanted as reading them with liquid present increased variation in the data.

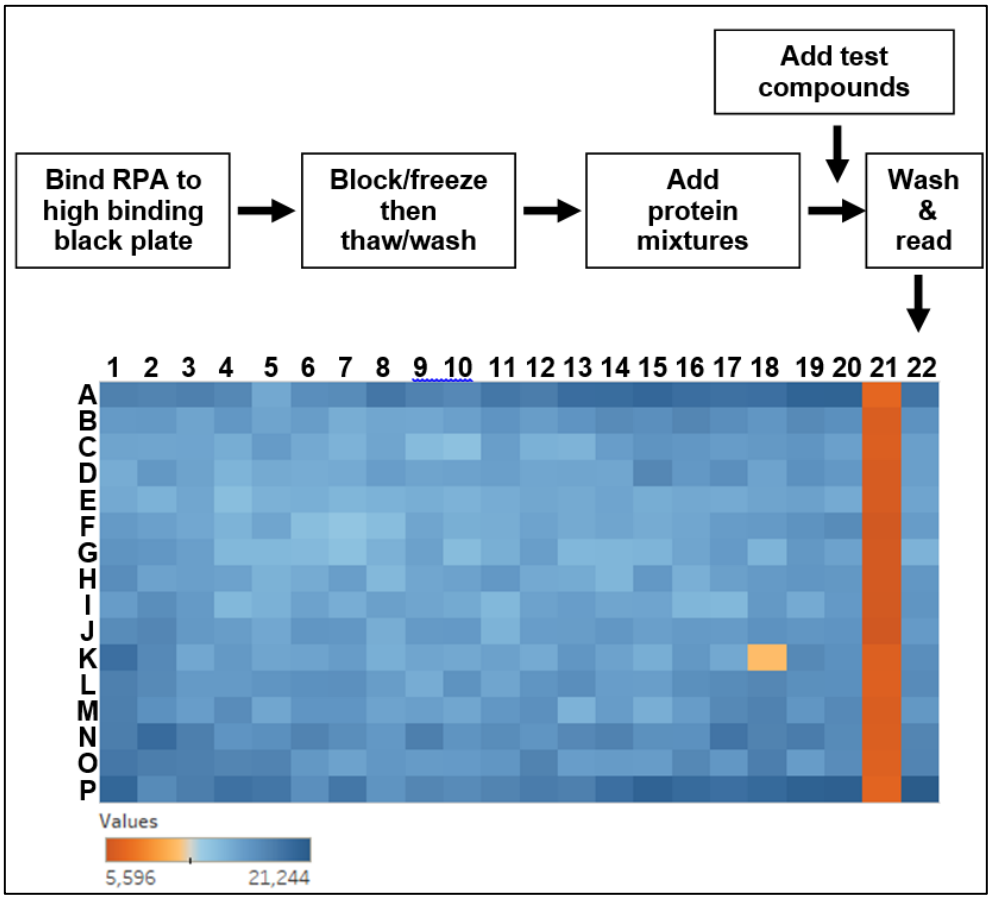
Add test compounds
Bind RPA to high binding black plate
Block/freeze then thaw/wash
Add protein mixtures
Wash & read
1 2 3 4 5 6 7 8 9 10 11 12 13 14 15 16 17 18 19 20 21 22
A B C D E F G H I J K L M N O P
Values
5,596
21,244

Figure 2.4 HTS FluorIA procedure diagram and representative data. Columns 1-20 are the screen of a chemical library. Column 21 is inhibited with RAD52(1-303) control and column 22 is buffer control. Column 21 is the PC and column 22 is the NC in wquation 2. Well K18 is a hit.

2.3.3. Strategy for screening libraries of compounds. For large library screening, a single concentration is used (e.g. 100 μM). Plates are repeated to eliminate false hits. Then triplicate repeats further verify hits. With this strategy, it is possible to screen up to 10,000 compounds per day with two workers.

2.3.4. Statistical analysis. A screening window coefficient (denoted Z-factor) is used to assess the quality of the signal throughout screen optimization and application.

$$Z = 1 - \frac{3SD \text{ of sample} + 3 \text{ SD of control}}{|\text{mean of sample} - \text{mean of control}|} \quad (1)$$

Here, the assay value in the absence of potential inhibitor is the "sample" while the "control" is the value in the presence of the known competitive inhibitor RAD52(1-303). In some early pilot assays EGFP was the control. If $1 > Z \geq 0.5$ then the separation band between the sample and control is large enough and the assay is considered excellent.

Candidate SMI hits are identified as follows: On each screening plate, the average value of a designated column containing no potential inhibitors and buffer only is a negative control (NC). The average value of a column containing the known inhibitor RAD52(1-303), is the positive control (PC). Then

$$Xhit = \left(NC - \frac{NC - PC}{2}\right) 100 \quad (2)$$

A SMI is considered a hit if Xhit is 50% or lower (Figure 2.4, shown as light orange in well K18). A value of 50% is used for this example because the RAD52:RPA PPI under study probably involves two binding surfaces and a hit might bind to only half of the uncharacterized surface. The hits are also three standard deviations below the NC.

2.4. Results and discussion

Previously, we used an ELISA-based method that required antibodies and chemiluminescence for detection to analyze the domains of RPA interaction on RAD52 and vice versa.[103]. This method worked well for biochemical type assays but is too cumbersome, expensive, and uses far too many wash steps to be practical for HTS. The FluorIA is a new approach that obviates the need for antibodies, thus avoiding problems of non-specificity, and detects PPI simply with purified proteins with a minimal number of steps and low cost. Here, purified RPA is directly bound to a black, high-binding microtiter plate and the PPI detected with RAD52 tagged with EGFP (Figure 2.1C and Figure 2.3). An increased relative fluorescent unit (RFU) is detected when EGFP-RAD52 is added to RPA (Figure 2.5). A similar response is not detected with the EGFP tag alone indicating the interaction is between RPA and RAD52 not between RPA and the EGFP tag. Z-factor analysis with EGFP tag as a control helped us select minimal protein levels that gave an optimal response (Figure 2.5). The best Z-factor value along with lower variation in replicates was obtained for 20 pmol of EGFP-RAD52 per well added to 10 pmol of RPA. Despite higher signal value with 40 pmol EGFP-RAD52, we use 20 pmol concentration for HTS as it gives a consistently good Z-score in repeats and meets the goal of lowering the cost of reagents. We tested pilot assays with 25 µL/well or 75 µL/ well reaction (data not shown). A 75 µL volume gives the best signal as it filled the small 384-well without overflowing and allowed RPA to bind the flat bottom as well as the walls of the well for increased signal. As optimization progressed, we increased the amount of RPA to 15 pmol to ensure sufficient RPA per well after multiple washing and handling procedures.

Excellent Z-factors greater than 0.5 are obtained in the FluorIA mainly due to the low standard deviation of the screen and large difference between PC and NC.

Temperature is another factor to consider. To see the effect of temperature, two plates were incubated at 22 °C and 28 °C individually (Figure 2.6). The results suggest that it is best to perform the screen at room temperature and to watch the thermostat. Higher temperature fluctuations probably result in detachment of the bound RPA from the wells resulting in lower signal. Therefore, the FluorIA is conveniently conducted at room temperature.

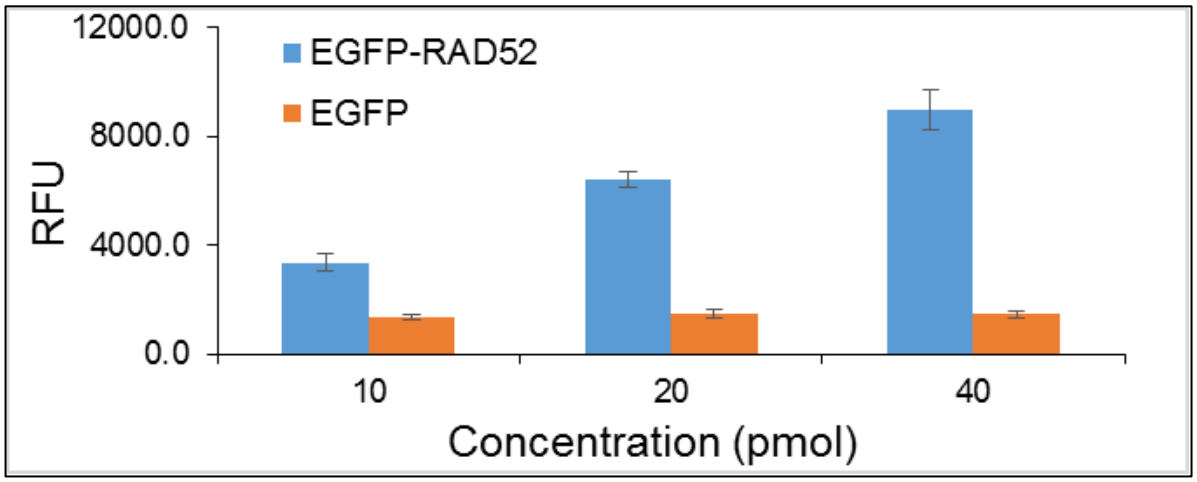
12000.0
8000.0
4000.0
0.0
RFU
EGFP-RAD52
EGFP
10
20
40
Concentration (pmol)

Figure 2.5 Optimization of protein levels per well. Z-factors were 0.39, 0.73 and 0.66 for 10, 20, and 40 pmol respectively.

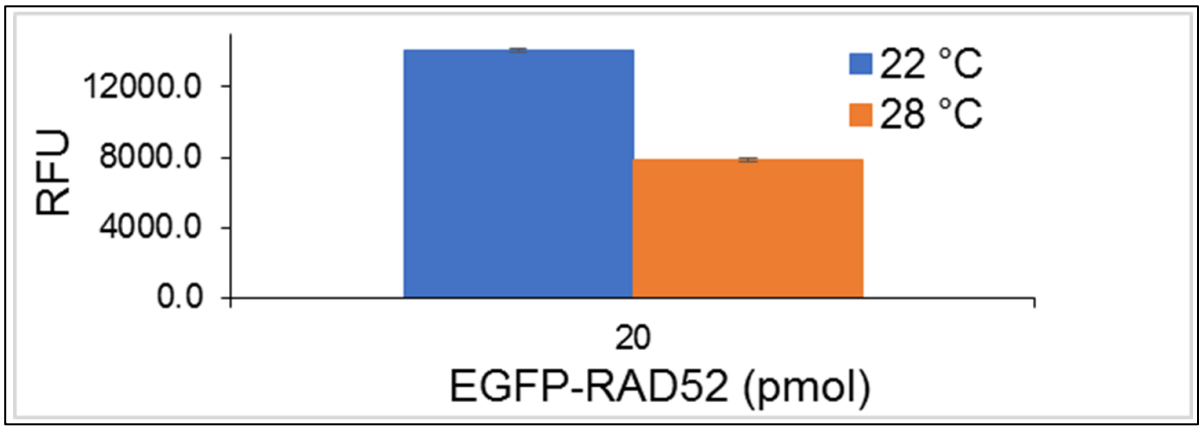
22 °C
28 °C
RFU
12000.0
8000.0
4000.0
0.0
20
EGFP-RAD52 (pmol)

Figure 2.6 The effect of temperature on FluorIA. The reaction was done at 22 ºC and 28 ºC.

Further development of the assay required the use of a robust known inhibitor for the statistical analysis of each plate and hit identification. Previous work by our group shows that RAD52:RPA electrostatic interaction can be disrupted by increased salt concentration.[103] Therefore, we diluted the EGFP-RAD52 with a range of 0-1 M KCl before adding it to the RPA plate. Consistent with our previous findings, inhibition was evident by a progressive decrease in fluorescence signal with increased salt concentration (Figure 2.7A). However, it was evident that a much larger salt concentration was required to achieve the desired baseline inhibition. The possibility of salt interfering with the chemical libraries motivated us to search for an alternative inhibitor.

Previously, we demonstrated that the primary interaction sites for RPA on RAD52 are within residues 193-303 [103]. Also RAD52(1-303), which has intact RPA binding domains but is missing the remaining 115 residues at the C-terminus, exhibits a slightly higher RPA binding activity compared to full length RAD52 [103]. Interestingly, Plate and coworkers reported an enhanced repair activity for a yeast Rad52(1-307) construct compared to full-length Rad52 [78]. Accordingly, RAD52(1-303) inhibits the FluorIA by competing with EGFP-RAD52 for RPA binding. In a pilot screen, 20 pmol of EGFP-RAD52 was incubated with increasing concentrations of RAD52(1-303) in the RPA plate (Figure 2.7B). At a molar ratio of 1:1, 50% inhibition is observed and with increased concentration of RAD52(1-303), baseline inhibition is achieved. Therefore, 100 pmol of RAD52(1-303) is used as a known inhibitor (positive control) in the FluorIA.

At this juncture, it was necessary to assess the resilience of the FluorIA readout signal with the added challenges of a HTS. Typically, compounds in chemical libraries are dissolved in 100% DMSO and that could be detrimental to the integrity of purified proteins,

the main components of the FluorIA. We plan to limit the final concentration of DMSO to no more than 5% per reaction well in HTS. To see any effects, different amounts of DMSO were added with EGFP-RAD52 before incubating in the RPA plates (Figure 2.8). Fortunately, up to 5% DMSO has no significant effect on the FluorIA signal.

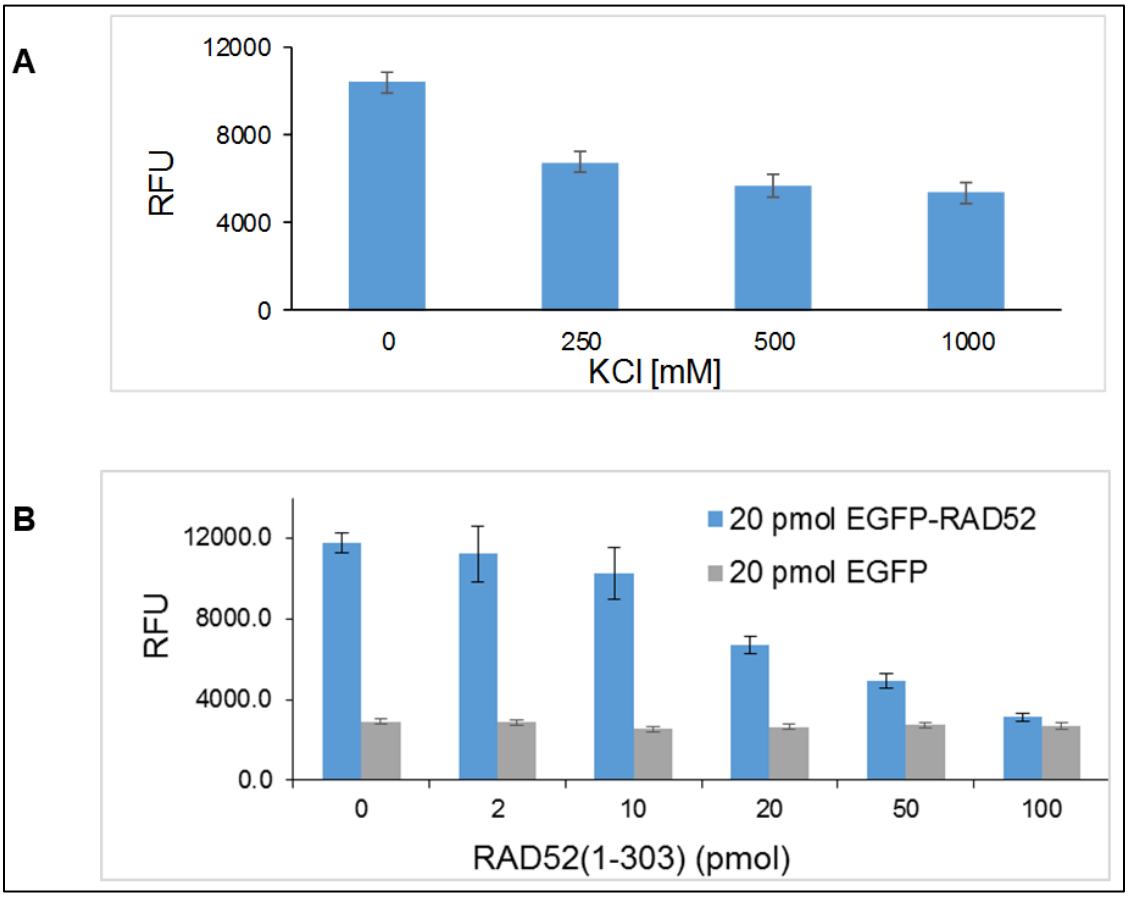
A
12000
8000
4000
0
RFU
0
250
500
1000
KCl [mM]
B
20 pmol EGFP-RAD52
20 pmol EGFP
12000.0
8000.0
4000.0
0.0
RFU
0
2
10
20
50
100
RAD52(1-303) (pmol)

Figure 2.7 Known inhibitor. Finding suitable competitive inhibitors to serve as control (A) KCl or (B) RAD52(1-303).

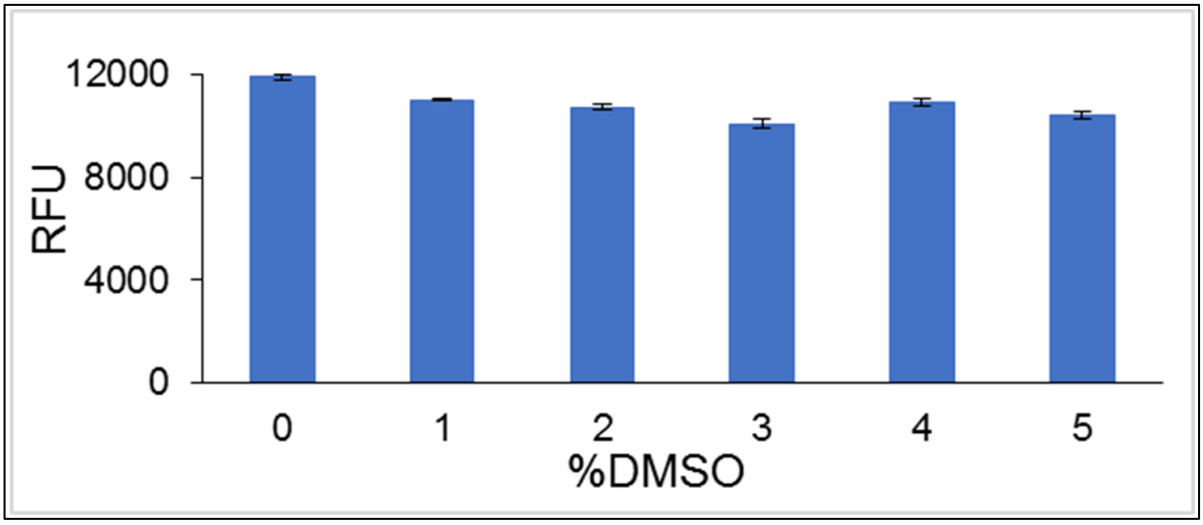
12000
8000
4000
0
RFU
0
1
2
3
4
5
%DMSO

Figure 2.8 Testing the effect of DMSO. DMSO was added up to 5% in the FluorIA reaction.

The parameters defined above provide the essentials for an HTS assay, namely, sensitivity, reliability, and homogeneity. Subsequent work creates a successful process for screening large libraries with minimum time and maximum cost efficiency. Assay steps need to be minimized and automated for simplicity and speed. The storage of assay plates over various times and to optimize proper storage conditions was addressed. Once the storage condition in 30% glycerol at the blocking step was found to be optimal, three different RPA plates were tested after freezing overnight to assess plate-to-plate variability (Figure 2.9A). As no difference was detected, we conducted the freezing test for up to two weeks and freezing did not lead to change in signal output (Figure 2.9B). Thus, making the RPA plates ahead of time and freezing them provides a convenient stopping place in the FluorIA protocol. Also, having the RPA incubation, washing, and blocking steps done ahead significantly mitigates the number of steps to be done on the day of HTS, reduces the risk of costly errors and allows for screening of several thousand chemicals a day. The case is not the same with EGFP-RAD52. The EGFP signal diminishes with time stored (Figure 2.9C). EGFP-RAD52 must be freshly purified the week of the screen. On a HTS day, it is critical to perform a test plate of all proteins and buffers to test activity and Z-factor before committing to a long day of screening.

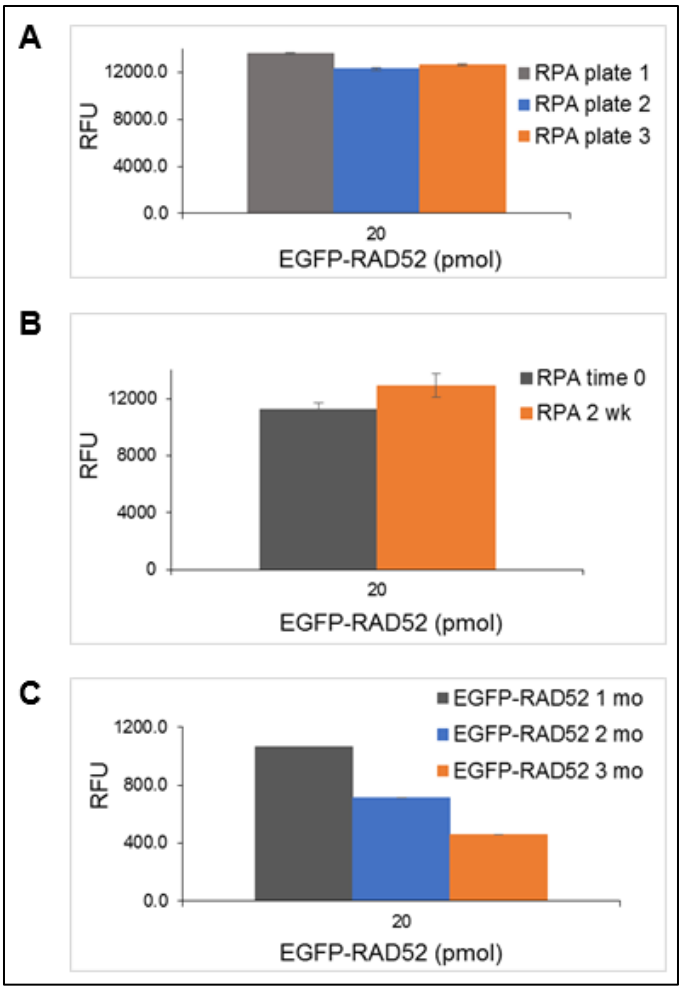
A
12000.0
8000.0
4000.0
0.0
RFU
20
EGFP-RAD52 (pmol)
RPA plate 1
RPA plate 2
RPA plate 3
B
12000
8000
4000
0
RFU
20
EGFP-RAD52 (pmol)
RPA time 0
RPA 2 wk
C
1200.0
800.0
400.0
0.0
RFU
20
EGFP-RAD52 (pmol)
EGFP-RAD52 1 mo
EGFP-RAD52 2 mo
EGFP-RAD52 3 mo

Figure 2.9 Reagent shelf life. (A) RPA plate variation with three different RPA assay plates prepared, sealed and frozen overnight. (B) Effect of short term freezing on RPA plates. (C) Effect of freezing on purified EGFP-RAD52 signal. For part C, nonbinding plates and gain setting of 1000 was used.

The final optimized parameter is the buffer system. For most of the pilot optimization screens, an EDTA-containing buffer system was used. By exploring other buffer systems we found that 1x PBS gives a larger change between positive and negative controls contributing to the statistical quality of the assay (Figure 2.10).

PPIs are important in biological processes as well as pathology. Here we demonstrate how the simple FluorIA protocol can be used to find SMIs that disrupt the RAD52:RPA interaction. Future HTS of SMI libraries will follow the full FluorIA optimization described here. The well-coordinated flow of the FluorIA and analysis makes it possible to screen up to 10,000 compounds per day. FluorIA is applicable to PPI where the purified protein maintains activity. FluorIA is not restricted to screening SMIs and is suitable to test aptamers as well.

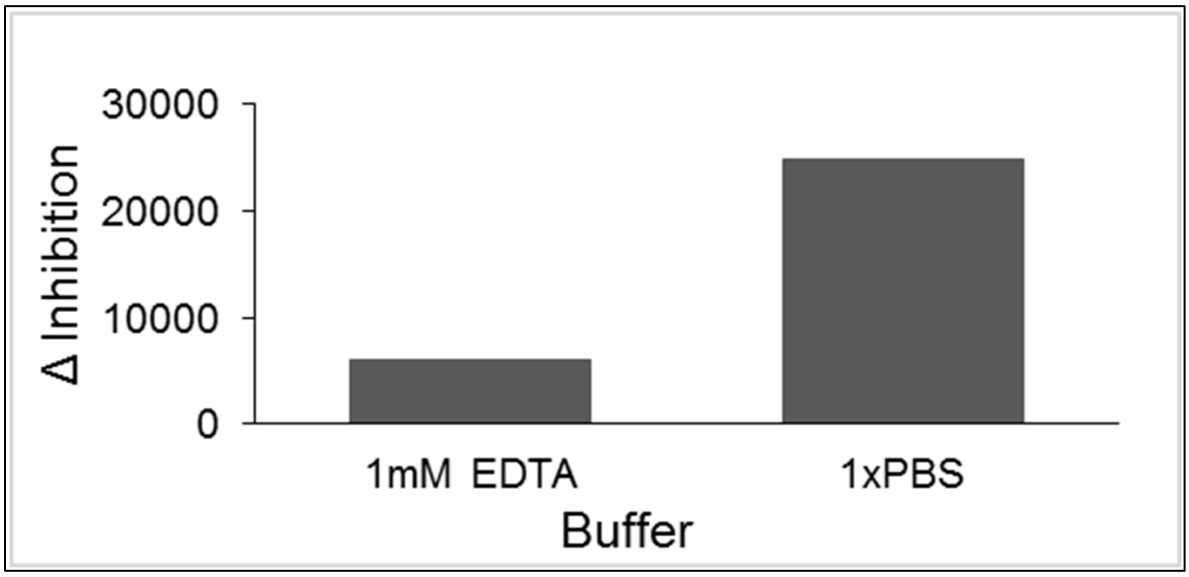
30000
20000
10000
0
Δ Inhibition
1mM EDTA
1xPBS
Buffer

Figure 2.10 Optimal buffer choice. Testing EDTA and 1x PBS buffers in FluorIA.

2.5. Conclusion

PPI take central importance in biological processes and their pathological changes. Early developments of HTS were based on targets other than PPI. We now realize that modulating PPI with small molecule is not only possible but advantageous in the quest of targeted therapeutics.

We developed FluorIA to find SMIs that can disrupt RAD52:RPA interaction. Following full optimization, we were able to do an unbiased screen of three large libraries of potential SMIs. The flow of the HTS and analysis was well coordinated, and it was possible to screen up to 10, 000 compounds per a screen day.

Chapter 3
Characterizing the RAD52:RPA complex

3.1. Abstract

RAD52 interaction with RPA constitutes a crucial step in its known and newly emerging roles in DNA damage repair. RPA's main function in the cell is to protect ssDNA strands and relax DNA secondary structures during the process of normal DNA replication or repair. RAD52 plays a role in repair processes such as HRR, SSA, or break-induced repair processes, RAD52 requires direct interaction with the RPA occupying the ssDNA at the damage site for activity. Recently, there is an increased appreciation for RAD52's role in the maintenance of tumorigenesis. The molecular and dynamic details of RAD52:RPA interaction are of great interest with increasing efforts to target RAD52 DNA repair activity to kill tumor cells. Here we use the FluorIA we developed along with kinetic and thermodynamic measurements to investigate the RAD52:RPA interacting. The interaction of RPA with RAD52 has dissociation constant of 0.1 μM and the interaction appears strong enough to be physiologically relevant and has the potential to be a therapeutic target.

3.2. Introduction

HRR is one of five major DNA repair pathways that make it possible for cells to combat DNA lesions encountered during the course of replication [104]. HRR is a specialized and accurate repair for DNA DSBs, a type of DNA damage that is of a particular significance in cancer [105]. Not surprisingly, PPIs in this repair pathway are of central importance in tumorigenesis development and potential candidates in targeted therapy [106, 107].

RPA is a heterotrimer composed of three subunits and binds ssDNA intermediates of DNA metabolism and repair processes [77, 108]. The dynamic nature of this binding

stretches beyond protection into specific and essential interaction with protein partners to ensure the efficiency of these processes [109]. RAD52 is an important protein partners that functions in HRR, SSA, BIR, RNA-templated DSBs repair [57, 66, 75]. With RPA being an early responder, when RAD52 seek to repair damaged DNA, RPA had already proceeded to the site making this PPI crucial in initiating the repair processes. RPA interaction is reported to either dictate or stimulate RAD52 repair activity. Plate and co-workers demonstrated that there is a requirement for direct interaction with RPA for Rad52 to carry out its role in HR repair [78]. Moreover, in the newly characterized role for RAD52 in RNA-templated DSBs repair, the addition of RPA to the reaction clearly stimulated the repair activity [72].

RAD52 and RPA proteins received great interest from researchers due to their significant roles in normal and pathological processes. Flexible linkers connecting the three subunits of RPA hindered efforts for a full structural view of the protein [110-116], while RAD52 was revealed as a ring structure using electron microscopy and X-ray crystallography [117-120]. The RAD52 ring was predicted by Singleton to provide a positively charged groove as a binding pocket for ssDNA [120]. This structural knowledge along with emerging understanding of RAD52 role in tumorigenesis, motivated the search for therapeutic agents that can disrupt the RAD52 ring to target its activity [62, 74]. Our past data showed that conformational changes offered by RPA interaction dictate the activity of RAD52 in DNA repair. Namely, we found that in the absence of RPA, RAD52 existed in rings and aggregates of rings. However, monomer RAD52 purified in a stable complex with RPA-ssDNA. Additionally, we found that RPA alone was capable of promoting the breakage of the RAD52 ring structure. These

findings motivated our interest in the RAD52 monomers as the potential active form in DNA repair [79, 103].

Here, we aim to characterize the RAD52:RPA complex and validate its candidacy for targeted therapeutics. FluorIA, was used to delineate the RPA-binding domains on RAD52. Using the same method, the RAD52 interaction surface on RPA, based on previously reported NMR data, was investigated [121]. SPR was then utilized to study the affinity of RPA interaction with full-length and truncated mutants of RAD52. Finally, ITC analysis was used to validate our SPR findings for the full-length proteins.

3.3. Materials and methods

3.3.1. Proteins purification.

RPA purification was done as described in Chapter 2. To make the ssDNA:RPA complex, RPA was mixed with an excess molar concentration of a 25-mer oligonucleotide (GCTAGCTCAATTCATCGACAAACCTT) (1:1.1 ratio) that was synthesized and reconstituted as described by Deng and coworkers [79]. The complex was incubated on ice for one hour before purification using size exclusion column (see above) with 300 mM KCl in HI-0 buffer described in Chapter 2. Fractions containing the complex were selected guided by the 260/280 ratio read by NanoDrop1000 and purity of the sample as judged by SDS-PAGE (Figure 3.1A).

The 6xHis-tagged RPA was expressed using the pET-Duet system. The plasmids were made by GenScript with codons optimized for *E.coli*. RPA70 was cloned into multiple cloning site 2 (MCS2) of pCOLA Duet-1 with kanamycin resistance. His-RPA14 and RPA32 were cloned into MCS1 and MCS2, respectively, in pACYC Duet-1

plasmid with chloramphenicol resistance. These were transformed into BL21(DE3) *E.coli* with chloramphenicol and kanamycin selection. The expression procedure was as described for RPA in Chapter 2. A 5 g cell pelleted His-tagged RPA was resuspended in 25 mL of buffer A with 250 µL of PIC and lysed. Clarified and filtered lysate was then loaded onto a HisTrap FF column (5 mL, GE Life Sciences). The protein eluted with a 25 CV gradient to 1 M imidazole in buffer A. The purity of the protein fractions were examined by 10% SDS-PAGE (Figure 3.1B).

6xHis tagged RPA32(172-270), also known as the winged-helix-loop-helix region (wHLH) (MW 9.4kDa), a generous gift from Dr. Marc Wold and was transformed into Rosetta2(DE3) with chloramphenicol and kanamycin selection. Protein expression was as described for RPA in Chapter 2. For purification, a RPA32(172-270) pellet was thawed and resuspended in buffer D [10 mM $NaPO_4$ pH 7.5, 150 mM NaCl, 10 mM imidazole, and 2 mM β-ME] with 250 µL of PIC and lysed. Clarified lysate was filtered through a 0.45 µM filter then loaded onto a His Trap FF column (1 mL, GE Life Sciences). The protein eluted with a 25 CV gradient to 1 M imidazole in buffer E. Pooled fractions were diluted with 4 volumes of buffer F [20 mM $NaPO_4$, pH 7.5, 50 mM NaCl, 2 mM β-mercaptoethanol (β-ME), 0.5 mM EDTA] and polished using a monoQ anion exchange column (1 mL, GE Life Sciences # 17-5166-01). The protein was eluted in a 25 CV gradient of 0-100% 1 M KCl in buffer F. Since 6xHis-RPA32(172-270) has no tryptophan, a UV absorbance at 210 nanometers was necessary for detection of protein fractions. Fractions were also examined by 12% SDS-PAGE (Figure 3.1C). The bicinchoninic acid assay (BCA assay) was used to measure protein concentration.

The His-tag was removed from a portion of the purified wHLH by thrombin digestion (10 U/mg tagged protein) to use it in SPR as an analyte over RAD52-bound to NTA chip. Thrombin, loose His tags, and still-tagged protein were removed from the digestion mixture by adding benzamidine resin (removes thrombin) and nickel resin (removes His). Tagged and detagged wHLH were examined by 12% SDS-PAGE (Figure 3.1C).

RAD52(1-418), RAD52(1-303), and RAD52(1-212) all in in pET28, were transformed into Rosetta2(DE3) *E.coli* with chloramphenicol and kanamycin selection. RAD52 (168-306) and EGFP-RAD52(1-212) in pET28a (GenScript) were transformation in BL21(DE3) *E.coli* with kanamycin selection. Expression and purification for all these RAD52 constructs was done in the same manner described for RAD52(1-303) in Chapter 2. Purification of, RAD52 (168-306) and EGFP-RAD52(1-212) expression and purification included an additional size exclusion (Superdex 200, HiLoad 16/60, GE Life Sciences) purification step preceded by an overnight dialysis into a high-salt buffer (20 mM HEPES pH 7.5, 400 mM NaCl, 100 mM KCl, 1 mM EDTA, 2 mM β-ME, and 10% glycerol). RAD52 (168-306) sequence contains no tryptophan so a UV absorbance at 210 nm was necessary for detection of protein fractions during purification. Fractions were examined by 10% SDS-PAGE with Coomassie stain (Figure 3.2). The RAD52(257-274) peptide was purchased (GenScript). Peptides was diluted to 10 mM in nuclease-free water and stored frozen at -20 °C

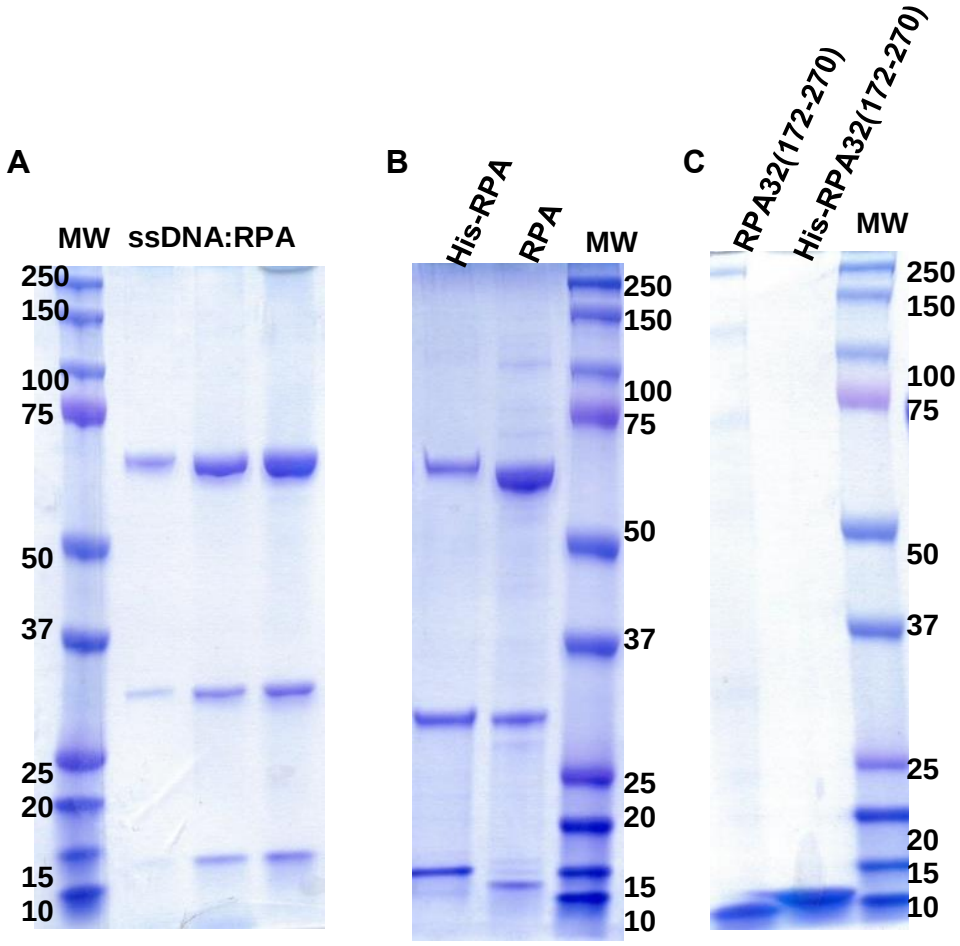
A
MW
ssDNA:RPA
250
150
100
75
50
37
25
20
15
10
B
His-RPA
RPA
MW
250
150
100
75
50
37
25
20
15
10
C
RPA32(172-270)
His-RPA32(172-270)
MW
250
150
100
75
50
37
25
20
15
10

Figure 3.1 Purified proteins in SDS PAGE gels. (A) Fractions of ssDNA: RPA, (B) 6xHis- tagged on RPA14 subunit next to untagged RPA14, (C) RPA32(172-270) with or without 6xHis tag

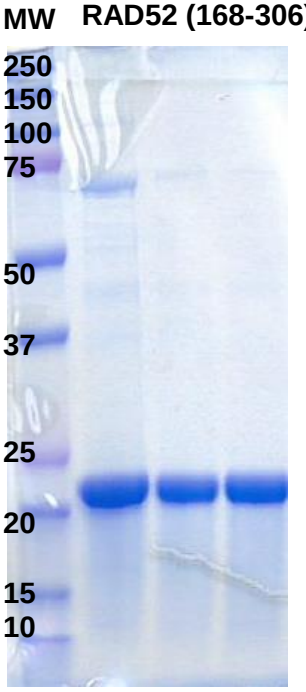
MW
RAD52 (168-306)
250
150
100
75
50
37
25
20
15
10

Figure 3.2 SDS PAGE gels shown His-RAD52(168-306).

3.3.2 Isothermal titration calorimetry procedure and sample preparation. ITC titrations were performed on an iTC200 (Malvern Instruments Inc. Northampton, MA). A total of 15 injections of RPA with concentration 150-300 µM were performed into a 0.2 mL reaction cell containing a solution of RAD52 with concentration about ten times smaller than the titrant. The total injection volume was 37 µL with individual injection of 2 or 3 µL. All experiments were carried out at room temperature and mixing rate 1000 rpm. Reaction heats were measured by integration of the area of the injection curve, corrected for the dilution heat of the titrant, and normalized by the moles of titrant added. Experiments with a low range of RPA concentrations (150-170 µM) were performed to measure the heat of reaction directly in initial steps of the titration. The average of 4-5 injections at concentrations less than saturation provides the reaction enthalpy, ΔH_{ITC}. The resultant thermograms were analyzed using single set of binding sites model of the MicroCal LLC software based on the Levenberg-Marquardt non-linear least square curve fitting algorithm to provide binding affinity, binding stoichiometry and enthalpy of binding ($\Delta H°$). The binding free energy ($\Delta G°$) and the entropic contribution to binding were then calculated using standard thermodynamic relationships.

Purified RPA and RAD52 were first concentrated separately using spin concentrators (30,000 and 3,000 MWCO respectively). RPA and RAD52 were then dialyzed separately against 1x PBS buffer with 1 mM EDTA and 2 mM βME overnight followed by a second round the next day for a minimum of three hours. Concentrations of the proteins were checked before and after dialysis using a NanoDrop1000 applying ε_{280}=87.2 $M^{-1}cm^{-1}$ for RPA and ε_{280}= 20.4 $M^{-1}cm^{-1}$ for RAD52.

3.3.5. Surface plasmon resonance analysis. OpenSPR instrument (Nicoya Lifesciences,) as well as Biacore 3000 (Biacore AB, Uppsala, Sweden) were used. OpenSPR utilizes gold nanoparticles instead of traditional gold SPR films for the sensor chip. Also the OpenSPR instrument uses LSPR that differs from traditional SPR in that it employs readings of absorption of the sensor substrate chip.

For the OpenSPR analyses, sensor chips (SEN-Au-100-12-NTA) was installed and Nickel labeled according to manufacturer's recommendations. Based on experimental pilot tests, 25-50 μg/mL of the His-tagged ligand could be bound on a chip. When the ligand was a RAD52 construct, we used the HBS-PE running buffer [10 mM HEPES pH 7.4, 150 mM NaCl, 3.4 mM EDTA, and 0.005% Tween20] at a higher salt concentration of (500 mM NaCl) to ensure best binding and activity. To analyze multiple analyte concentrations, multiple two or three-fold dilutions were made typically: 900, 300, 100, 33, and 11 nM along with a zero (HBS-PE buffer only) condition. HBS-PE buffer at 150 mM NaCl buffer was used as the running buffer in the system throughout the analyte binding and regeneration processes. The salt concentration of 150 mM for ligand-analyte binding was based on our previous work in making the RAD52:RPA complex [79]. Resulting data were processed using TraceDrawer software provided by Nicoya. Each experiment was repeated several times and repeats with the best fit Chi^2 value were selected for average, standard deviation and variance calculations.

Interaction analyses of full-length RPA and RAD52 were also done using a Biacore. For this kinetic analysis, amine coupling with a CM5 sensor chip was performed. RAD52 was chosen to be the ligand to bind the carboxymethyl groups containing CM5 chip while RPA was flowed over as the analyte.

A 20 mM MES buffer (pH 5.5) was chosen for immobilization of ligand while 1x PBS containing 0.005% Tween was used for running the analyte. Then 10 mM glycine/NaOH (pH 10) was used for regeneration. The CM5 used chip used preconditioned with two short pulses of 50 mM NaOH, 100 mM HCl and 0.5% SDS. To prepare for ligand binding, individual ligand flow channels were activated with a mixture of 1-ethyl-3-[3-dimethylaminopropyl carbodiimide hydrochloride) (0.2 M) and sulfo-*N*-hydroxysuccinimide (0.05 M). RAD52 (5-20 μg/mL) was prepared for immobilization in 20 mM MES buffer (pH 5.5). Ethanolamine-HCl was used to block the remaining excess ester groups. The immobilization process resulted in the coupling of RAD52 at a density of 1200 RUs (an arbitrary response unit which corresponds to 1 pg/mm^2).

Analyte buffer replaced the immobilization buffer and a series of RPA dilutions were prepared for programed injections over the chip. Activation, regeneration, and blocking solutions were provided by BIAcore. All data were collected at 25 ºC and evaluated using BIAevaluation software (version 3.0). Out of the several experimental repeats, two are selected for their lowest Chi^2 values of 2.1 and 6.6.

3.4. Results and discussion

3.4.1. Analysis of reported RPA-binding domains on RAD52. Min Park used GST-pull down studies to identify that the RAD52 region which mediates RPA interaction was located within the basic region composed of residues 221 to 280 [122]. Plate and colleagues used yeast Rad52 in a series of mutational and biochemical studies to identify that RPA is able to interact with Rad52(169-260) (yeast Rad52 numbering) [78]. None of the studies mentioned above or others can exclude the possibility for the existence of additional RPA-interaction domains on RAD52.

Previously, our group estimated that the interaction site for RPA is within the RAD52 region encompassing residues 193-303 by ELISA analysis using different RAD52 constructs and RPA domains [103]. Interestingly, RAD52(1-303) and RAD52(218-418) showed slightly higher binding activity than full-length RAD52 [103]. These results lead our curiosity to find out if this binding activity is due to an additional RPA binding site in the N-terminus besides the known binding domain in the C-terminus (residues 221 to 280).

We used FluorIA to analyze the competitive binding capacity of RAD52(1-303) and RAD52(1-212) versus EGFP-RAD52. 20 pmol of full length EGFP-RAD52 was mixed with 100 pmol of either RAD52(1-303) or RAD52(1-212) to incubate with RPA. The results shown in Figure 3.3 suggest that the RAD52(1-212) can compete for RPA binding with full length EGFP-RAD52 albeit less strongly than observed with RAD52(1-303). To explore this further, we tested direct interaction of RPA with EGFP-RAD52(1-212) and the results depicted in Figure 3.4 suggest binding activity to RPA.

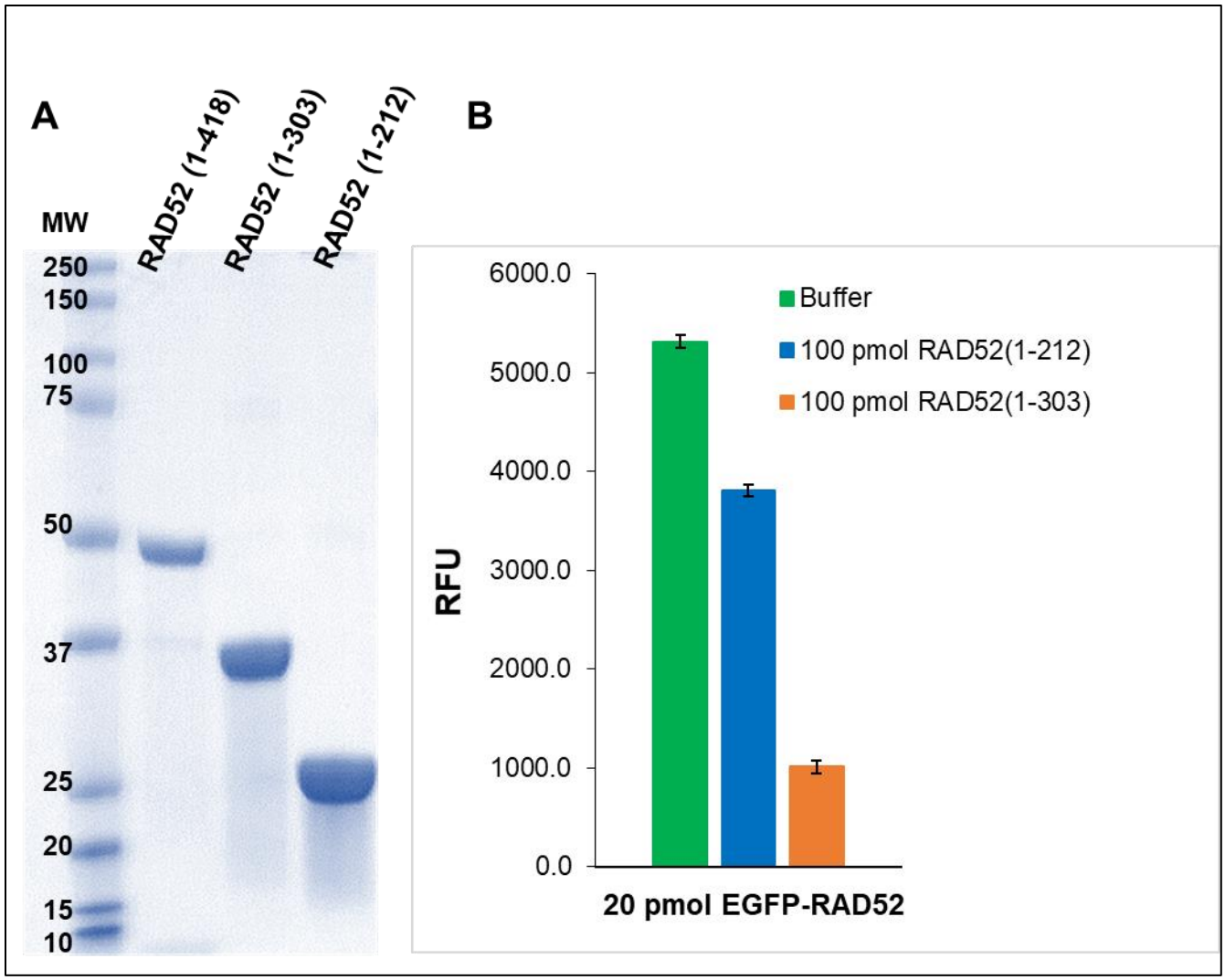
A
RAD52 (1-418)
RAD52 (1-303)
RAD52 (1-212)
MW
250
150
100
75
50
37
25
20
15
10
B
6000.0
5000.0
4000.0
3000.0
2000.0
1000.0
0.0
RFU
Buffer
100 pmol RAD52(1-212)
100 pmol RAD52(1-303)
20 pmol EGFP-RAD52

Figure 3.3 Competitive binding in FluorIA. A) SDS-PAGE gel shown full-length RAD52(1-418) to the left of the molecular weight marker, RAD52(1-303), and RAD52(1-212). B) FluorIA reaction in which 20 pmol of EGFP tagged full-length RAD52 is incubated with RPA alone or with a 100 pmol of unlabeled RAD52(1-303) or (1-212) to compete with EGFP-RAD52 for RPA binding. Reduction in RFU signal signifies more binding activity of the unlabeled RAD52 construct.

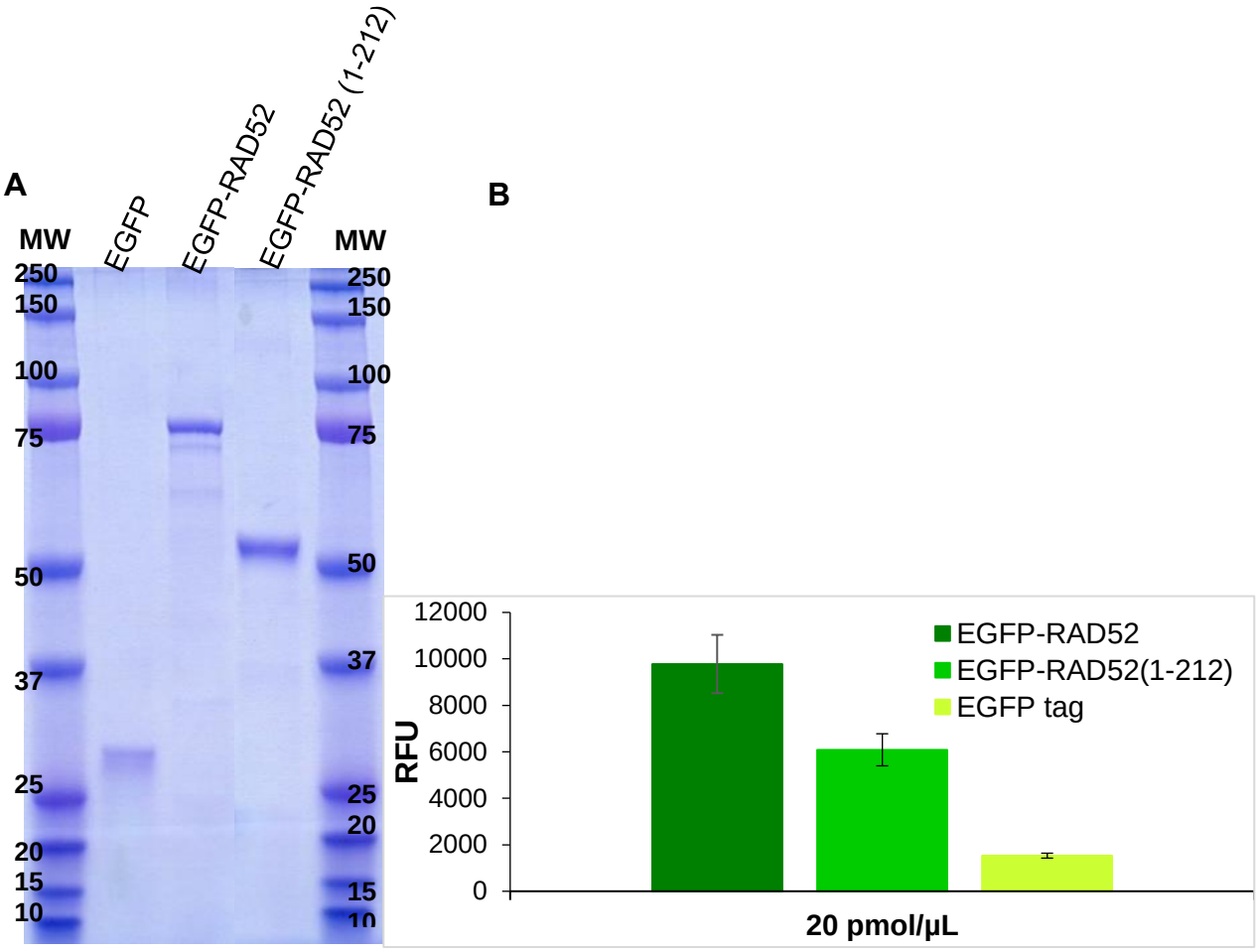
A
MW
EGFP
EGFP-RAD52
EGFP-RAD52 (1-212)
MW
250
150
100
75
50
37
25
20
15
10
B
RFU
12000
10000
8000
6000
4000
2000
0
EGFP-RAD52
EGFP-RAD52(1-212)
EGFP tag
20 pmol/µL

Figure 3.4 RAD52(1-212) binding to RPA. A) SDS-PAGE gel shown left to right, EGFP-tag, N-terminal EGFP-tagged full-length RAD52(1-418), and N-terminal EGFP-tagged RAD52(1-212). B) FluorIA reaction in which 20 pmol of EGFP tagged full-length RAD52, EGFPRAD52(1-212), or EGFP tag are incubated with RPA. Decreasing RFU signal signifies less binding activity as guided by baseline signal of EGFP tag alone with RPA.

Further work is needed to dissect the role of each of these two RPA-binding domains in the DNA "hand-off" mechanism during the repair process but most importantly, this information is vital when a therapeutic inhibitor of RAD52 interaction with RPA is selected.

3.4.2. Surface plasmon resonance. The outcome of our FluorIA analysis of RAD52:RPA binding activity motivated an investigation to determine the kinetic parameters of these interactions. SPR analysis was conducted using the different RAD52 constructs and the results are summarized in Table 3.1. A representative SPR curves for the different complexes each showing the different analyte concentrations are presented in figure 3.4. The primary function of RPA is to bind ssDNA and this complex provides further stability to the RAD52 interaction [79, 115, 123]. SPR analysis confirmed that the RPA:ssDNA complex had stronger affinity with RAD52 than RPA alone. RPA interaction with RAD52(1-303) was similar to full-length RAD52. More precise experimental measurements of EGFP-RAD52(213-418) show similar interaction affinity to full-length RAD52 and RAD52(1-303) with RPA. RAD52(1-212) and RAD52(168-306) interactions with RPA also show similar binding affinities. The interaction of these construct is, after all, electrostatic and thus show similar values. The data here disprove previously-speculated negative regulation role for the RAD52 C-terminus.

Table 3.1. Binding affinities of different RAD52 and RPA constructs.

Complex[a]	**K_D (M)**[b]
wtRPA:wtRAD52	$1.9*10^{-7}$ ($2.0*10^{-8}$ S)
(ssDNA:RPA):wtRAD52	$1.1*10^{-7}$ ($1.5*10^{-8}$ V)
wtRAD52:RPA(1-303)	$1.7*10^{-7}$ ($9.2*10^{-8}$ V)
wtRAD52:RPA(1-212)	$4.8*10^{-7}$ ($1.7*10^{-7}$ S)
RPA:EGFP-RAD52(213-418)	$2.9*10^{-7}$ ($1.1*10^{-7}$ V)
RPA:RAD52(168-306)	$3.2*10^{-7}$ ($1.2*10^{-7}$ S)
RAD52(257-274): RPA	$7.3*10^{-6}$ ($7.7*10^{-13}$ V)
RAD52(257-274):RPA32(172-270)	$4.6*10^{-6}$ ($1.6*10^{-7}$ V)
RPA32(172-270)RAD52(1-303)	$1.2*10^{-9}$ ($3.9*10^{-19}$ V)

[a] For the complexes, the protein on the left is the analyte and the protein on the right is the ligand and attached to the chip via His tag.

[b] The parentheses on the in the right-hand columns are the errors estimated from the standard deviation (S) or as variation (V) if only two trials were done.

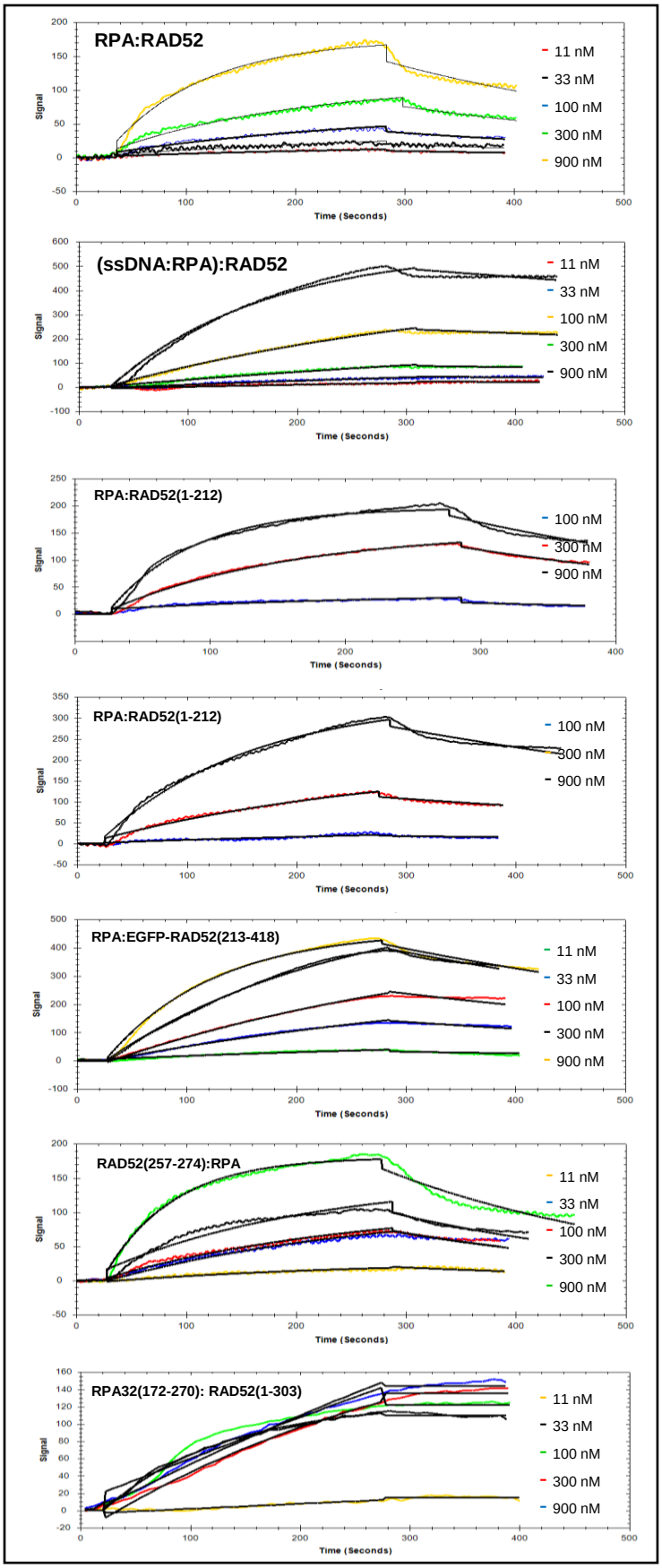
RPA:RAD52
11 nM
33 nM
100 nM
300 nM
900 nM
Signal
Time (Seconds)
(ssDNA:RPA):RAD52
11 nM
33 nM
100 nM
300 nM
900 nM
Signal
Time (Seconds)
RPA:RAD52(1-212)
100 nM
300 nM
900 nM
Signal
Time (Seconds)
RPA:RAD52(1-212)
100 nM
300 nM
900 nM
Signal
Time (Seconds)
RPA:EGFP-RAD52(213-418)
11 nM
33 nM
100 nM
300 nM
900 nM
Signal
Time (Seconds)
RAD52(257-274):RPA
11 nM
33 nM
100 nM
300 nM
900 nM
Signal
Time (Seconds)
RPA32(172-270): RAD52(1-303)
11 nM
33 nM
100 nM
300 nM
900 nM
Signal
Time (Seconds)

Figure3.5 Representative SPR curves. Legend on the right shows different analyte concentrations flown over ligand and regenerating in between. Complex names are on the top left corner with the analyte shown on the left side of the colon while the ligand is on the right hand.

It was based on HR activity analyses of different RAD52 truncations, that most of the C-terminal half was excluded to obtain a crystal structure with a good diffraction quality [119]. To explore this further, we designed a new His-tagged RAD52(168-306) construct, which excluded the C-terminus beyond the RPA binding domain and included the linear sequence arm known to facilitate oligomerization [119, 124]. The binding affinity of this construct of RPA is the same as of RAD52(1-303) and RAD52 (1-212). The results further support the idea that a portion of the N-terminal region of RAD52 is involved in binding of RPA. Additionally, comparing the K_D values of RPA with RAD52(168-306) to that with EGFP-RAD52(213-418) in table 3.1, we observe that the interaction affinity was not significantly reduced. This information suggests the absence of a domain of RAD52 C-terminus that might be negatively regulating the PPI.

RPA(172-270) is a region which contains a wHLH structure required for DNA repair and a site for PPIs [115]. RAD52 is among the interacting partners on this region and its interaction affinity was of interest. As our data indicates that RAD52(1-303) contains the entire RPA binding sites, interaction with RPA(172-270) yielded a strong binding affinity $1*10^{-9}$ M. This is interesting as affinity was lower when a full RPA trimer ($1.9*10^{-7}$) suggesting that the full-length is offering inhibitory regions that are of importance to the dynamic of interaction. Early work by Bochkarev and colleagues in their work showing a DNA-binding activity within the RPA32/14 complex, suggested that N- and/or C-terminus of RPA32 harbor domains that inhibit ssDNA binding. In later structural work by the group, suggested that those RPA32 inhibitory domains are near the L45 loop known for promoting ssDNA binding and might be affecting its mobility and reducing affinity of interaction with DNA [110]. The strong affinity of interaction of RPA32 C-

terminus with RAD52(1-303) we observed here suggests a regulatory mechanism for this domain in supporting PPI and DNA interaction. Further work is needed to understand if increase in affinity for RAD52 is an an accompanying event with reduced affinity for ssDNA.

Interestingly, Mer and colleagues carried NMR analysis of RPA(172-270) with RAD52(257-274) and found that the exchange between free and bound state of the RAD52 peptide was fast on the time scale of chemical shifts, indicating a weak binding [121]. The K_D of two other protein partners, UNG and XPA, were reported in their study to be 1 and 5 μM respectively and RAD52 peptide was speculated to be weaker. We measured RPA(172-270) interaction with RAD52(257-274) and obtained a K_D of $4.6*10^{-6}$ M) which is in excellent agreement with their reported K_D values.

We explored the potential inhibitory effect of RAD52(257-274) peptide of RAD52:RPA interaction when added as an SMI in FluorIA reaction (Chapter 2). No inhibition was observed for up to 100 μM. This suggest that a binding affinity greater than $7*10^{-6}$ is needed to inhibit the complex. Similar reactions were carried out with other RAD52 peptides we designed (detailed in Appendix I) and no inhibition was observed in singles or synergy. These results is probably attributed to weaker affinity as found with RAD52(257-274) but it is also possible that the peptides probably do not assume a structure that mimics the PPI.

The kinetics of RAD52:RPA interaction was also analyzed with a different SPR instrument and method of coupling. Biacore 3000 was used as described, utilizing amine coupling technique to immobilize RAD52 on the CM5 chip and conduct kinetic analysis with RPA. Out of the several experimental repeats, two were selected for their lowest

Chi^2 values of 2.1 and 6.6. The average K_D value was $7.8*10^{-7}(\pm 1.3*10^{-7}$ V). This K_D value obtained was close to that obtained from the OpenSPR system ($1.9*10^{-7}$) despite the different instruments and coupling methods employed for immobilization.

3.4.3. Isothermal titration calorimetry. The thermodynamic parameters for the RAD52:RPA interaction were investigated using ITC. A high concentration of RPA (150-300 μM) was titrated against about one-tenth concentration of wt.RAD52 to obtain the binding isotherms of the reaction (Figure 3.6). Binding was confirmed in ITC but the value we obtained was off by one order of magnitude probably due to experimental conditions. We further calculated thermodynamic parameters using the exothermic ΔH value (Table 3.2).

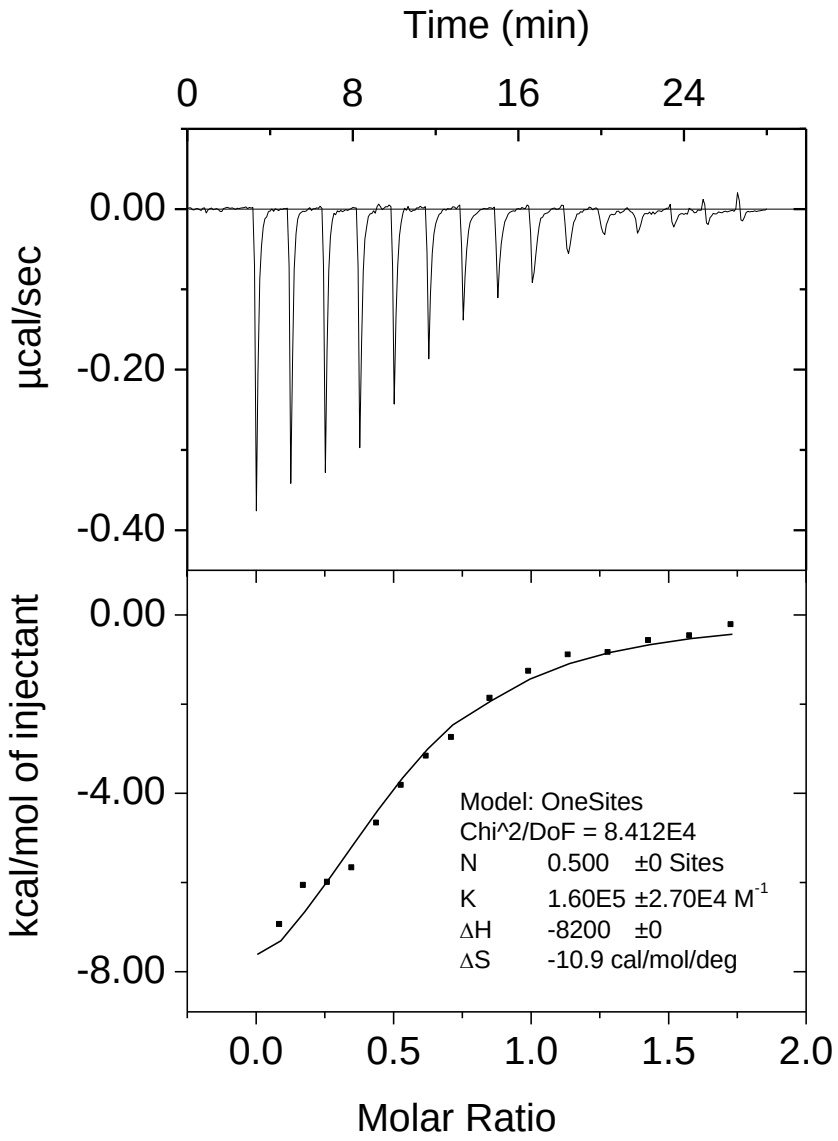
Time (min)
0
8
16
24
0.00
-0.20
-0.40
µcal/sec
0.00
-4.00
-8.00
kcal/mol of injectant
Model: OneSites
Chi^2/DoF = 8.412E4
N 0.500 ±0 Sites
K 1.60E5 ±2.70E4 M-1
ΔH -8200 ±0
ΔS -10.9 cal/mol/deg
0.0
0.5
1.0
1.5
2.0
Molar Ratio

Figure 3.6 ITC profiles for the titration of RAD52 with RPA. The top panel represents a sequential injection of RPA into a solution of RAD52 and the bottom panel shows the integrated heat data against molar ratio of [RPA] / [RAD52] after correction of heat of dilution. Data points were fitted to one site model and the solid line represents the best fit data with fixed N=0.5 and fixed ΔH=8.2 kcal/mol.

Table 3.2 Thermodynamic parameters for RAD52:RPA interaction.

ITC experiments	K (M^{-1})	ΔG^o (kcal/mol)	$T\Delta S$ (kcal/mol)
RPA on RAD52 (run #1)	$1.6*10^5$ ($2.7*10^4$)	-97.7	-89.50
RPA on RAD52 (run #2)	$7.0*10^5$ ($1.7*10^4$)	-404.5	-396.3

Two ITC runs are selected (run 1 is shown in Figure 3.5). ΔG^o = -RT*In(K) equation was used to calculate ΔG^o and this value was used to calculate $T\Delta S$ according to the equation $\Delta G = \Delta H - T\Delta S$ and using the average ΔH= -8.188 Kcal/mol

3.5. Conclusion

RAD52 interaction with RPA is a promising candidate therapeutic target. Inhibiting RAD52 repair activity can deprive tumors of an important survival and maintenance factor. RAD52 activity is guided and dictated by RPA which guards the ssDNA near the damage site. It was imperative, therefore, to understand the nature of this PPI.

Given the formidable nature of both proteins to full structural analysis, we utilized multiple techniques by which we moved from global understanding of binding activities to detailed calculations of binding affinity and thermodynamic parameters. With this information and close examination of available structural information, we developed a new understanding for RPA-interacting domains on RAD52.

Number of important findings were presented here in characterizing RAD52 interaction with RPA. First, we confirmed previous supposition for the presence of an additional RPA-binding domain within the RAD52 N-terminus. Second, our data here disperse key aspects that will be of significant value to further investigate domains involved in regulating the dynamic process of DSB repair. Our data disproves previously-speculated negative regulation role for the RAD52 C-terminus as including the rest of the C-terminus did not reduce the affinity of interaction with RPA. Further, measurements of the C-terminus wHLH region of RPA32 with RAD52(1303) yielded a strong interaction affinity, which was reduces when full-trimer RPA was used. This indicates the presence of a domain in the RPA trimer that weakens the interaction with RAD52. What is interesting about our finding here is that the C-terminus of RPA32 containing the wHLH region, was implicated in offering structural dynamics that reduces the affinity of interaction with ssDNA. We have yet to understand whether the strong interacting

affinity with RAD52 is an accompanying event that supports the hand-off mechanism in repair.

Overall, the measured K_D values makes RAD52:RPA interaction a viable target for SMIs. The information here will facilitates tailoring the appropriate method to find a fitting therapeutic agent that can target this RAD52:RPA with an appropriate affinity and selectivity. Moreover, the map and affinity of RAD52 interaction with RPA will guide potential pharmaceutical inhibitors or modulators of this interaction.

New information here includes regions in RAD52(1-212) are important for binding RPA. Also, it is clear that there is a large electrostatic component to the formation of the complex.

Chapter 4

HTS analysis and identification of potential RAD52 inhibitors

4.1 Abstract

RAD52 activity has been shown to support the establishment and maintenance of tumors by addressing their most challenging DNA repair problems such as DSBs and collapsed replication forks. In HRR-defective cancer cells, RAD52 becomes particularly important in providing a backup repair pathway and therefore, holds a promising therapeutic value through synthetic lethality. While there has been several published SMIs for RAD52, we differ here in our approach by seeking to prevent RAD52 repair activity by impairing its interaction with RPA, an abundantly present protein on ssDNA at DNA damage sits. RPA meets RAD52 at every junction in the latter's quest to reach damaged DNA. Beyond this obligatory physical interaction, we and others have demonstrated that RPA dictates RAD52 recruitment and function in repair. Through a HTS using FluorIA, we identified SMIs that inhibited RAD52 interaction with RPA that selectively kill HRR-defective cancer cells.

4.2. Introduction

DNA damage response and repair have always been at the center of common cancer chemotherapeutic and radiotherapy treatments directed to overwhelm repair machineries with mounting DNA lesions. Cancer cells often show dependence on unique DNA repair pathways due to frequent mutations in repair-related genes or proteins and their higher demand for repair to sustain their active division. The evolving avenues in targeted cancer therapeutics are not far from these principles, but aspire to zero-in on selected factors that are dispensable for normal cells thus sparing them from collateral damage [125]. Coupling maladaptive mutations in cancer with pharmacological inactivation of another target to induce selective cell death is called synthetic lethality

[101]. This approach minimizes side effects that exhaust patients and has the potential to lift the roadblocks for the treatment of aggressive subtypes of cancers for which there are currently no effective therapies. High-grade serous ovarian and triple negative breast cancers, for example, are among the most lethal subtypes characterized by poor prognosis, high rate of reoccurrence and metastasis [23, 126]. Many patients with these specific subtypes harbor somatic mutations in BRCA1 or BRCA2 contributing to the development and progress in PARP inhibitors [49, 127, 128].

Poly (ADP-ribose) polymerase (PARP) enzymes catalyze polymerization of ADP-ribose moieties (PARsylation). Serial of PARsylation facilitate the repair of SSBs in DNA. Inhibiting this catalytic activity impairs SSB repair and cause the formation of DSBs [129]. The exacerbating amount of DSBs is purposefully induced by PARP inhibitors to challenge cancer cells. This approach appears to be effective against cancers that are defective in HRR [130]. Cross-reactivity among some PARP family members to developed inhibitors has unfortunately caused side effects emerged [131]. Also, resistance to PARP inhibitors is a problem, so there is a need for additional selective treatments for HRR-defective cancers.

The specialty and high fidelity of HRR for DSBs make it a candidate pathway to look for cancer targets as exemplified by the story of PARP inhibitors [8]. Importantly, cells with defective BRCA2 or related proteins shows dependency on RAD52 protein to maintain functional RAD51-mediated HRR repair activity of DSBs [100]. In fact, other RAD52 repair activities such as SSA were reported to increase in BRCA-related defects in HRR [69, 71]. These findings helped establish a body of research targeting RAD52 activity to induce selective killing of BRCA-deficient tumors [60, 62, 74].

New findings about the role of RAD52 in tumorigenesis further qualifies it as an anti-cancer target [132]. RAD52, for example, is specifically recruited to in break-induced repair (BIR) and the restart of collapsed replication forks [66]. Supporting role in the establishment and maintenance of tumors, *RAD52* expression was found to be associated with increased risk for lung cancer and its upregulation was observed in hepatocarcinoma [19, 133]. Beyond the scope of its synthetic lethal relationship with the BRCAs, RAD52 inactivation was demonstrated to augment the immune response and improve therapeutic response [73].

Development of an effective modulator or inhibitor are usually guided by comprehensive structural and biomolecular aspects of the target. For this reason, we characterized RAD52 interaction with RPA by SPR, ITC, and FluorIA as described in Chapter 3. The data obtained was based on previous work done by our group that delineated domains of interactions using an ELISA-based assay [103], stoichiometry by SEC-MALS [79], structural analyses by crystallography methods [115], and posttranslational modifications by various experimental methods [134].

Here we elaborate on using the FluorIA procedure, described in chapter 1, to conduct a high throughput screening for SMIs targeting RAD52:RPA interaction. Over 101,500 compounds were screened from three different libraries. Eleven candidate hits were obtained, five of which showed the strongest inhibition as determined by their high EC_{50} values *in vitro*. Three out of the five are FDA approved and two of these are anti-cancer drugs.

4.3. Materials and methods

4.3.1. Chemical libraries screened and handling of compounds. The FluorIA procedure described in Chapter 2 was used here to screen for SMIs from three large libraries: 1) The 355-member SelleckChem Kinase Inhibitor Library, the 1200-member Prestwick Chemical Library, and the 100,000-member ChemBridge library. Compounds from each library had been stocked at 10 mM in 100% DMSO and stored at -80 ºC in 384 plates (Nunc, 267460) termed as "master plates". Daughter plates are prepared from master plates by a 1:5 or 1:50 dilution in 100% DMSO of each compound into new 384-well clear, round-bottom plates and stored in -20 ºC.

The screen of the SelleckChem Kinase Inhibitor and the Prestwick were done in two concentrations of the drugs: 10 and 100 μM each in duplicate. As we moved to screen the large ChemBridge library, we carried out the screen at a single concentration of 100 μM. Questionable readings were repeated either as single wells or a whole plate. It was possible to screen up to 10,000 compounds in a screen day. At the end of all screens, we selected eleven chemicals that met the statistical criteria for a hit as described in Chapter 2, method section. Each of these hits were further verified in triplicate at 10 and 100 μM in a separate FluorIA screen.

4.3.2. Dose response analysis of hits. Each compound determined to be a hit was taken through a secondary screening to confirm its response. Subsequently, as dose response curve (DRC) was generated to analyze the half-maximal effective concentration (EC_{50}) value *in vitro*. A source plate is created by hand-pipetting compounds from master plates thawed at room temperature starting at 10 mM and serially diluted in half down to 6.0 μM using 100% DMSO. From each dilution point, a 12 μL/well were hand-pipetted in

quadruplicate in a clear, round bottom 384-well source plate. Then100% DMSO was pipetted in the same manner in one column of the source plate. Working plates are then prepared by first binding 15 pmol/well of freshly purified RPA in the same way described in Chapter 2. The RPA plate, however, is not subjected to freezing and is washed and blocked. Then FluorIA protocol is followed as described in Chapter 2. Using the Biomek, 4 uL of each compound or DMSO are transferred from the source plate into the working plate. At this point each well contains the experimental or control reaction in a final DMSO concentration of 5%. With the addition of 4 µL from each compound in to a 75 µL reaction mixture, the concentration of chemicals would be reduced approximately 20x generating final concentration series that ranges from 500 µM to 0.3 µM. Based on the results of these experiments, hits that showed a dose response were ordered. Candidate SMIs were purchased and a 1D NMR analyses was carried out to verify their identities. Using the molecular weight value, each compound was dissolved in 100% DMSO to achieve a stock concentration of 10 mM. Stocks of compounds were aliquoted and stored frozen at -20°C. For *in vitro* DRC experiments, 5×10^3 where the response is the average RFU of a triplicate at each concentration point, T_0 is the average RFU of a triplicate the negative control, and T_{100} is average RFU of a triplicate the zero-inhibition condition.

4.3.3. Cancer cell lines. Two cancer cell lines were used: 1) HCC1937 cell line (a generous gift from Dr. Simon Powell) is derived from mammary gland, primary ductal carcinoma at early onset of a tumor. This triple negative patient carried germ line mutation in *BRCA1* resulting in COO-terminal truncation protein and loss of the second *BRCA1* allele. A BRCA1-restored and an empty vector lines were also obtained by transfection of a vector containing full-length human BRCA1 cDNA or an empty vector,

respectively. 2) PE01 cell line derived from an ovarian cancer patient, with BRCA2 mutation, ascites at her first relapse post cisplatin chemotherapeutic treatment was provided Dr. Tadayoshi Bessho along with a BRCA2-proficient revertant cell line, C4-2. The latter line is one of eight clones from cultured PE01with restored BRCA2 due to secondary mutation in *BRCA2* that cancelled the original mutation as described in Sakai *et al.* [135].

4.3.4. Cell viability assay. Cells were seeded 5 x 10^3 cells per well in 96-well plates in a 90 µL volume per well one day before treatment with exception to the HCC1937 BRCA1-restored cell line which required a higher density of around 5 x 10^4 cells per well due to consistently observed slow growth and division behavior. For treatment, master plates were made from the stock aliquots of compounds described above making 1:2 serial dilution starting from 10 mM down to 0.02 µM in 100% DMSO. 1:10 dilution was made from there in 100% DMSO followed by another 1:10 dilution in cell culture media. Finally, 10 µL of this compound solution is transferred onto the 90 µL of cells bringing the final DMSO to 1%. Cells in 96-well plates were incubated with increasing concentrations, adjusted to the level of sensitivity of the cells to the compound, or vehicle control (1% DMSO) for 72 hours. For HCC1937 BRCA1-restord cell line, treatments duration was extended to 96 hours accounting for the observed slow division and to allow for enough doubling events while in treatment. Each treatment plate contained nine 1:2 dilution points of a drug in six replicates each: P1 (0–10 µM), P2 or P3 (0–2.5 µM). Cell viability was determined using PrestoBlue reagent (Life Technologies, # A13261). Fluorescent measurements were taken using a Spectramax M5 plate reader (MDS). To assess cells' replication in the absence of compounds as a control, six wells on each plate

were treated with vehicle to be read in triplicate at the initial treatment day as time zero (T_0) and at 72-hour read as time 100 (T_{100}). The PE01 and C-42 cells lines were treated in the same manner but due to higher sensitivity, the top concentrations were lower: P1 (0–5 μM), P2 (0–5 μM), or P3 (0–1.25 μM).

4.4. Results and discussion

4.4.1. High throughput screen and hits. Libraries screened, and hits obtained from each are summarized in Table 4.1. No hits were obtained from SelleckChem Kinase Inhibitor Library as expected. There were three hits from the Prestwick library: P1, P2, and P3 and they showed the strong inhibition of RAD52:RPA interaction compared to the rest of the hits (Figure 4.1). Eight hits were obtained from the Chembridge library with C2 and C8 being the strongest inhibition of the RAD52:RPA PPI (Figure 4.2). Based on their strong *in vitro* inhibition and their significance as FDA-approved drugs, the three Prestwick hits were selected for further cell-based characterization.

Table 4.1 Chemical libraries screened by FluorIA and hits obtained.

Chemical Library	Hits
SellekChem	none
Prestwick	P1, P2, P3
Chembridge	C1, C2, C3, C4, C5, C6, C7, C8

P signifies hits from the Prestwick library while C is for Chembrige library.

A

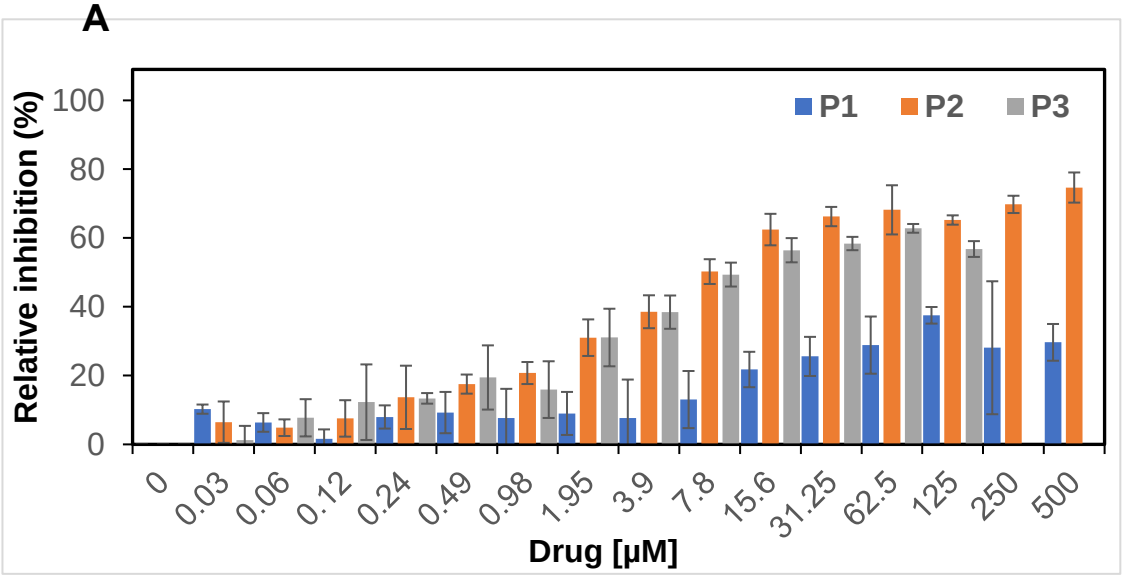
Relative inhibition (%)
100
80
60
40
20
0
P1
P2
P3
0
0.03
0.06
0.12
0.24
0.49
0.98
1.95
3.9
7.8
15.6
31.25
62.5
125
250
500
Drug [μM]

B

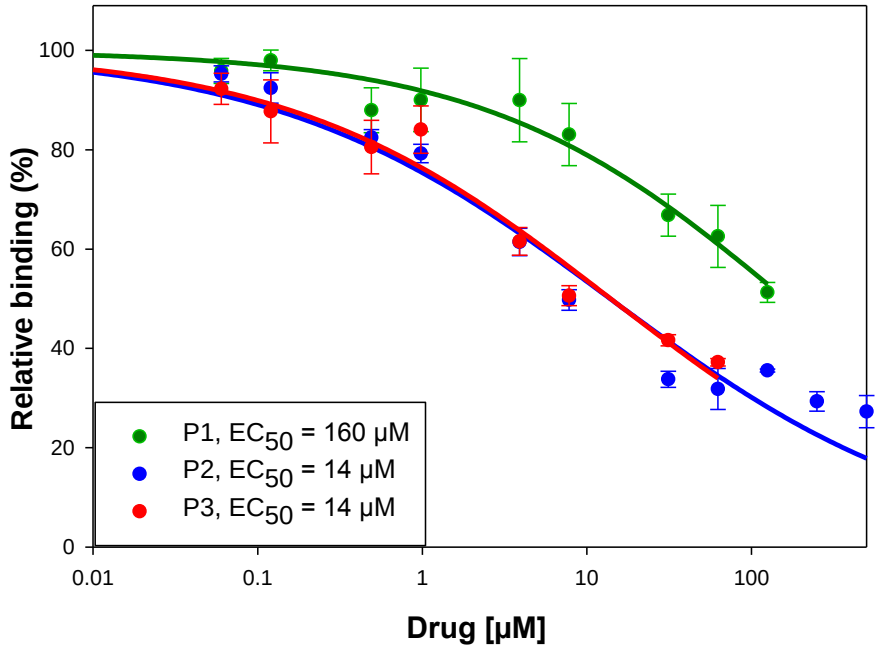
Relative binding (%)
100
80
60
40
20
0
P1, EC50 = 160 μM
P2, EC50 = 14 μM
P3, EC50 = 14 μM
0.01
0.1
1
10
100
Drug [μM]

Figure 4.1 Dose response curve and relative inhibition values of Prestwick hits. (A) Prestwick drugs were added in the series of concentrations up to 500 µM as described in Materials and methods employing the FluorIA. Relative inhibition values were calculated against EGFP tag or RAD52(1-303) as controls. (B) Half-maximal effective concentration (EC_{50}) for each drug was calculated using SigmaPlot 13.0 software with minimum and maximum adjusted to zero and 100 respectfully. Experiments were repeated three times for each drug. P1 and P3 precipitated in solution at high concentrations and data points were eliminated for clarity.

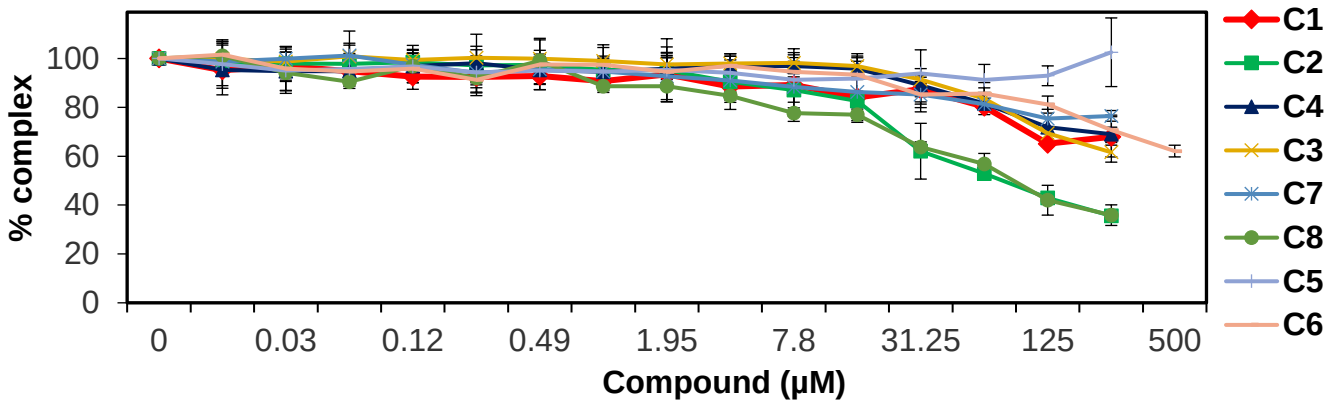
% complex
100
80
60
40
20
0
0
0.03
0.12
0.49
1.95
7.8
31.25
125
500
Compound (µM)
C1
C2
C4
C3
C7
C8
C5
C6

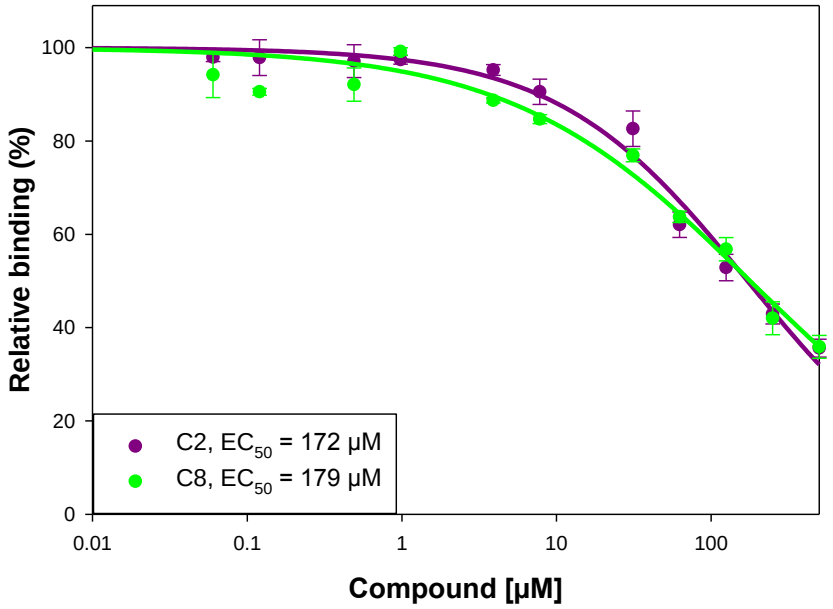
Relative binding (%)
100
80
60
40
20
0
0.01
0.1
1
10
100
Compound [µM]
C2, EC50 = 172 µM
C8, EC50 = 179 µM

Figure 4.2 Dose response curve and relative inhibition values of Chembridge hits (A) Chembridge compounds were added in the series of concentrations up to 500 µM to FluorIA reaction as described in Materials and methods. Relative inhibition values were calculated against EGFP tag or RAD52(1-303) as controls. (B) EC_{50} for each drug was calculated using SigmaPlot 13.0 software with minimum and maximum adjusted to zero and 100 respectfully. Experiments were repeated three times for each drug.

4.4.2 Inhibition of BRCA-deficient cancer cells' viability following treatments with P1, P2, and P3. BRCA1 and BRCA2 are the main pathway in mammalian cells to mediate the formation of RAD51 presynaptic filaments and catalyze the repair of DSBs by HRR [33, 97]. RAD52, through its interaction with RPA, composes an alternative pathway for cells lacking functional BRCA [100]. Targeting RAD52 activity in BRCA-deficient cancer cells was shown to induce synthetic lethality making it a valuable cancer target [58, 59].

As an initial cell-based assessment, we obtained cancer breast and ovarian cancer cell lines with impaired BRCA1 or BRCA2 function and tested their viability with P1, P2, and P3 treatments. We rationalized that if these P1, P2, and P3 can inhibit RAD52:RPA interaction, BRCA-deficient cell lines will be sensitive to those drugs. For the BRCA1-deficient HCC1937 triple negative cell line, the results are summarized in Figure 4.3. Following 72 or 96-hour treatment with increasing concentrations of either compound P1 P2, or P3 (0–5 μM) the viability of each cell line was analyzed. The effect of P1 treatment on viability was difficult to determine with an unexpected spur in overall growth behavior. Treatment with P2 reduced cell viability in a dose-dependent manner for BRCA1-deficient parental line (not shown) as it did in the empty-vector control while inserted BRCA1 plasmid supported survival. P3 treatment indicates an overall cytotoxic effect which might have masked any potential difference. Interestingly, treatment with lower doses of P2 or P3 showed noticeable spur of growth albeit less than that observed with P1.

A

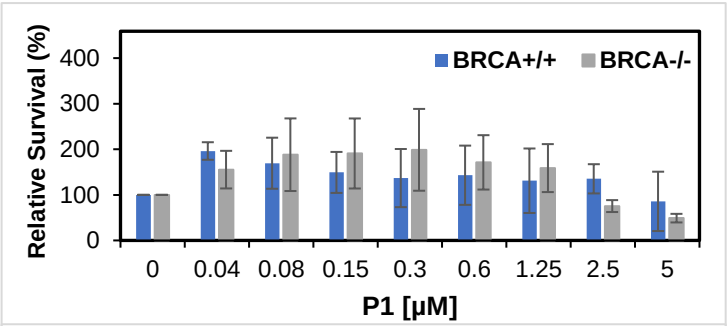
Relative Survival (%)
400
300
200
100
0
BRCA+/+
BRCA-/-
0
0.04
0.08
0.15
0.3
0.6
1.25
2.5
5
P1 [µM]

B

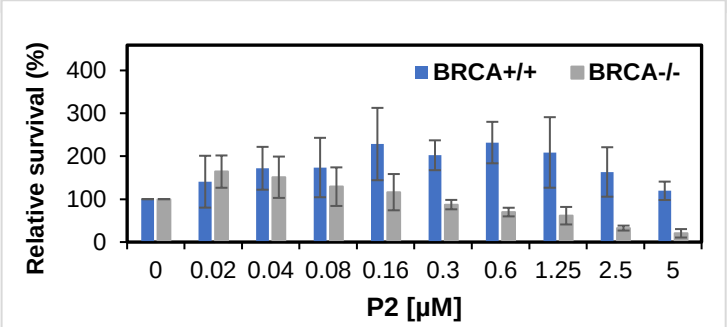
Relative survival (%)
400
300
200
100
0
BRCA+/+
BRCA-/-
0
0.02
0.04
0.08
0.16
0.3
0.6
1.25
2.5
5
P2 [µM]

C

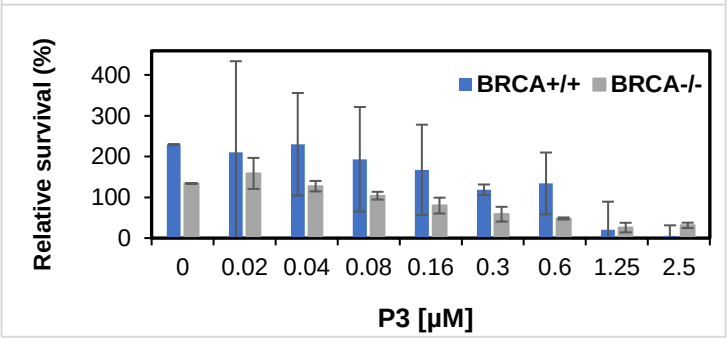
Relative survival (%)
400
300
200
100
0
BRCA+/+
BRCA-/-
0
0.02
0.04
0.08
0.16
0.3
0.6
1.25
2.5
P3 [µM]

Figure 4.3 BRCA1-defective cancer cell line survival assay. HCC1937 corrected ($BRCA^{+/+}$), empty vector ($BRCA^{-/-}$), and parental (not shown here) were treated with increasing concentrations of (A) P1, (B) P2 and (C) P3 and incubated for three days at 37 °C. Corrected line needed additional 24 hr. in treatment due to slower growth behavior. PrestoBlue reagent was used to assess the viabilities of the treated cells as detailed in Material and methods, and the obtained results were normalized to vehicle control.

The BRCA2-deficient PE01 ovarian cell line and it BRCA2 restored mutant C4-1 displayed different patterns of sensitivity. PE01 was sensitive to all three drugs showing an overall reduced cell viability in a dose-dependent manner and ~75% inhibition with as low as 0.31μM of P2 or P3 treatment. With P1 treatment, 5 μM was needed to reach a similar level of inhibition. The interpretation of treatments' effect for any lower dosages was masked by enhanced growth for all three drugs in both cell lines in similar way observed with HCC1937 cell lines (Figure 4.4) (lower data point with this issue are eliminated for clarity). The EC_{50} values were determined through curve fitting and are summarized in Table 4.2.

Unlike the HCC1937 with inserted BRCA1 plasmid, C4-2, with restored BRCA2, shows evident reduction in viability in a dose-dependent manner with all three drugs despite better survival rate than PE01. PE01 was derived from a patient with ovarian adenocarcinoma at stage III who was sensitive initially to cisplatin and AG14361 PARP inhibitor. However, she acquired cisplatin resistance and PARP inhibition resistance upon a secondary revertant point mutation in *BRCA2* [135, 136].

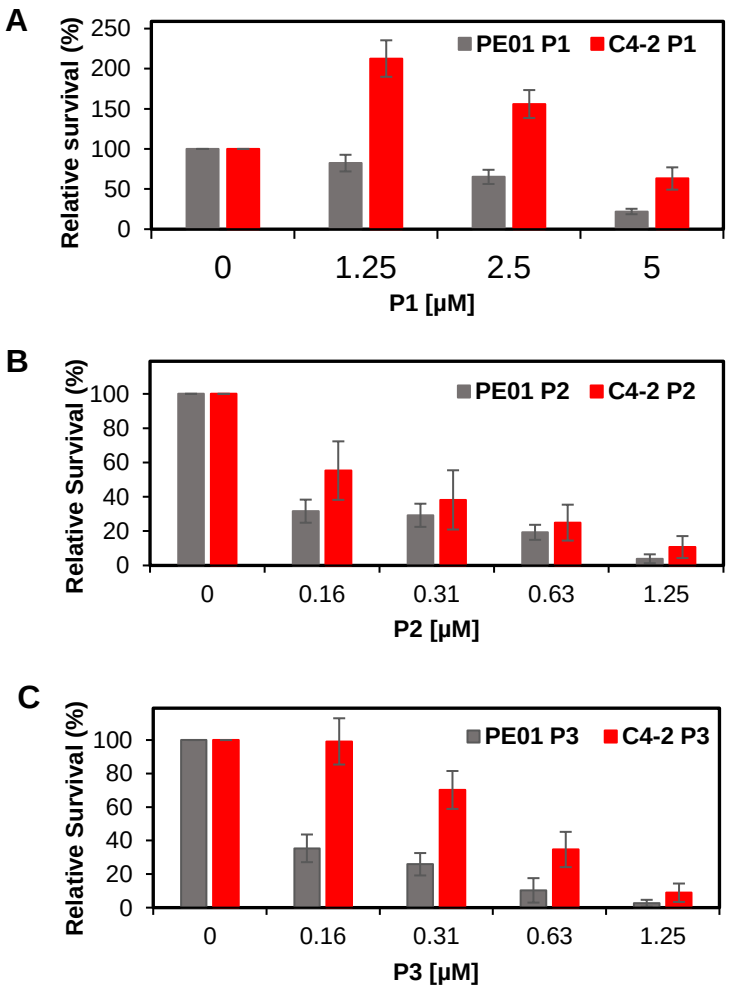
A
Relative survival (%)
250
200
150
100
50
0
PE01 P1
C4-2 P1
0
1.25
2.5
5
P1 [μM]
B
Relative Survival (%)
100
80
60
40
20
0
PE01 P2
C4-2 P2
0
0.16
0.31
0.63
1.25
P2 [μM]
C
Relative Survival (%)
100
80
60
40
20
0
PE01 P3
C4-2 P3
0
0.16
0.31
0.63
1.25
P3 [μM]

Figure 4.4 BRCA2-defective cancer cell line survival assay PE01 and C4-2 cell lines were treated with increasing concentrations of (A) P1, (B) P2 and (C) P3 and incubated for three days at 37°C. PrestoBlue reagent was used to assess the viabilities of the treated cells as detailed in Material and methods, and the obtained results were normalized to vehicle control.

Table 4.2 EC_{50} for P1, P2, and P3-treated PE01 and C4-2.

Cell line	P1	P2	P3
PEO1	2.9 (0.32)	0.11 (0.036)	0.15 (0.07)
C4-2	5.4 (0.62)	0.37 (0.12)	0.43 (0.29)

EC_{50}values here are experimental replicates with technical triplicates.

C4-2 was among several PE01 clones obtained after four weeks in culture where BRCA2 was restored. Functional significance of this type of restoration is unclear particularly with the heterogeneity in resistance observed among these clones. No reports of administering the anti-cancer P2 or P3 drugs in that patient's chemotherapeutic rounds after acquiring this secondary *BRCA2* mutation were found. This data here suggest a level of sensitivity in C4-2 and might be of therapeutic value to explore whether RAD52:RPA inhibition bolstered this sensitivity.

The observed inhibition of the viability for these artificial BRCA2 mutants suggest an impact on alternative repair and survival pathway in the absence of BRCA2. In addition to the finding of the screen with respect to inhibition of RAD52:RPA interaction, further work is needed to validate whether RAD52 activity is specifically targeted here and whether that explains the compromised survival observed in BRCA-deficient cell line. Collectively, cell viability assays revealed higher potency for P2 and therefore, it was selected for this analysis.

The viability tests above guided a general understanding of BRCA-deficient cell lines sensitivities to these three hit drugs. However, the varying phenotype and heterogeneity in response were inevitable features of cancer cell lines. To validate inhibition of RAD52:RPA interaction as we found in FluorIA, it was is necessary to examine drugs' effect on specialized RAD52 pathway.

RAD52 is a primary driver of SSA type of HR where a search for homology usually carried by RAD51 is dispensable when DSBs take place within direct repeats. RPA covers the ssDNA exonuclease products at the DSB site and through interaction with RAD52 ends are re-joining concludes the repair process with inevitable deletion of

flanking sequences between the direct repeats. Pretreatment of SA-GFP U2OS with P2 was done by Dr. Bessho prior to expression of I-SceI and analysis by flow cytometry. Similar treatment was carried out using D-I03, a RAD52 inhibitor recently published by Dr. Mazin's group [63]. DSBs repair activity by SSA was scored by GFP^+ cells and blotted as a function of P2, D-I03, or vehicle treatment. As will be soon reported in a manuscript for publication, with 5 nM, P2 lowered SSA activity by over 50%, which is 4000-fold less concentration than D-I03 to reach this effect. The data suggests that RAD52 repair activity is part of the mechanism of action for P2 and can be of great value to explain the varied sensitivity to this drug among cancer patients.

4.5. Conclusion

RAD52 repair activity is valuable for the progress of tumorigenesis and we have demonstrated through multidisciplinary studies that its complex with RPA is a candidate to target for the development of selective anti-cancer therapies. While development of a new targeted cancer drugs is an ambitious goal that we strive for, investigating the mechanism of action of existing anti-cancer drugs should be a concomitant effort. As we are understanding more about the genetic background behind cancer, it is vital to revisit the therapeutic drugs in use and delineate the molecular maps behind their sensitivities and resistance. The outcome of such studies will be of great benefit to the clinical assignment of candidate patients for such drugs, building on the goal of personalized medicine in cancer therapeutics.

We identified eleven potential SMIs for RAD52 interaction with RPA to induce synthetic lethality in BRCA-deficient tumors. Surprisingly, three of those hits were FDA-approved drugs, two of which are known for their anti-cancer activities. While the

general mechanism of these two drugs are known, varied sensitivities to them in patients is not completely understood. Our work here leads to molecular clues that may explain that variation. We show selective targeting of P2 to RAD52 repair activity; however, further work is needed to identify its selectivity to RAD52 proteins and ways to enhance its inhibitory action.

Chapter 5

Conclusion and future directions

A common starting feature in malignancies is uncontrolled cell division. There are molecular factors that enable such behavior and others that work to maintain it in the face of all defense mechanisms our bodies had developed. DNA damage and repair are central processes in cancer and candidate enabling and maintenance factors can be identified within these pathways.

RAD52 is currently recognized to promote tumorigenesis because of its crucial roles in a number of repair activities at DNA damage stress sites. RAD52 repair activity was specifically explored in different cancers and affirmed to be parallel to maintenance of cancer cells' survival. Work by Cramer-Morales and colleagues showed that BCR-ABL1- mediated leukemia (BRCA1-deficient) relies on RAD52 to repair increased levels due to enhanced ROS-induced damage [60]. Remarkably, their work also showed that depletion of RAD52 suppressed both cancer stem and progenitor cells expansion and increased their apoptosis. In support of their work, a recent $RAD52^{-/-}$ mice model not only demonstrated resistance to squamous cell lung carcinoma, but also augmented the activity of CD^{8+} T cells and NK effectors [73].

Our work focused on characterizing the candidacy of RAD52 interaction with RPA as a cancer target and development of a high throughput assay to screen libraries of SMIs for this interaction. Previous successes scored in targeting PPIs was attributed to thorough, multidisciplinary characterization of protein targets. Targeting PPI to inhibit or modulate their activity is becoming an attractive approach in various therapeutics due to their observed altered behavior of interaction or expression in disease. Large PPI interfaces had traditionally posed a challenge for the idea of being modulated by small molecules. However, protein mutational studies demonstrated that only some residue

areas or “hot spots” may provide the binding energy for the small molecules to bind and exclude the targeted protein partner [85, 90]. Successful HTS screens, for example, have been credited for the discoveries of most enzyme-targeted small molecules that were later adapted for other protein targets. To name a few, NMR-based screens [91], differential scanning fluorimetry (DSF) [92], and 3D molecular modeling to select candidates for HTS [94].

While these were useful approaches, their applications is usually costly and requires the presence of specific instruments that are not readily available for every researcher. FluorIA (Chapter 2) has no demand for expensive instrumentation yet is a robust and homogeneous assay. We were able to screen large libraries of molecules with efficacy in time, cost, and output. On a low-scale, FluorIA was proved valuable use in detecting PPIs using full-length or truncated mutant proteins. This was particularly useful in delineating the domains of interactions and coordinating such data with available kinetic and structural data to characterize RAD52 interaction with RPA (Chapter 3).

The libraries we screen yielded interesting potential SMIs in terms of identity and structure (Chapter 4). We focused particular attention on the three FDA-approved drugs hits. We characterized several BRCA1/2-deficient cancer cell lines’ survival with these three hits treatment. Despite the challenges encountered with the heterogeneous behavior of culturing cancer cell lines, we observed a general survival in the presence of BRCA1/2. P2, being an anti-cancer drug was particularly interesting. The data we have suggest that targeting RAD52 repair activity might be part of the mechanism of action for P2 and can be of great value to explain the varied sensitivity to this drug among cancer patients.

Understanding the mechanism of action of existing anti-cancer drugs is equally important as discovering new ones. Varied resistance and sensitivities to current therapies has always been a challenge and delineating the molecular basis for this variation is valuable in the quest for personalized cancer therapy. A great example for this was demonstrated through vorinostat, a drug that showed significant success in reducing brain metastases particular experienced by TNBC patients. The known mechanism-of-action for vorinostat was its action as a histone-modifying agent [137]. Palmier and colleagues demonstrated that decreased RAD52 expression augments vorinostat's action by promoting accumulation of unrepaired DSBs [138].

In clinical literature, P2 was reported to have the highest anti-cancer activity in patients with BRCAness. There is a generally accepted mechanism of action for P2 that does not address the varied sensitivity in BRCA-deficient tumors. Interestingly, there are reported efforts to sensitize other non BRCA-deficient subtypes of breast cancers to P2 through targeting other DNA repair pathways. Accordingly, we anticipate that our research will explain a new mechanism-of-action in which the success in P2 use with BRCA-deficient breast or ovarian cancer patients might be attributed to the synthetic lethality achieved by inhibition of RAD52 activity.

We will further characterize the eleven potential SMIs, particularly the strongest five, by *in vivo* and *in vitro* experiments. Additional future work will include determining the protein partner binding (RPA or RAD52) and the affinity of binding. We will also use protein painting method and crystallography to further understanding binding pockets and interacting residues [139]. With the knowledge we have of interacting domains of RPA on RAD52, we plan to link the best of the SMI with each other or with other published

SMIs which inhibit binding directly to ssDNA to achieve more specific binding and selective targeting of RAD52.

Appendix I.

RAD52 peptides design and analysis in the FluorIA

Introduction

The RPA32(172-270) wHLH region is known to be a site for PPI. The interaction interfaces of UNG2, XPA, and RAD52 with this region has been examined by NMR analyses. Residues of UNG2 protein involved in long-range Nuclear Overhauser enhancements (NOEs) were aligned with corresponding residues of XPA and RAD52 [121]. We used the RAD52(257-274) from this group plus an additional eleven RAD52 peptides based on analyses of the RAD52(1-212) crystal structure in the FluorIA assay to further investigate the overall RAD52:RPA interaction domains. The rational for peptides was that this is a route frequently used to find PPI inhibitors.

Method

RAD52 peptides. Eleven RAD52 peptides were designed and purchased (China peptide) (Table A1.1, peptides 1-11). The full RAD52(257-274) peptide was obtained as well (GenScript) (Table A1.1, peptide 12). A stock was made at of RAD52(257-274) at10 mM using nuclease-free water and stored frozen at -20 °C. All other peptides were peptides were diluted to 10 mM using DMSO and stored frozen at -20 °C.

Two peptides (260-RQKQQQFR-269 and 253-ATHQRKLRQK-262) were generated from NMR analysis where UNG2 residues involved in intermolecular NOE signals were assigned, and the corresponding alignments with RAD52(257-274) were determined for interaction with RPA32(172-270) [121]. An additional peptide (269-RERMEKQQVR-278) was made from the last segment of RAD52(257-274). The remaining eight peptides were designed from structural analysis of the self-association domain of RAD52 [119].

Table A1.1 The sequences RAD52 peptides

Peptide	Amino acid sequence	Rational for design
Peptide 1	34-EEYQAIQKAL-43	RAD52 self-association
Peptide 2	42-ALRQRLGPEY-51	
Peptide 3	69-HRVINLANEM-78	
Peptide 4	81-YNGWAHSITQQ-91	
Peptide 5	115-LKDGSYHEDV-124	
Peptide 6	141-KARKEAVTDG-150	
Peptide 7	167-LDKDYLRS-174	
Peptide 8	191-AKRQDKEPSV-200	
Peptide 9	253-ATHQRKLRQK-262	RPA-binding domain
Peptide 10	260-RQKQLQQQFR-269	
Peptide 11	269-RERMEKQQVR-278	
Peptide 12	257-RKLRQKQLQQQFRERMEK-274)	RPA binding region

RAD52 short peptides with labeled as P1-P11 with their amino acid sequences. RAD52(257-274) peptide labeled P12.

Screening peptides by FluorIA. Each peptide was added first to a single well of the FluorIA reaction as an inhibitor at 100 and 10 μM in the same manner described Chapter 2 (Figure A1.1). Additional FluorIA assays were done with peptide combinations to look for any potential synergetic inhibitory effects. The final concentration of each peptide in the synergy reaction was 50 μM per well. The layout for the experiment is shown in Figure A1.2. This experiment will be redone at 100 μM in the future.

Results

In FluorIA, peptide1-11 was added at 10 or 100 μM in the hope of detecting an inhibitory effect. No signal reduction was detected from any single peptide (Figure A1.1) or synergy combination of two peptides per well at 50 μM (Figure A1.2).

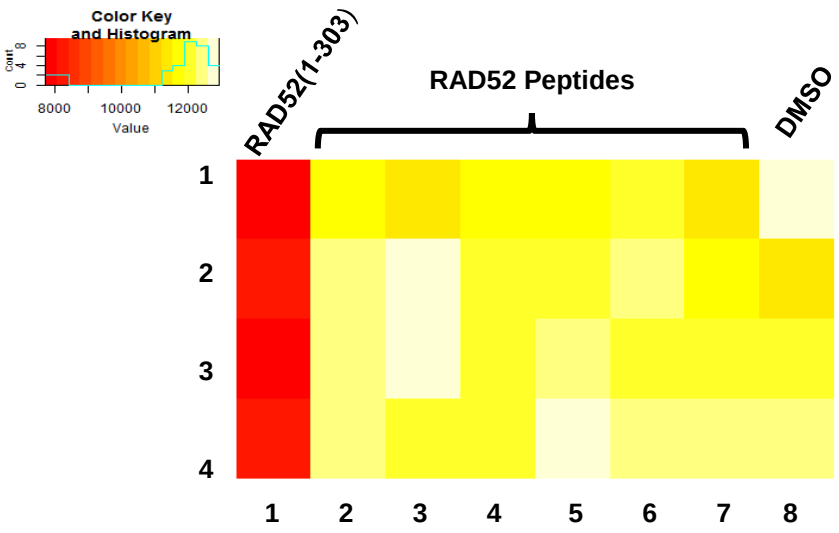
Color Key
and Histogram
Count
0
4
8
8000
10000
12000
Value
RAD52(1-303)
RAD52 Peptides
DMSO
1
2
3
4
1
2
3
4
5
6
7
8

Figure A1.1 FluorIA results with RAD52 peptides in singles. Heat map created by R studio using FluorIA data testing each of the RAD52 peptides as potential SMIs for RAD52:RPA interaction. The red colored column (column 1) has low RFU readings as a result of inhibition by Rad52(1-303) and servers as a positive control. The eleven peptides are laid out horizontally row 1-7 (row 1 and 2) with 10 μM on top and 100 μM in the bottom (row 3 and 4). Column 8 is a negative control.

	1	2	3	4	5	6	7	8	9	10	11
1	P1:P1	P1:P2	P1:P3	P1:P4	P1:P5	P1:P6	P1:P7	P1:P8	P1:P9	P1:P10	P1:P11
2	P2:P1	P2:P2	P2:P3	P2:P4	P2:P5	P2:P6	P2:P7	P2:P8	P2:P9	P2:P10	P2:P11
3	P3:P1	P3:P2	P3:P3	P3:P4	P3:P5	P3:P6	P3:P7	P3:P8	P3:P9	P3:P10	P3:P11
4	P4:P1	P4:P2	P4:P3	P4:P4	P4:P5	P4:P6	P4:P7	P4:P8	P4:P9	P4:P10	P4:P11
5	P5:P1	P5:P2	P5:P3	P5:P4	P5:P5	P5:P6	P5:P7	P5:P8	P5:P9	P5:P10	P5:P11
6	P6:P1	P6:P2	P6:P3	P6:P4	P6:P5	P6:P6	P6:P7	P6:P8	P6:P9	P6:P10	P6:P11
7	P7:P1	P7:P2	P7:P3	P7:P4	P7:P5	P7:P6	P7:P7	P7:P8	P7:P9	P7:P10	P7:P11
8	P8:P1	P8:P2	P8:P3	P8:P4	P8:P5	P8:P6	P8:P7	P8:P8	P8:P9	P8:P10	P8:P11
9	P9:P1	P9:P2	P9:P3	P9:P4	P9:P5	P9:P6	P9:P7	P9:P8	P9:P9	P9:P10	P9:P11
10	P10:P1	P10:P2	P10:P3	P10:P4	P10:P5	P10:P6	P10:P7	P10:P8	P10:P9	P10:P10	P10:P11
11	P11:P1	P11:P2	P11:P3	P11:P4	P11:P5	P11:P6	P11:P7	P11:P8	P11:P9	P11:P10	P11:P11

Figure A1.2 RAD52 peptide synergy analysis. RAD52 peptides screened as small molecule inhibitors in pairs according to the FluorIA method described in Chapter 1. The final concentration of each peptide in a well is 50 μM.

Appendix II

Additional cell lines for survival analysis with candidate hits

Cancer cell lines

1) **EUF423 cell line.** This cell line contains biallelic truncation of the COOH-terminal region of both *BRCA2* genes also obtained from Dr. Simon Powell along with restored BRCA2 line. The stable transfection procedures along with culturing conditions for each cell line are described in Treszezamsky *et al*., [140].

2) **Capan-1 cell lines.** Three Capan-1 cell lines were also tested with our hits: BRCA2 mutant Capan-1-neo, empty vector, and is BRCA2-corrected Capan-1-236-BRCA2. These lines were cultured in DMEM with glutamine, supplemented with 20% FBS, 100U/mL penicillin, 100ug/mL streptomycin.

Western Blot. Cell lysates were separated by 6% SDS-PAGE and BRCA1, BRCA2, HA-tagged BRCA1 were analyzed by western blots. The Antibodies (Abs) used are: affinity purified rabbit anti-BRCA1 Ab (Bethyl, #A301-377A), anti-BRCA2 (Ab-1) mouse monoclonal clone 2B (EMD Millipore, OP95), ECL anti-rabbit IgG-HRP HA (GE Life Sciences, #NA934), and ECL anti-mouse IgG-HPR (GE Life Sciences, #NA931). Bands were detected using ECL Clarity (BioRad).

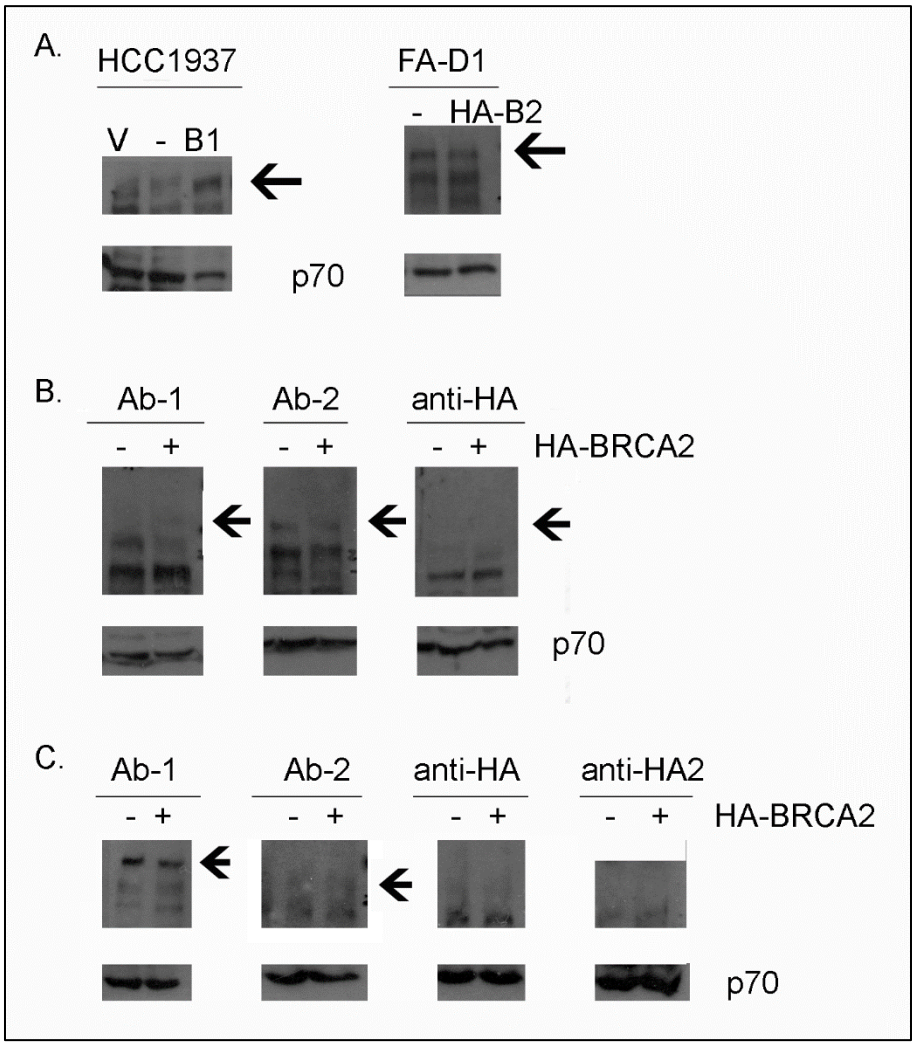
A.
HCC1937
FA-D1
V - B1
- HA-B2
p70
B.
Ab-1
Ab-2
anti-HA
- + - + - +
HA-BRCA2
p70
C.
Ab-1
Ab-2
anti-HA
anti-HA2
- + - + - + - +
HA-BRCA2
p70

Figure A2.1 Western blot analysis for BRCA1 and BRCA2 status in HCC1937 and EUFA432 cell lines. (A) Left: HCC1937 corrected (3rd lane labeled B1) show a band for BRCA1. None was detected in empty vector (labeled as "V") or parental line (labeled as "-"). Right: EUFA423 cell line showed a BRCA1 band in both parental (labeled as "-") and corrected (labeled as HA-B2). (B and C) Repeats of the EUFA423 lines listed above with two regular anti-BRCA2 antibodies and two anti-HA antibodies. The results show that the corrected EUFA423 might have lost its BRCA2 insert plasmid. Upon treatment with P1, P2, and P3; no difference in survival was observed. The level of BRCA2 expression could be have been sufficient to rescue cellular phenotype.

Results

No difference was observed in survival upon treatment of parental or BRCA1/2 plasmid-inserted derivative of Capan-1 or EUFA423 cell lines respectively. A western blot analysis revealed residual BRCA2 in EUFA423 that might have contributed to equal survival (Figure A2.1B and C).

Non-cancer CRISPR-generated BRCA2 mutant cell lines.

HeLa-DR cell line that was specifically designed homology-mediated gene conversion (HR) was used to generate BRCA2 mutants by CRISPR/Cas9 technology. Expression of BRCA2 in CRISPR-generated BRCA2 mutants. Whole cell lysate was prepared from each cell line and the levels of BRCA2 protein were examined by western blots. A large subunit of RPA, p70, was used as loading control. A parental HeLa-DR that contains wild type BRCA2 and two BRCA2 mutants: g2-10 and g2-37. Each cell line was seeded at 300 cells/well in 24-well plates and grew overnight. The cells were treated with the indicated concentrations of MMC for one day. After removing MMC, the cells were grown in fresh medium for 4-5 days until colonies formed. The cells were stained by crystal violet, the numbers of colonies were counted, and surviving fraction was determined. A HeLa-derived cell line, HeLa-DR-13-9 (a generous gift from Dr. Jeffrey Parvin at the Ohio State University) was used to measure HR activity. Each cell line was seeded at 3×10^4 cells per well in 12-well plates one day before transfection. The cells were transfected by the expression plasmid of I-SceI endonclease (a generous gift from Dr. Maria Jasin at Memorial Sloan Kettering Cancer Center) to induce DSBs. On the third day of the transfection, the HR activity (scored as GFP positive cells) was determined by FACS.

Results

The effect of treatment with P1, P2, and P3 on wt.HeLa (DR) and the BRCA2 mutants' survival was examined in the same manner described above with cancer cell lines. However, due to reported higher sensitivity of HeLa cell lines to DNA-damaging agents treatment with lower doses of concentration series were done. As seen in Figure A2.2, treatment with P3 showed the most sensitivity compared with treatment of P2 while treatment with P1 impact the wt.HeLa line and higher concentration series of it was needed to observe the effect.

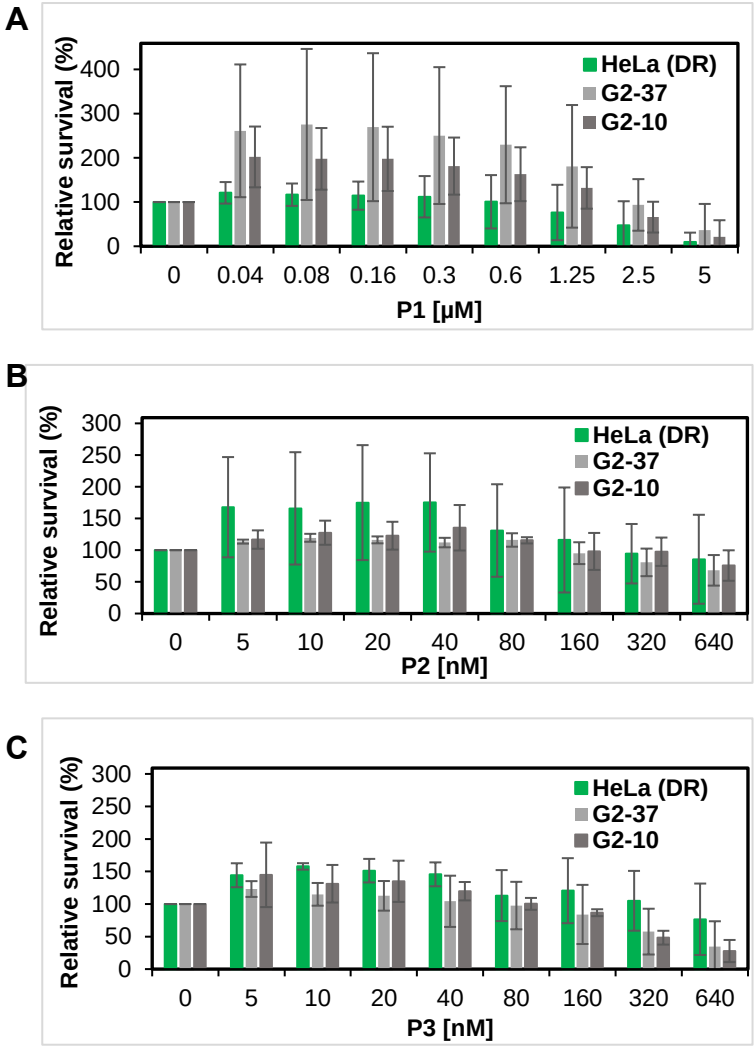
A
Relative survival (%)
400
300
200
100
0
HeLa (DR)
G2-37
G2-10
0
0.04
0.08
0.16
0.3
0.6
1.25
2.5
5
P1 [μM]
B
Relative survival (%)
300
250
200
150
100
50
0
HeLa (DR)
G2-37
G2-10
0
5
10
20
40
80
160
320
640
P2 [nM]
C
Relative survival (%)
300
250
200
150
100
50
0
HeLa (DR)
G2-37
G2-10
0
5
10
20
40
80
160
320
640
P3 [nM]

Figure A2.2 CRISPR-generated BRCA2 mutants HeLa-DR, BRCA2 mutants. The g2-10, BRCA2 mutant g2-37 were treated with increasing concentrations of (A) P1, (B) P2 and (C) P3 and incubated for three days at 37°C. PrestoBlue reagent was used to assess the viabilities of the treated cells as detailed in Material and methods, and the obtained results were normalized to vehicle control.

Appendix III

Development of SSA activity assay

Introduction

Sugiyama and co-workers exploited the selective binding of DAPI dsDNA to fluorescently follow the annealing activity of a Rad52:RPA complex in the presence of a heat-denatured DNA plasmid [75]. Their work demonstrated the important role for RPA in promoting SSA activity of RAD52. Given our great interest in RAD52 interaction with RPA, we developed a similar but more robust SSA activity assay employing longer DNA in the reaction, human proteins, and a much more sensitive method of detection (SYBR Dyes) that exhibits >1000-fold fluorescence enhancement upon binding to nucleic acids and has a high quantum yield (~0.6) upon binding to ds or ssDNA [141].

Method

Purified 8D-RPA and RAD52 (Figure A3.1 A and B respectively) were used in this assay. Purification for each followed the same protocol detailed in Chapter 2. A 50 ng of pBlueScript KS(+/-) plasmid DNA linearized by ScaI (dsDNA) and heat-denatured linearized (hdDNA). The hdDNA was preincubated with 8D-RPA for one hour before the addition of RAD52 in a 1:2 ratio. The products were separated by 1% agarose gel (100 voltage for 1 hour and 40 minutes in 1x TAE buffer). SYBR stains (SYBR Green for dsDNA and SYBR Gold for both dsDNA and ssDNA, Molecular Probes) were diluted in 1x TAE buffer according to manufacturer instructions and used to stain the gels for 20 minutes before washing 2x with ddH2O and imaging with Safe Imager 2.0 (Invitrogen).

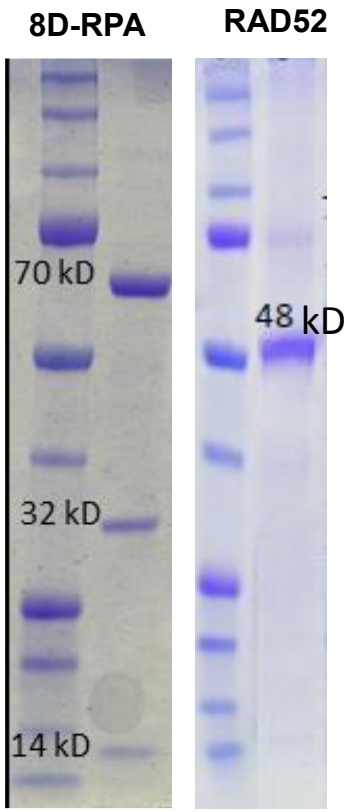
8D-RPA
RAD52
70 kD
32 kD
14 kD
48 kD

Figure A3.1 SDS-PAGE gel of purified protein constructs. A) Purified hetero-trimeric 8D-RPA. B) Different constructs of RAD52 shown from left to right: full length RAD52, full-length RAD52 with an EGFP tag, and RAD52(1-212) construct.

Results

We observed the characteristic hdDNA band at about ~2900 base pair (Figure A3.2, red box) disappeared in the presence of 8D-RPA and a band above the 10,000 base-pair mark appeared, (Figure A3.2, blue box), indicating multiple RPAs binding to the ssDNA. RAD52:DNA cpmplex have been noted to accumulate as large molecular weight aggregates in the gel wells [142]. Our result confirms this phenomoneon, as seen in the last four lanes containing decreasing concentrations of RAD52 added to an RPA-bound ssDNA. Nevertheless, we demonstrated the annealing of the plasmid as indicated by the dose-related reappearance of the dsDNA at its expected size of 3500 bp. We will use this assay to test the effect of RPA phosphorylation and candidate SMIs on RAD52 activity.

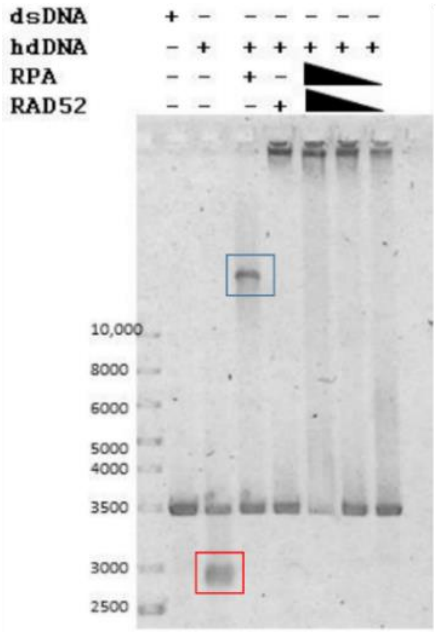
dsDNA + – – – – – –
hdDNA – + + + + + +
RPA – – + –
RAD52 – – – +
10,000
8000
6000
5000
4000
3500
3000
2500

Figure A3.2 RAD52 SSA assay. Gel based assay using 8D-RPA and RAD52. The gel was stained with SYBR Gold and our interpretation was confirmed with SYBR Green (not shown).

Appendix IV

8D-RPA SAXS analysis

Introduction

RPA is phosphorylated in a cell cycle-dependent manner to regulate its interaction with DNA and protein partners. Specific phosphorylation events on multiple serine residues of RPA32 subunit as this site is a hub for PPI, including RAD52. An RPA phosphmimic was created by Wolds and co-workers to mimic hyperphosphorylated RPA. It contains the following mutations on RPA32: S8D, S11D, S12D, S13D, T21D, S25D, S29D, and S33D.

It has not been possible to obtain full structural data on RPA using crystallography or NMR due to flexible nature of the regions linking the different domains. Here we used SAXS to analyze an overall low-resolution structural measurement of 8DRPA.

Methods

The plasmid for 8D RPA was a generous gift from Dr. Marc Wolds. Transformation was done into Rosetta2(DE3). Expression and growth were the same as described for RPA in chapter 2 with the addition of purification using size exclusion column with 300 mM KCl in HI-0 buffer described in Chapter 2. Fractions were then collected individually and assessed by DLS for monodispersity.

Two monodispersed samples were obtained, and concentrations were determined by NanoDrop1000. The two samples were concentrated separately using spin concentrators (30,000 MWCO) achieving 6 mg/mL and 8 mg/mL. The flow-through resulting from the concentration process was collected to use as blank buffer in SAXS analysis. Column void volume is the buffer volume before the elution of the protein in the size exclusion purification step was also collected for the same purpose.

Images were collected for 1.5 hours at room temperature on Rigaku BioSAXS 1000 system with an FR-E rotating anode X-ray generator (λ= 1.54 Å). Resulting data were processed using Automated Analysis Pipline in SAXSLab software which provides a GUI for the ARSAS Package (Rigaku). The buffer effect was automatically subtracted by the software and the Guinier plot, radius of gyration, molecular weight and volume, pair distribution function, Kratky plot, an infinite dilution scattering curve, and *ab initio* bead model fits to the data were calculated as well. Finally, Dmax was calculated from the X-intercept of the P(r) curve were calculated. Models were generated using PyMOL (SchrÖdinger, LLC).

Results and discussion

SAXS is a low-resolution technique that is of great value to obtain an overall shape and dimension data that can be paired with higher resolution structural data from crystallography or NMR techniques. It is also a feasible technique to analyze full-length proteins in solution [143]. At the time of this investigation, we had the 8DRPA expression and purification resolved and therefore was used in the SAXS analysis. We anticipated no difference from the wild-type RPA. The data were collected over two concentrations: 6 and 8mg/mL that were checked for monodispersity using DLS.

The scattering pattern indicate q of about 0.2 demonstrating less noise and good quality data at the concentrations analyzed (Figure A4.1 A). Using the Guinier approximation and scattering data, the radius of gyration (Rg) was obtained and reported in table A4.1. Kratky plot shown in figure A3.1B indicates partial folding as the curves increase at higher q values after reaching a peak. Finally, maximum dimensions (Dmax)

(Table A4.1) was calculated from the probability distribution function, P(r), plot (Figure A4.1C). The maximum dimension for 8DRPA seems to be around 175 Å.

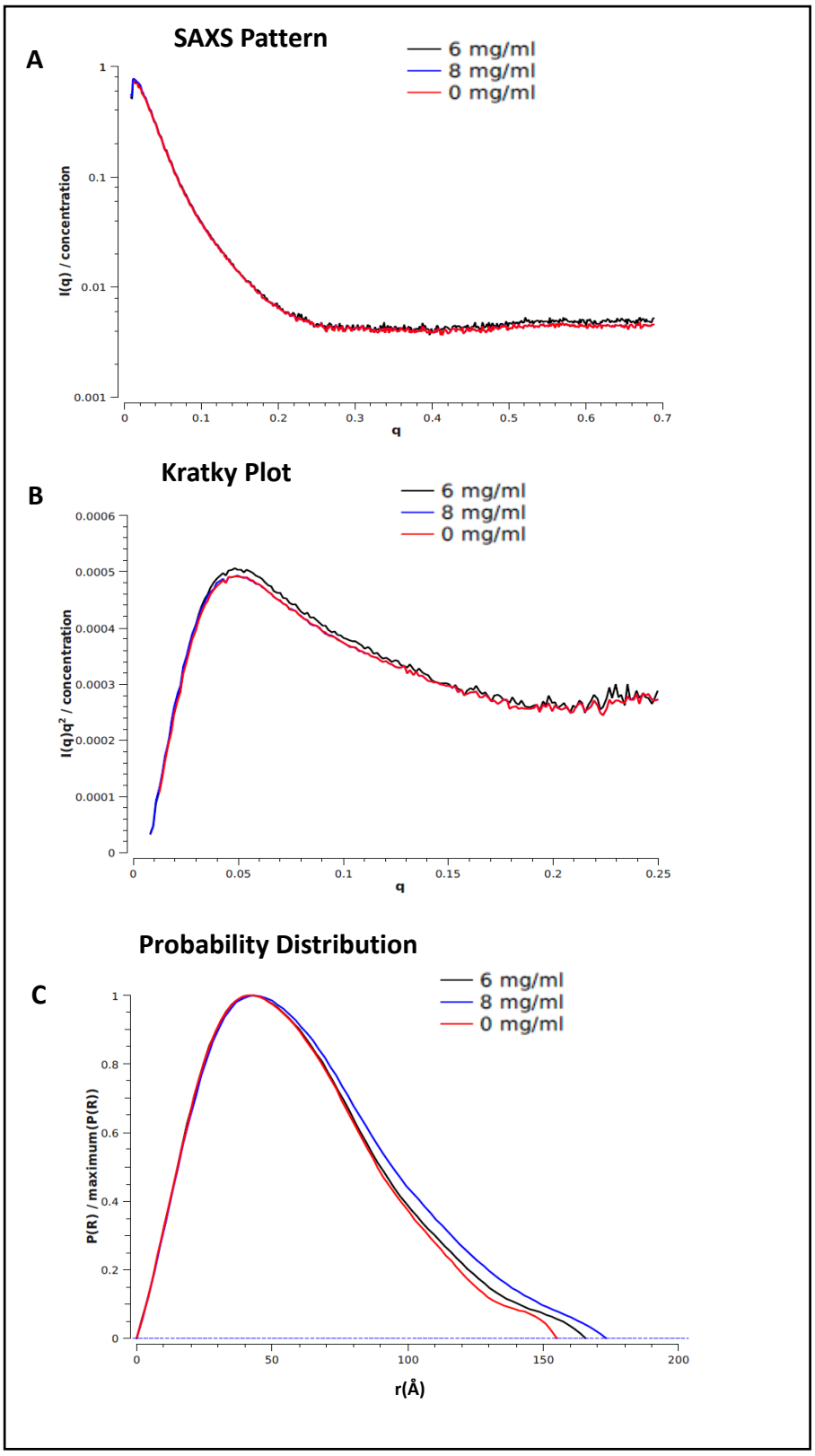
A
SAXS Pattern
6 mg/ml
8 mg/ml
0 mg/ml
I(q) / concentration
q
B
Kratky Plot
6 mg/ml
8 mg/ml
0 mg/ml
I(q)q² / concentration
q
C
Probability Distribution
6 mg/ml
8 mg/ml
0 mg/ml
P(R) / maximum(P(R))
r(Å)

Figure A4.1 SAXS profile data for 8DRPA. A) SAXS scattering, B) Kratky plot, C) probability distribution of 8DRPA at the two different concentrations analyzed.

Table A4.1 Predictions of 8DRPA dimension values.

8DRPA concentration (mg/mL)	Rg	D_{max}
6	49	166
8	51	173

SAXSLab software calculation of the radius of gyration (Rg) using the SAXS scattering pattern and maximum dimension (Dmax) using from the x-intercept of the P(r) curve.

The relative topology of 8DRPA is demonstrated by the *Ab initio* bead models that were fit to the P(r) function. The molecular envelop shows an extended structure for the most parts of the protein with semi-globular conformation in most of the central and terminal region (Figure A4.2).

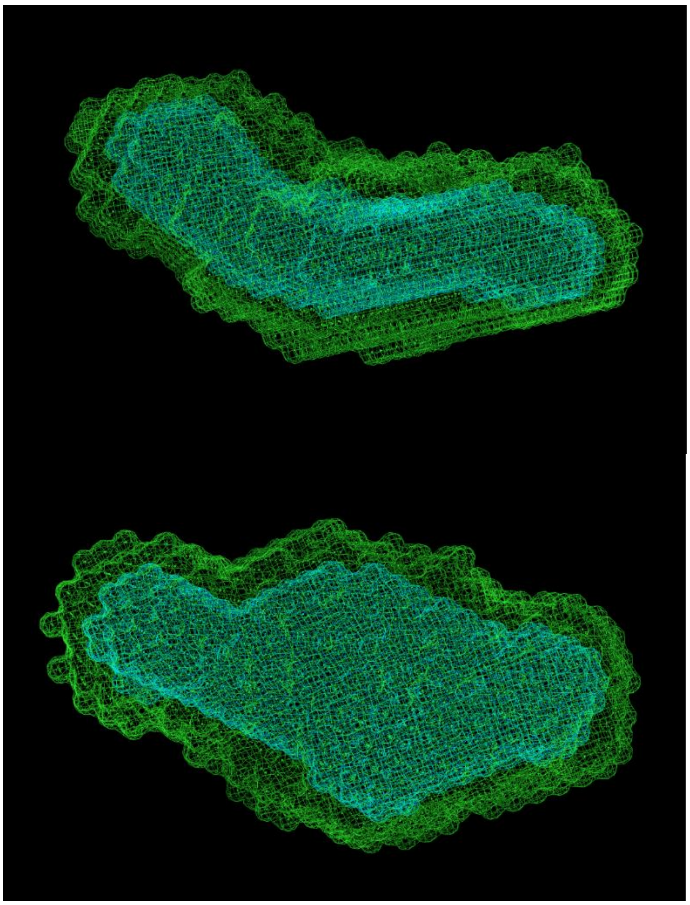

Front view

Side view

Figure A4.2 SAXS model for 8DRPA.

Ab initio bead models to predict the molecular envelop of full-length 8DRPA.

References

1. Heldt, F.S., et al., *A comprehensive model for the proliferation-quiescence decision in response to endogenous DNA damage in human cells.* Proc Natl Acad Sci U S A, 2018. **115**(10): p. 2532-2537.
2. Bakkenist, C.J. and M.B. Kastan, *DNA damage activates ATM through intermolecular autophosphorylation and dimer dissociation.* Nature, 2003. **421**(6922): p. 499-506.
3. Sun, Y., et al., *DNA damage-induced acetylation of lysine 3016 of ATM activates ATM kinase activity.* Mol Cell Biol, 2007. **27**(24): p. 8502-9.
4. Kozlov, S.V., et al., *Autophosphorylation and ATM activation: additional sites add to the complexity.* J Biol Chem, 2011. **286**(11): p. 9107-19.
5. Jackson, S.P. and J. Bartek, *The DNA-damage response in human biology and disease.* Nature, 2009. **461**(7267): p. 1071-8.
6. Hoeijmakers, J.H., *DNA damage, aging, and cancer.* N Engl J Med, 2009. **361**(15): p. 1475-85.
7. Vamvakas, S., E.H. Vock, and W.K. Lutz, *On the role of DNA double-strand breaks in toxicity and carcinogenesis.* Crit Rev Toxicol, 1997. **27**(2): p. 155-74.
8. Ranjha, L., S.M. Howard, and P. Cejka, *Main steps in DNA double-strand break repair: an introduction to homologous recombination and related processes.* Chromosoma, 2018.
9. Rothkamm, K., et al., *Pathways of DNA double-strand break repair during the mammalian cell cycle.* Mol Cell Biol, 2003. **23**(16): p. 5706-15.
10. Saleh-Gohari, N. and T. Helleday, *Conservative homologous recombination preferentially repairs DNA double-strand breaks in the S phase of the cell cycle in human cells.* Nucleic Acids Res, 2004. **32**(12): p. 3683-8.
11. Karanam, K., *Quantitative live cell imaging reveals a gradual shift between DNA repair mechanisms and a maximal use of HR in mid S phase.* Molecular cell, 2012. **47**(2): p. 320-329.
12. Stark, J.M., et al., *Genetic steps of mammalian homologous repair with distinct mutagenic consequences.* Mol Cell Biol, 2004. **24**(21): p. 9305-16.
13. Hanahan, D. and R.A. Weinberg, *Hallmarks of cancer: the next generation.* Cell, 2011. **144**(5): p. 646-74.
14. Flavahan, W.A., E. Gaskell, and B.E. Bernstein, *Epigenetic plasticity and the hallmarks of cancer.* Science, 2017. **357**(6348).
15. Kunkel, T.A. and K. Bebenek, *DNA replication fidelity.* Annu Rev Biochem, 2000. **69**: p. 497-529.
16. Davis, L. and N. Maizels, *Two Distinct Pathways Support Gene Correction by Single-Stranded Donors at DNA Nicks.* Cell Rep, 2016. **17**(7): p. 1872-1881.
17. Polyak, K. and J. Garber, *Targeting the missing links for cancer therapy.* Nat Med, 2011. **17**(3): p. 283-4.
18. Ciriello, G., et al., *Emerging landscape of oncogenic signatures across human cancers.* Nat Genet, 2013. **45**(10): p. 1127-33.
19. Hironaka, K., et al., *Dysregulation of DNA repair pathways in a transforming growth factor alpha/c-myc transgenic mouse model of accelerated hepatocarcinogenesis.* Lab Invest, 2003. **83**(5): p. 643-54.
20. Maacke, H., et al., *Over-expression of wild-type Rad51 correlates with histological grading of invasive ductal breast cancer.* Int J Cancer, 2000. **88**(6): p. 907-13.
21. Kato, M., et al., *Identification of Rad51 alteration in patients with bilateral breast cancer.* J Hum Genet, 2000. **45**(3): p. 133-7.

22. Thomas, G., et al., *A multistage genome-wide association study in breast cancer identifies two new risk alleles at 1p11.2 and 14q24.1 (RAD51L1).* Nat Genet, 2009. **41**(5): p. 579-84.
23. Cancer Genome Atlas Research, N., *Integrated genomic analyses of ovarian carcinoma.* Nature, 2011. **474**(7353): p. 609-15.
24. Hopkins, B.B. and T.T. Paull, *The P. furiosus mre11/rad50 complex promotes 5' strand resection at a DNA double-strand break.* Cell, 2008. **135**(2): p. 250-60.
25. Oakley, G.G. and S.M. Patrick, *Replication protein A: directing traffic at the intersection of replication and repair.* Front Biosci (Landmark Ed), 2010. **15**: p. 883-900.
26. Carra, C. and F.A. Cucinotta, *Accurate prediction of the binding free energy and analysis of the mechanism of the interaction of replication protein A (RPA) with ssDNA.* J Mol Model, 2012. **18**(6): p. 2761-83.
27. Audry, J., et al., *RPA prevents G-rich structure formation at lagging-strand telomeres to allow maintenance of chromosome ends.* EMBO J, 2015. **34**(14): p. 1942-58.
28. Baumann, P., *Human Rad51 protein promotes ATP-dependent homologous pairing and strand transfer reactions in vitro.* Cell (Cambridge), 1996. **87**(4): p. 757-766.
29. Tarsounas, M., D. Davies, and S.C. West, *BRCA2-dependent and independent formation of RAD51 nuclear foci.* Oncogene, 2003. **22**(8): p. 1115-23.
30. Chen, J., et al., *Stable interaction between the products of the BRCA1 and BRCA2 tumor suppressor genes in mitotic and meiotic cells.* Mol Cell, 1998. **2**(3): p. 317-28.
31. Scully, R., et al., *Association of BRCA1 with Rad51 in mitotic and meiotic cells.* Cell, 1997. **88**(2): p. 265-75.
32. Paull, T.T., et al., *Direct DNA binding by Brca1.* Proc Natl Acad Sci U S A, 2001. **98**(11): p. 6086-91.
33. Moynahan, M.E., et al., *Brca1 controls homology-directed DNA repair.* Mol Cell, 1999. **4**(4): p. 511-8.
34. Lord, C.J. and A. Ashworth, *BRCAness revisited.* Nat Rev Cancer, 2016. **16**(2): p. 110-20.
35. Durant, S.T. and J.A. Nickoloff, *Good timing in the cell cycle for precise DNA repair by BRCA1.* Cell Cycle, 2005. **4**(9): p. 1216-22.
36. Liu, J., et al., *Human BRCA2 protein promotes RAD51 filament formation on RPA-covered single-stranded DNA.* Nat Struct Mol Biol, 2010. **17**(10): p. 1260-2.
37. Liu, Y. and S.C. West, *Distinct functions of BRCA1 and BRCA2 in double-strand break repair.* Breast Cancer Res, 2002. **4**(1): p. 9-13.
38. Miki, Y., et al., *A strong candidate for the breast and ovarian cancer susceptibility gene BRCA1.* Science, 1994. **266**(5182): p. 66-71.
39. Wooster, R., et al., *Identification of the breast cancer susceptibility gene BRCA2.* Nature, 1995. **378**(6559): p. 789-92.
40. Liede, A., B.Y. Karlan, and S.A. Narod, *Cancer risks for male carriers of germline mutations in BRCA1 or BRCA2: a review of the literature.* J Clin Oncol, 2004. **22**(4): p. 735-42.
41. Breast Cancer Linkage, C., *Cancer risks in BRCA2 mutation carriers.* J Natl Cancer Inst, 1999. **91**(15): p. 1310-6.
42. Casarsa, S., et al., *BRCA2 germline mutations in primary cancer of the fallopian tube.* Oncol Rep, 2004. **12**(2): p. 313-6.
43. Johannsson, O., et al., *Incidence of malignant tumours in relatives of BRCA1 and BRCA2 germline mutation carriers.* Eur J Cancer, 1999. **35**(8): p. 1248-57.
44. Howlett, N.G., et al., *Biallelic inactivation of BRCA2 in Fanconi anemia.* Science, 2002. **297**(5581): p. 606-9.

45. Garcia-Higuera, I., et al., *Interaction of the Fanconi anemia proteins and BRCA1 in a common pathway.* Mol Cell, 2001. **7**(2): p. 249-62.
46. Lobitz, S. and E. Velleuer, *Guido Fanconi (1892-1979): a jack of all trades.* Nat Rev Cancer, 2006. **6**(11): p. 893-8.
47. Konstantinopoulos, P.A., et al., *Gene expression profile of BRCAness that correlates with responsiveness to chemotherapy and with outcome in patients with epithelial ovarian cancer.* J Clin Oncol, 2010. **28**(22): p. 3555-61.
48. Turner, N., A. Tutt, and A. Ashworth, *Hallmarks of 'BRCAness' in sporadic cancers.* Nat Rev Cancer, 2004. **4**(10): p. 814-9.
49. Domagala, P., et al., *BRCA1/2-negative hereditary triple-negative breast cancers exhibit BRCAness.* Int J Cancer, 2017. **140**(7): p. 1545-1550.
50. George, S.H. and P. Shaw, *BRCA and Early Events in the Development of Serous Ovarian Cancer.* Front Oncol, 2014. **4**: p. 5.
51. Andreopoulou, E., et al., *Therapies for triple negative breast cancer.* Expert Opin Pharmacother, 2015. **16**(7): p. 983-98.
52. Kroeger, P.T., Jr. and R. Drapkin, *Pathogenesis and heterogeneity of ovarian cancer.* Curr Opin Obstet Gynecol, 2017. **29**(1): p. 26-34.
53. McIlwraith, M.J., et al., *Reconstitution of the strand invasion step of double-strand break repair using human Rad51 Rad52 and RPA proteins.* J Mol Biol, 2000. **304**(2): p. 151-64.
54. Yamaguchi-Iwai, Y., et al., *Homologous recombination, but not DNA repair, is reduced in vertebrate cells deficient in RAD52.* Mol Cell Biol, 1998. **18**(11): p. 6430-5.
55. Rijkers, T., et al., *Targeted inactivation of mouse RAD52 reduces homologous recombination but not resistance to ionizing radiation.* Mol Cell Biol, 1998. **18**(11): p. 6423-9.
56. Feng, Z., et al., *Rad52 inactivation is synthetically lethal with BRCA2 deficiency.* Proc Natl Acad Sci U S A, 2011. **108**(2): p. 686-91.
57. New, J.H., et al., *Rad52 protein stimulates DNA strand exchange by Rad51 and replication protein A.* Nature, 1998. **391**(6665): p. 407-10.
58. Lok, B.H., et al., *RAD52 inactivation is synthetically lethal with deficiencies in BRCA1 and PALB2 in addition to BRCA2 through RAD51-mediated homologous recombination.* Oncogene, 2013. **32**(30): p. 3552-8.
59. Lok, B.H. and S.N. Powell, *Molecular pathways: understanding the role of Rad52 in homologous recombination for therapeutic advancement.* Clin Cancer Res, 2012. **18**(23): p. 6400-6.
60. Cramer-Morales, K., et al., *Personalized synthetic lethality induced by targeting RAD52 in leukemias identified by gene mutation and expression profile.* Blood, 2013. **122**(7): p. 1293-304.
61. Hanamshet, K., O.M. Mazina, and A.V. Mazin, *Reappearance from Obscurity: Mammalian Rad52 in Homologous Recombination.* Genes (Basel), 2016. **7**(9).
62. Sullivan, K., et al., *Identification of a Small Molecule Inhibitor of RAD52 by Structure-Based Selection.* PLoS One, 2016. **11**(1): p. e0147230.
63. Huang, F., et al., *Targeting BRCA1- and BRCA2-deficient cells with RAD52 small molecule inhibitors.* Nucleic Acids Res, 2016. **44**(9): p. 4189-99.
64. Hengel, S.R., et al., *Small-molecule inhibitors identify the RAD52-ssDNA interaction as critical for recovery from replication stress and for survival of BRCA2 deficient cells.* Elife, 2016. **5**.

65. Hengel, S.R., M.A. Spies, and M. Spies, *Small-Molecule Inhibitors Targeting DNA Repair and DNA Repair Deficiency in Research and Cancer Therapy.* Cell Chem Biol, 2017. **24**(9): p. 1101-1119.
66. Sotiriou, S.K., et al., *Mammalian RAD52 Functions in Break-Induced Replication Repair of Collapsed DNA Replication Forks.* Mol Cell, 2016. **64**(6): p. 1127-1134.
67. Mijic, S., et al., *Replication fork reversal triggers fork degradation in BRCA2-defective cells.* Nat Commun, 2017. **8**(1): p. 859.
68. Wray, J., et al., *Distinct RAD51 associations with RAD52 and BCCIP in response to DNA damage and replication stress.* Cancer Res, 2008. **68**(8): p. 2699-707.
69. Deniz, M., et al., *Increased single-strand annealing rather than non-homologous end-joining predicts hereditary ovarian carcinoma.* Oncotarget, 2017. **8**(58): p. 98660-98676.
70. Zhang, W., et al., *Alu distribution and mutation types of cancer genes.* BMC Genomics, 2011. **12**: p. 157.
71. Bennardo, N., et al., *Alternative-NHEJ is a mechanistically distinct pathway of mammalian chromosome break repair.* PLoS Genet, 2008. **4**(6): p. e1000110.
72. Mazina, O.M., et al., *Rad52 Inverse Strand Exchange Drives RNA-Templated DNA Double-Strand Break Repair.* Mol Cell, 2017. **67**(1): p. 19-29 e3.
73. Lieberman, R., et al., *Rad52 deficiency decreases development of lung squamous cell carcinomas by enhancing immuno-surveillance.* Oncotarget, 2017. **8**(21): p. 34032-34044.
74. Chandramouly, G., et al., *Small-Molecule Disruption of RAD52 Rings as a Mechanism for Precision Medicine in BRCA-Deficient Cancers.* Chem Biol, 2015. **22**(11): p. 1491-504.
75. Sugiyama, T., J.H. New, and S.C. Kowalczykowski, *DNA annealing by RAD52 protein is stimulated by specific interaction with the complex of replication protein A and single-stranded DNA.* Proc Natl Acad Sci U S A, 1998. **95**(11): p. 6049-54.
76. Seroussi, E. and S. Lavi, *Replication protein A is the major single-stranded DNA binding protein detected in mammalian cell extracts by gel retardation assays and UV cross-linking of long and short single-stranded DNA molecules.* J Biol Chem, 1993. **268**(10): p. 7147-54.
77. Wyka, I.M., et al., *Replication protein A interactions with DNA: differential binding of the core domains and analysis of the DNA interaction surface.* Biochemistry, 2003. **42**(44): p. 12909-18.
78. Plate, I., et al., *Interaction with RPA is necessary for Rad52 repair center formation and for its mediator activity.* J Biol Chem, 2008. **283**(43): p. 29077-85.
79. Deng, X., et al., *Human replication protein A-Rad52-single-stranded DNA complex: stoichiometry and evidence for strand transfer regulation by phosphorylation.* Biochemistry, 2009. **48**(28): p. 6633-43.
80. Stefan, E., J. Troppmair, and K. Bister, *Targeting the Architecture of Deregulated Protein Complexes in Cancer.* Adv Protein Chem Struct Biol, 2018. **111**: p. 101-132.
81. Radha, G. and S.C. Raghavan, *BCL2: A promising cancer therapeutic target.* Biochim Biophys Acta, 2017. **1868**(1): p. 309-314.
82. Fox, S., et al., *High-throughput screening: update on practices and success.* J Biomol Screen, 2006. **11**(7): p. 864-9.
83. Inglese, J., et al., *High-throughput screening assays for the identification of chemical probes.* Nat Chem Biol, 2007. **3**(8): p. 466-79.
84. Wells, J.A. and C.L. McClendon, *Reaching for high-hanging fruit in drug discovery at protein-protein interfaces.* Nature, 2007. **450**(7172): p. 1001-9.

85. Laraia, L., et al., *Overcoming Chemical, Biological, and Computational Challenges in the Development of Inhibitors Targeting Protein-Protein Interactions.* Chem Biol, 2015. **22**(6): p. 689-703.
86. Scott, D.E., et al., *Small molecules, big targets: drug discovery faces the protein-protein interaction challenge.* Nat Rev Drug Discov, 2016. **15**(8): p. 533-50.
87. Mayer, J.P. and R.D. Dimarchi, *Drugging the undruggable.* Chem Biol, 2005. **12**(8): p. 860-1.
88. Murray, J.K. and S.H. Gellman, *Targeting protein-protein interactions: lessons from p53/MDM2.* Biopolymers, 2007. **88**(5): p. 657-86.
89. Villoutreix, B.O., et al., *Drug-Like Protein-Protein Interaction Modulators: Challenges and Opportunities for Drug Discovery and Chemical Biology.* Mol Inform, 2014. **33**(6-7): p. 414-437.
90. Arkin, M.R., Y. Tang, and J.A. Wells, *Small-molecule inhibitors of protein-protein interactions: progressing toward the reality.* Chem Biol, 2014. **21**(9): p. 1102-14.
91. Yu, J.L., et al., *NMR-based platform for fragment-based lead discovery used in screening BRD4-targeted compounds.* Acta Pharmacol Sin, 2016. **37**(7): p. 984-93.
92. Wan, K.F., et al., *Differential scanning fluorimetry as secondary screening platform for small molecule inhibitors of Bcl-XL.* Cell Cycle, 2009. **8**(23): p. 3943-52.
93. Du, Y., *Fluorescence polarization assay to quantify protein-protein interactions in an HTS format.* Methods Mol Biol, 2015. **1278**: p. 529-44.
94. Szelag, M., et al., *Identification of STAT1 and STAT3 specific inhibitors using comparative virtual screening and docking validation.* PLoS One, 2015. **10**(2): p. e0116688.
95. Yasui, T., et al., *Discovery of a novel B-cell lymphoma 6 (BCL6)-corepressor interaction inhibitor by utilizing structure-based drug design.* Bioorg Med Chem, 2017. **25**(17): p. 4876-4886.
96. Sameshima, T., et al., *Discovery of an Irreversible and Cell-Active BCL6 Inhibitor Selectively Targeting Cys53 Located at the Protein-Protein Interaction Interface.* Biochemistry, 2018.
97. Moynahan, M.E., A.J. Pierce, and M. Jasin, *BRCA2 is required for homology-directed repair of chromosomal breaks.* Mol Cell, 2001. **7**(2): p. 263-72.
98. Sung, P., *Mediating repair.* Nat Struct Mol Biol, 2005. **12**(3): p. 213-4.
99. Jensen, R.B., A. Carreira, and S.C. Kowalczykowski, *Purified human BRCA2 stimulates RAD51-mediated recombination.* Nature, 2010. **467**(7316): p. 678-83.
100. Liu, J. and W.D. Heyer, *Who's who in human recombination: BRCA2 and RAD52.* Proc Natl Acad Sci U S A, 2011. **108**(2): p. 441-2.
101. Shaheen, M., et al., *Synthetic lethality: exploiting the addiction of cancer to DNA repair.* Blood, 2011. **117**(23): p. 6074-82.
102. Chandramouly, G., et al., *Small-Molecule Disruption of RAD52 Rings as a Mechanism for Precision Medicine in BRCA-Deficient Cancers.* Chem Biol, 2015. **22**(11): p. 1491-1504.
103. Jackson, D., et al., *Analysis of the human replication protein A:Rad52 complex: evidence for crosstalk between RPA32, RPA70, Rad52 and DNA.* J Mol Biol, 2002. **321**(1): p. 133-48.
104. Chatterjee, N. and G.C. Walker, *Mechanisms of DNA damage, repair, and mutagenesis.* Environ Mol Mutagen, 2017. **58**(5): p. 235-263.
105. Srivastava, M., *DNA Double-Strand Break Repair Inhibitors as Cancer Therapeutics.* Chemistry & biology, 2015. **22**(1): p. 17-29.
106. Mao, Z., et al., *DNA repair by homologous recombination, but not by nonhomologous end joining, is elevated in breast cancer cells.* Neoplasia, 2009. **11**(7): p. 683-91.

107. Jasin, M., *Homologous repair of DNA damage and tumorigenesis: the BRCA connection.* Oncogene, 2002. **21**(58): p. 8981-93.
108. Chen, H., M. Lisby, and L.S. Symington, *RPA coordinates DNA end resection and prevents formation of DNA hairpins.* Mol Cell, 2013. **50**(4): p. 589-600.
109. Chen, R. and M.S. Wold, *Replication protein A: single-stranded DNA's first responder: dynamic DNA-interactions allow replication protein A to direct single-strand DNA intermediates into different pathways for synthesis or repair.* Bioessays, 2014. **36**(12): p. 1156-61.
110. Bochkarev, A., et al., *The crystal structure of the complex of replication protein A subunits RPA32 and RPA14 reveals a mechanism for single-stranded DNA binding.* EMBO J, 1999. **18**(16): p. 4498-504.
111. Habel, J.E., J.F. Ohren, and G.E. Borgstahl, *Dynamic light-scattering analysis of full-length human RPA14/32 dimer: purification, crystallization and self-association.* Acta Crystallogr D Biol Crystallogr, 2001. **57**(Pt 2): p. 254-9.
112. Fanning, E., *A dynamic model for replication protein A (RPA) function in DNA processing pathways.* Nucleic acids research, 2006. **34**(15): p. 4126-4137.
113. Brosey, C.A., *Preparation of the modular multi-domain protein RPA for study by NMR spectroscopy.* Methods in molecular biology (Clifton, N.J.), 2012. **831**: p. 181-195.
114. Prakash, A. and G.E. Borgstahl, *The structure and function of replication protein A in DNA replication.* Subcell Biochem, 2012. **62**: p. 171-96.
115. Deng, X., et al., *Structure of the full-length human RPA14/32 complex gives insights into the mechanism of DNA binding and complex formation.* J Mol Biol, 2007. **374**(4): p. 865-76.
116. Bochkareva, E., et al., *Structure of the RPA trimerization core and its role in the multistep DNA-binding mechanism of RPA.* EMBO J, 2002. **21**(7): p. 1855-63.
117. Ranatunga, W., et al., *Human RAD52 exhibits two modes of self-association.* J Biol Chem, 2001. **276**(19): p. 15876-80.
118. Stasiak, A.Z., *The human Rad52 protein exists as a heptameric ring.* Current biology, 2000. **10**(6): p. 337-340.
119. Kagawa, W., et al., *Crystal structure of the homologous-pairing domain from the human Rad52 recombinase in the undecameric form.* Mol Cell, 2002. **10**(2): p. 359-71.
120. Singleton, M.R., et al., *Structure of the single-strand annealing domain of human RAD52 protein.* Proc Natl Acad Sci U S A, 2002. **99**(21): p. 13492-7.
121. Mer, G., et al., *Structural basis for the recognition of DNA repair proteins UNG2, XPA, and RAD52 by replication factor RPA.* Cell, 2000. **103**(3): p. 449-56.
122. Park, M.S., et al., *Physical interaction between human RAD52 and RPA is required for homologous recombination in mammalian cells.* J Biol Chem, 1996. **271**(31): p. 18996-9000.
123. Prakash, A., et al., *Identification of the DNA-Binding Domains of Human Replication Protein A That Recognize G-Quadruplex DNA.* J Nucleic Acids, 2011. **2011**: p. 896947.
124. Kagawa, W., et al., *Homologous pairing promoted by the human Rad52 protein.* J Biol Chem, 2001. **276**(37): p. 35201-8.
125. Dietlein, F., L. Thelen, and H.C. Reinhardt, *Cancer-specific defects in DNA repair pathways as targets for personalized therapeutic approaches.* Trends Genet, 2014. **30**(8): p. 326-39.
126. Guestini, F., et al., *Triple Negative Breast Cancer Chemosensitivity and Chemoresistance: Current Advances in Biomarkers Indentification.* Expert Opin Ther Targets, 2015.

127. Banerjee, S., S.B. Kaye, and A. Ashworth, *Making the best of PARP inhibitors in ovarian cancer.* Nat Rev Clin Oncol, 2010. **7**(9): p. 508-19.
128. Audeh, M.W., et al., *Oral poly(ADP-ribose) polymerase inhibitor olaparib in patients with BRCA1 or BRCA2 mutations and recurrent ovarian cancer: a proof-of-concept trial.* Lancet, 2010. **376**(9737): p. 245-51.
129. Morales, J., et al., *Review of poly (ADP-ribose) polymerase (PARP) mechanisms of action and rationale for targeting in cancer and other diseases.* Crit Rev Eukaryot Gene Expr, 2014. **24**(1): p. 15-28.
130. Lord, C.J. and A. Ashworth, *Targeted therapy for cancer using PARP inhibitors.* Curr Opin Pharmacol, 2008. **8**(4): p. 363-9.
131. Papeo, G., et al., *Insights into PARP Inhibitors' Selectivity Using Fluorescence Polarization and Surface Plasmon Resonance Binding Assays.* J Biomol Screen, 2014. **19**(8): p. 1212-9.
132. Lieberman, R. and M. You, *Corrupting the DNA damage response: a critical role for Rad52 in tumor cell survival.* Aging (Albany NY), 2017. **9**(7): p. 1647-1659.
133. Lieberman, R., et al., *Functional characterization of RAD52 as a lung cancer susceptibility gene in the 12p13.33 locus.* Mol Carcinog, 2016. **55**(5): p. 953-63.
134. Borgstahl, G.E., et al., *Interplay of DNA damage and cell cycle signaling at the level of human replication protein A.* DNA Repair (Amst), 2014. **21**: p. 12-23.
135. Sakai, W., et al., *Functional restoration of BRCA2 protein by secondary BRCA2 mutations in BRCA2-mutated ovarian carcinoma.* Cancer Res, 2009. **69**(16): p. 6381-6.
136. Sakai, W., et al., *Secondary mutations as a mechanism of cisplatin resistance in BRCA2-mutated cancers.* Nature, 2008. **451**(7182): p. 1116-20.
137. Munshi, A., et al., *Vorinostat, a histone deacetylase inhibitor, enhances the response of human tumor cells to ionizing radiation through prolongation of gamma-H2AX foci.* Mol Cancer Ther, 2006. **5**(8): p. 1967-74.
138. Palmieri, D., et al., *Vorinostat inhibits brain metastatic colonization in a model of triple-negative breast cancer and induces DNA double-strand breaks.* Clin Cancer Res, 2009. **15**(19): p. 6148-57.
139. Luchini, A., V. Espina, and L.A. Liotta, *Protein painting reveals solvent-excluded drug targets hidden within native protein-protein interfaces.* Nat Commun, 2014. **5**: p. 4413.
140. Treszezamsky, A.D., et al., *BRCA1- and BRCA2-deficient cells are sensitive to etoposide-induced DNA double-strand breaks via topoisomerase II.* Cancer Res, 2007. **67**(15): p. 7078-81.
141. Singer, V.L., T.E. Lawlor, and S. Yue, *Comparison of SYBR Green I nucleic acid gel stain mutagenicity and ethidium bromide mutagenicity in the Salmonella/mammalian microsome reverse mutation assay (Ames test).* Mutat Res, 1999. **439**(1): p. 37-47.
142. Van Dyck, E., et al., *Visualisation of human rad52 protein and its complexes with hRad51 and DNA.* J Mol Biol, 1998. **284**(4): p. 1027-38.
143. Jacques, D.A., *Small-angle scattering for structural biology--expanding the frontier while avoiding the pitfalls.* Protein science, 2010. **19**(4): p. 642-657.